

5G Channel Model for bands up to 100 GHz

Revised version

(2.1 May 2016)

Contributors:

Aalto University

AT&T

BUPT

CMCC

Ericsson

Huawei

INTEL

KT Corporation

Nokia

NTT DOCOMO

New York University

Qualcomm

Samsung

University of Bristol

University of Southern California

Executive Summary

The future mobile communications systems are likely to be very different to those of today with new service innovations driven by increasing data traffic demand, increasing processing power of smart devices and new innovative applications. To meet these service demands the telecommunication industry is converging on a common set of 5G requirements which includes network speeds as high as 10 Gbps, cell edge rate greater than 100 Mbps and latency of less than 1 ms. To be able to reach these 5G requirements the industry is looking at new spectrum bands in the range up to 100 GHz where there is spectrum availability for wide bandwidth channels. For the development of the new 5G systems to operate in bands up to 100 GHz there is a need for accurate radio propagation models for these bands which are not addressed by existing channel models developed for bands below 6 GHz. This white paper presents a preliminary overview of the 5G channel propagation phenomena and channel models for bands up to 100 GHz. These have been derived based on extensive measurement and ray-tracing results across a multitude of bands. The following procedure was used to derive the channel model in this white paper.



Based on extensive measurements and ray-tracing across frequency bands from 6 GHz to 100 GHz, the white paper describes an initial 3D channel model which includes:

- a. Typical deployment scenarios for urban micro (UMi), urban macro (UMa) and indoor (InH) environments.
- b. A baseline model incorporating pathloss, shadow fading, line of sight probability, penetration and blockage models for the typical scenarios
- c. Preliminary fast fading models for the above scenarios
- d. Various processing methodologies (e.g. clustering algorithm, antenna decoupling etc.)

These studies have found some extensibility of the existing 3GPP models (e.g. 3GPP TR36.873) to the higher frequency bands up to 100 GHz. The measurements indicate that the smaller wavelengths introduce an increased sensitivity of the propagation models to the scale of the environment and show some frequency dependence of the path loss as well as increased occurrence of blockage. Further, the penetration loss is highly dependent on the material and tends to increase with frequency. The shadow fading and angular spread parameters are larger and the boundary between LOS and NLOS depends not only on antenna heights but also on the local environment. The small-scale characteristics of the channel such as delay spread and angular spread and the multipath richness is somewhat similar over the frequency range, which is encouraging for extending the existing 3GPP models to the wider frequency range.

Version 2.0 of this white paper provides significant updates to the baseline model that was disclosed in the first version. In particular, Version 2.0 provides concrete proposals for modeling important features, such as outdoor to indoor path loss. In addition, modeling proposals are provided for features that were not modeled in the first version, such as dynamic blockage, and spatial consistency.

Finally, version 2.0 provides significant updates to large and small-scale parameter modeling, including a newly proposed clustering algorithm and models that capture frequency dependency of various large and small-scale parameters.

While further work needs to be carried out to develop a complete channel model for these higher frequency bands, this white paper presents the first steps for an initial basis for the model development.

Contents

Executive Summary	2
1 Introduction	6
2 Requirements for new channel model	7
3 Typical Deployment Scenarios	8
3.1 Urban Micro (UMi) Street Canyon and Open Square with outdoor to outdoor (O2O) and outdoor to indoor (O2I)	9
3.2 Indoor (InH)– Open and closed Office, Shopping Malls	9
3.3 Urban Macro (UMa) with O2O and O2I.....	10
4 Characteristics of the Channel in 6 GHz-100 GHz	10
4.1 UMi Channel Characteristics	11
4.2 UMa Channel Characteristics	11
4.3 InH Channel Characteristics	11
4.4 Penetration Loss in all Environments	12
4.4.1 Outdoor to indoor channel characteristics	12
4.4.2 Inside buildings.....	15
4.5 Blockage in all Environments	15
5 Channel Modelling Considerations	19
5.1 Support for a large frequency range.....	23
5.2 Support for high bandwidths.....	23
5.3 Modelling of spatial consistency.....	23
5.3.1 Method using Spatially consistent random variables.....	24
5.3.2 Geometric Stochastic Approach	27
5.3.3 Method using geometric locations of clusters (Grid-based GSCM, GGSCM)	29
5.4 Support for large arrays	34
5.5 Dual mobility support	35
5.6 Dynamic blockage modelling	35
5.7 Foliage loss	38
5.8 Atmospheric losses	39
6 Pathloss, Shadow Fading, LOS and Blockage Modelling	41
6.1 LOS probability	41
6.2 Path loss models.....	44
6.3 Building penetration loss modelling	48
6.4 Blockage models.....	50
7 Fast Fading Modelling	50
7.1 UMi.....	50
7.2 UMa	54
7.3 InH.....	55

7.4	O2I channel modelling	57
8	Step-by-step procedure for generating channels	58
9	List of contributors.....	58
10	Acknowledgements.....	59
11	Appendix.....	59
11.1	Overview of measurement campaigns	59
11.2	Overview of ray-tracing campaigns	66
11.3	Fast Fading Model parameters from measurements and ray-tracing	71
11.3.1	UMi	71
11.3.2	UMa.....	76
11.3.3	InH.....	84
11.3.4	O2I.....	90
11.4	Processing Methodologies	94
11.4.1	Physical effects on propagation	94
11.4.2	The effects of the antenna pattern.....	95
11.4.3	Clustering	96
	References	98
	List of Acronyms.....	102

1 Introduction

Next generation 5G cellular systems will encompass frequencies from around 500 MHz all the way to around 100 GHz. For the development of the new 5G systems to operate in bands above 6 GHz, there is a need for accurate radio propagation models for these bands that include aspects that are not fully modelled by existing channel models below 6 GHz. Previous generations of channel models were designed and evaluated for operation at frequencies only as high as 6 GHz. One important example is the recently developed 3D-urban micro (UMi) and 3D-urban macro (UMa) channel models for LTE [3GPP TR36.873]. The 3GPP 3D channel model provides additional flexibility for the elevation dimension, thereby allowing modelling two dimensional antenna systems, such as those that are expected in next generation system deployments. It is important for future system design to develop a new channel model that will be validated for operation at higher frequencies (e.g., up to 100 GHz) and that will allow accurate performance evaluation of possible future technical specifications for these bands over a representative set of possible environments and scenarios of interest. Furthermore, the new models should be consistent with the models below 6 GHz. In some cases, the new requirements may call for deviations from the modelling parameters or methodology of the existing models, but these deviations should be kept to a minimum and only introduced when necessary for supporting the 5G simulation use cases.

There are many existing and ongoing research efforts worldwide targeting 5G channel measurements and modelling. They include METIS202 [METIS 2015], COST2100/COST[COST], IC1004 [IC], ETSI mmWave SIG [ETSI 2015], 5G mmWave Channel Model Alliance [NIST], MiWEBA [MiWEBA 2014], mmMagic [mmMagic], and NYU WIRELESS [Rappaport 2015, MacCartney 2015, Rappaport 2013, Samimi 2015]. METIS2020, for instance, has focused on 5G technologies and has contributed extensive studies in terms of channel modelling. Their target requirements include a wide range of frequency bands (up to 86 GHz), very large bandwidths (hundreds of MHz), fully three dimensional and accurate polarization modelling, spherical wave modelling, and high spatial resolution. The METIS channel models consist of a map-based model, stochastic model, and a hybrid model which can meet requirements for flexibility and scalability. The COST2100 channel model is a geometry-based stochastic channel model (GSCM) that can reproduce the stochastic properties of multiple-input/multiple output (MIMO) channels over time, frequency, and space. Ongoing, the 5G mmWave Channel Model Alliance¹ is a newly established group that will formulate guidelines for measurement calibration and methodology, modelling methodology, as well as parameterization in various environments and a database for channel measurement campaigns. NYU WIRELESS has conducted and published extensive urban propagation measurements at 28, 38 and 73 GHz for both outdoor and indoor channels, and has created large-scale and small-scale channel models and concepts of spatial lobes to model multiple multipath time clusters that are seen to arrive in particular directions [Rappaport 2013, Rappaport 2015, Samimi GCW2015, MacCartney 2015, Samimi EUCAP2016].

In this white paper, we present a brief overview of the channel properties for bands up to 100 GHz based on extensive measurement and ray-tracing results across a multitude of bands. In addition we

¹ <https://sites.google.com/a/corneralliance.com/5g-mmwave-channel-model-alliance-wiki/home>

present a preliminary set of channel parameters suitable for 5G simulations that are capable of modelling the main properties and trends.

2 Requirements for new channel model

The requirements of the new channel model that will support 5G operation across frequency bands up to 100 GHz are outlined below:

1. The new channel model should preferably be based on the existing 3GPP 3D channel model [3GPP TR36.873] but with extensions to cater for additional 5G modelling requirements and scenarios, for example:
 - a. Antenna arrays, especially at higher-frequency millimeter-wave bands, will very likely be 2D and dual-polarized both at the access point (AP) and the user equipment (UE) and will hence need properly-modelled azimuth and elevation angles of departure and arrival of multipath components.
 - b. Individual antenna elements will have antenna radiation patterns in azimuth and elevation and may require separate modelling for directional performance gains. Furthermore, polarization properties of the multipath components need to be accurately accounted for in the model.
2. The new channel model must accommodate a wide frequency range up to 100 GHz. The joint propagation characteristics over different frequency bands will need to be evaluated for multi-band operation, e.g., low-band and high-band carrier aggregation configurations.
3. The new channel model must support large channel bandwidths (up to 2 GHz), where:
 - a. The individual channel bandwidths may be in the range of 100 MHz to 2 GHz and may support carrier aggregation.
 - b. The operating channels may be spread across an assigned range of several GHz
4. The new channel model must support a range of large antenna arrays, in particular:
 - a. Some large antenna arrays will have very high directivity with angular resolution of the channel down to around 1.0 degree.
 - b. 5G will consist of different array types, e.g., linear, planar, cylindrical and spherical arrays, with arbitrary polarization.
 - c. The array manifold vector can change significantly when the bandwidth is large relative to the carrier frequency. As such, the wideband array manifold assumption is not valid and new modelling techniques may be required. It may be preferable, for example, to model arrival/departure angles with delays across the array and follow a spherical wave assumption instead of the usual plane wave assumption.
5. The new channel model must accommodate mobility, in particular:
 - a. The channel model structure should be suitable for mobility up to 350 km/hr.

- b. The channel model structure should be suitable for small-scale mobility and rotation of both ends of the link in order to support scenarios such as device to device (D2D) or vehicle to vehicle (V2V).
6. The new channel model must ensure spatial/temporal/frequency consistency, in particular:
- a. The model should provide spatial/temporal/frequency consistencies which may be characterized, for example, via spatial consistence, inter-site correlation, and correlation among frequency bands.
 - b. The model should also ensure that the channel states, such as Line Of Sight (LOS)/non-LOS (NLOS) for outdoor/indoor locations, the second order statistics of the channel, and the channel realizations change smoothly as a function of time, antenna position, and/or frequency in all propagation scenarios.
 - c. The spatial/temporal/frequency consistencies should be supported for simulations where the channel consistency impacts the results (e.g. massive MIMO, mobility and beam tracking, etc.). Such support could possibly be optional for simpler studies.
7. The new channel model must be of practical computational complexity, in particular:
- a. The model should be suitable for implementation in single-link simulation tools and in multi-cell, multi-link radio network simulation tools. Computational complexity and memory requirements should not be excessive. The 3GPP 3D channel model [3GPP TR36.873] is seen, for instance, as a sufficiently accurate model for its purposes, with an acceptable level of complexity. Accuracy may be provided by including additional modelling details with reasonable complexity to support the greater channel bandwidths, and spatial and temporal resolutions and spatial/temporal/frequency consistency, required for millimeter-wave modelling.
 - b. The introduction of a new modelling methodology (e.g. Map based model) may significantly complicate the channel generation mechanism and thus substantially increase the implementation complexity of the system-level simulator. Furthermore, if one applies a completely different modelling methodology for frequencies above 6 GHz, it would be difficult to have meaningful comparative system evaluations for bands up to 100 GHz.

3 Typical Deployment Scenarios

The traditional modelling scenarios (UMa, UMi and indoor hotspot (InH)) have previously been considered in 3GPP for modelling of the radio propagation in bands below about 6 GHz. The new channel model discussed in this paper is for a selective set of 5G scenarios and encompasses the following cases:

3.1 Urban Micro (UMi) Street Canyon and Open Square with outdoor to outdoor (O2O) and outdoor to indoor (O2I)



Figure 1. UMi Street Canyon



Figure 2. UMi Open Square

A typical UMi scenario is shown for street canyon and open square in Figure 1 and Figure 2, respectively. The cell radii for UMi is typically less than 100 m and the access points (APs) are mounted below rooftops (e.g., 3-20 m). The UEs are deployed outdoor at ground level or indoor at all floors.

3.2 Indoor (InH)– Open and closed Office, Shopping Malls

The indoor scenario includes open and closed offices, corridors within offices and shopping malls as examples. The typical office environment has open cubicle areas, walled offices, open areas, corridors, etc., where the partition walls are composed of a variety of materials like sheetrock, poured concrete, glass, cinder block, etc. For the office environment, the APs are mounted at a height of 2-3 m either on the ceilings or walls. The shopping malls are generally 2-5 stories high and often include an open area (“atrium”). In the shopping-mall environment, the APs are mounted at a height of approximately 3 m on the walls or ceilings of the corridors and shops. The density of the APs may range from one per floor to one per room, depending on the frequency band and output power. The typical indoor office scenario and shopping malls are shown in Figure 3 and Figure 4, respectively.

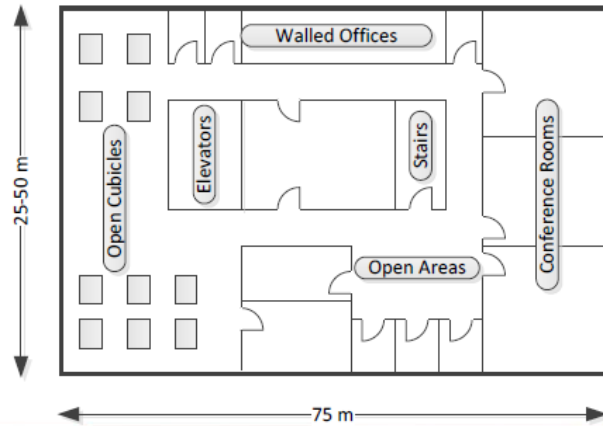


Figure 3. Typical Indoor Office



Figure 4. Indoor Shopping Malls

3.3 Urban Macro (UMa) with O2O and O2I



Figure 5. UMa Deployment

The cell radii for UMa is typically above 200 m and the APs are mounted on or above rooftops (e.g. 25-35 m), an example of which is shown in Figure 5. The UEs are deployed both outdoor at ground level and indoor at all floors.

4 Characteristics of the Channel in 6 GHz-100 GHz

Measurements over a wide range of frequencies have been performed by the co-signatories of this white paper. However, due to the more challenging link budgets at higher frequencies there are few

measurements at larger distances, e.g. beyond 200-300 m in UMi or in severely shadowed regions at shorter distances. In UMa measurements were able to be made at least in the Aalborg location at distances up to 1.24 km. An overview of the measurement and ray-tracing campaigns can be found in the Appendix. In the following sections we outline the main observations per scenario with some comparisons to the existing 3GPP models for below 6 GHz (e.g. [3GPP TR36.873]).

4.1 UMi Channel Characteristics

The LOS path loss in the bands of interest appears to follow Friis' free space path loss model quite well. Just as in lower bands, a higher path loss slope (or path loss exponent) is observed in NLOS conditions. The shadow fading in the measurements appears to be similar to lower frequency bands, while ray-tracing results show a much higher shadow fading (>10 dB) than measurements, due to the larger dynamic range allowed in some ray-tracing experiments.

In NLOS conditions at frequencies below 6.0 GHz, the RMS delay spread is typically modelled at around 50-500 ns, the RMS azimuth angle spread of departure (from the AP) at around 10-30°, and the RMS azimuth angle spread of arrival (at the UE) at around 50-80° [3GPP TR36.873]. There are measurements of the delay spread above 6 GHz which indicate somewhat smaller ranges as the frequency increases, and some measurements show the millimeter wave omnidirectional channel to be highly directional in nature.

4.2 UMa Channel Characteristics

Similar to the UMi scenario, the LOS path loss behaves quite similar to free space path loss as expected. For the NLOS path loss, the trends over frequency appear somewhat inconclusive across a wide range of frequencies. The rate at which the loss increases with frequency does not appear to be linear, as the rate is higher in the lower part of the spectrum. This could possibly be due to diffraction, which is frequency dependent, being a more dominating propagation mechanism at the lower frequencies. At higher frequencies reflections and scattering may be more predominant. Alternatively, the trends could be biased by the lower dynamic range in the measurements at the higher frequencies. More measurements are needed to better understand the UMa channel.

From preliminary ray-tracing studies, the channel spreads in delay and angle appear to be weakly dependent on the frequency and are generally 2-5 times smaller than in [3GPP TR36.873].

The cross-polar scattering in the ray-tracing results tends to increase (lower XPR) with increasing frequency due to diffuse scattering.

4.3 InH Channel Characteristics

In LOS conditions, multiple reflections from walls, floor, and ceiling give rise to a waveguide like propagation effect. Measurements in both office and shopping mall scenarios show that path loss exponents, based on a 1 m free space reference distance, are typically below 2, indicating a more favourable path loss than predicted by Friis' free space loss formula. The strength of the waveguiding effect is variable and the path loss exponent appears to increase very slightly with increasing frequency, possibly due to the relation between the wavelength and surface roughness.

Measurements of the small scale channel properties such as angular spread and delay spread have shown remarkable similarities between channels over a very wide frequency range. It appears as if the

main multipath components are present at all frequencies though with some smaller variations in amplitudes.

Recent work shows that polarization discrimination ranges between 15 and 25 dB for indoor millimeter wave channels [Karttunen EuCAP2015], with greater polarization discrimination at 73 GHz than at 28 GHz [MacCartney 2015].

4.4 Penetration Loss in all Environments

4.4.1 Outdoor to indoor channel characteristics

In both the UMa and the UMi scenario a significant portion of UEs or devices are expected to be indoors. These indoor UEs increase the strain on the link budget since additional losses are associated with the penetration into buildings. The characteristics of the building penetration loss and in particular its variation over the higher frequency range is therefore of high interest and a number of recent measurement campaigns have been targeting the material losses and building penetration losses at higher frequencies, see e.g. [Rodriguez VTC Fall 2014], [Zhao 2013], [Larsson EuCAP 2014], and the measurement campaigns reported in the Annex. The current understanding based on these measurements is briefly summarized as follows.

Different materials commonly used in building construction have very diverse penetration loss characteristics. Common glass tends to be relatively transparent with a rather weak increase of loss with higher frequency due to conductivity losses. "Energy-efficient" glass commonly used in modern buildings or when renovating older buildings is typically metal-coated for better thermal insulation. This coating introduces additional losses that can be as high as 40 dB even at lower frequencies. Materials such as concrete or brick have losses that increase rapidly with frequency. Figure 6 summarizes some recent measurements of material losses including those outlined in the Annex. The loss trends with frequency are linear to a first order of approximation. Variations around the linear trend can be understood from multiple reflections within the material or between different layers which cause constructive or destructive interference depending on the frequency and incidence angle.

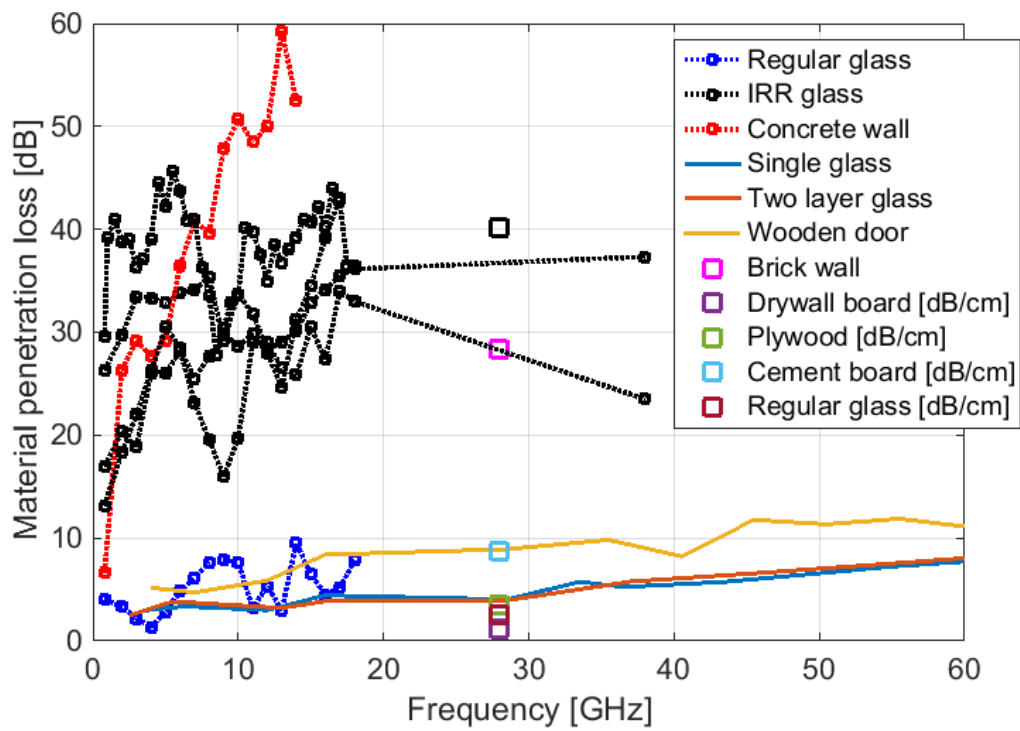


Figure 6. Measured material penetration losses. Sources: [Rodriguez VTC Fall 2014], [Zhao 2013], and measurements contributed by Samsung, Nokia, and Huawei.

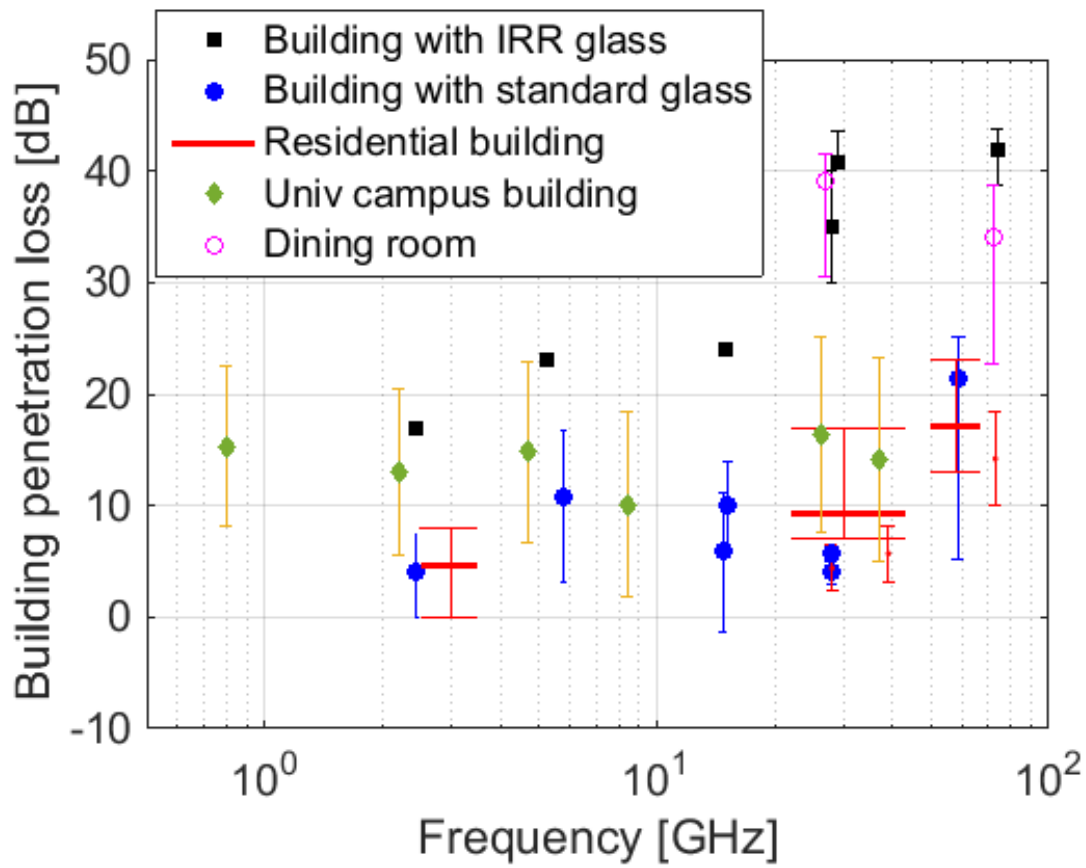


Figure 7. Effective building penetration loss measurements. The bars indicate variability for a given building. Sources: [Larsson EuCAP 2014] and measurements contributed by Qualcomm, NTT DOCOMO, Ericsson, Nokia, Huawei, and KT.

Typical building facades are composed of several materials, e.g. glass, concrete, metal, brick, wood, etc. Propagation of radio waves into or out of a building will in most cases be a combination of transmission paths through different materials, i.e. through windows and through the facade between the windows. The exception could be when very narrow beams are used which only illuminates a single material or when the indoor node is very close to the external wall. Thus, the effective penetration loss can behave a bit differently than the single material loss. A number of recent measurements of the effective penetration loss for close to perpendicular incidence angles are summarized in Figure 7. As indicated by the error-bars available for some of the measurements, there can be quite some variation even in a single building. The measurements can loosely be grouped into two categories: a set of high penetration loss results for buildings constructed with IRR glass, and a set of lower loss results for different buildings where regular glass has been used,

Increased penetration losses have been observed for more grazing incidence angles, resulting in up to 15-20 dB additional penetration loss in the worst case.

Propagation deeper into the building will also be associated with an additional loss due to internal walls, furniture etc. This additional loss appears to be rather weakly frequency-dependent but rather strongly dependent on the interior composition of the building. Observed losses over the 2-60 GHz range of 0.2-2 dB/m.

4.4.2 Inside buildings

Measurements have been reported for penetration loss for various materials at 2.5, 28, and 60 GHz for indoor scenarios [Rappaport Book2015] [Rappaport 2013] [And 2002] [Nie13] [Zhao 2013]. For easy comparisons, walls and drywalls were lumped into a common dataset and different types of clear glass were lumped into a common dataset with normalized penetration loss shown in Figure 8. It was observed that clear glass has widely varying attenuation (20 dB/cm at 2.5 GHz, 3.5 dB/cm at 28 GHz, and 11.3 dB/cm at 60 GHz). For mesh glass, penetration was observed to increase as a function of frequency (24.1 dB/cm at 2.5 GHz and 31.9 dB/cm at 60 GHz), and a similar trend was observed with whiteboard penetration increasing as frequency increased. At 28 GHz, indoor tinted glass resulted in a penetration loss 24.5 dB/cm. Walls showed very little attenuation per cm of distance at 28 GHz (less than 1 dB/cm).

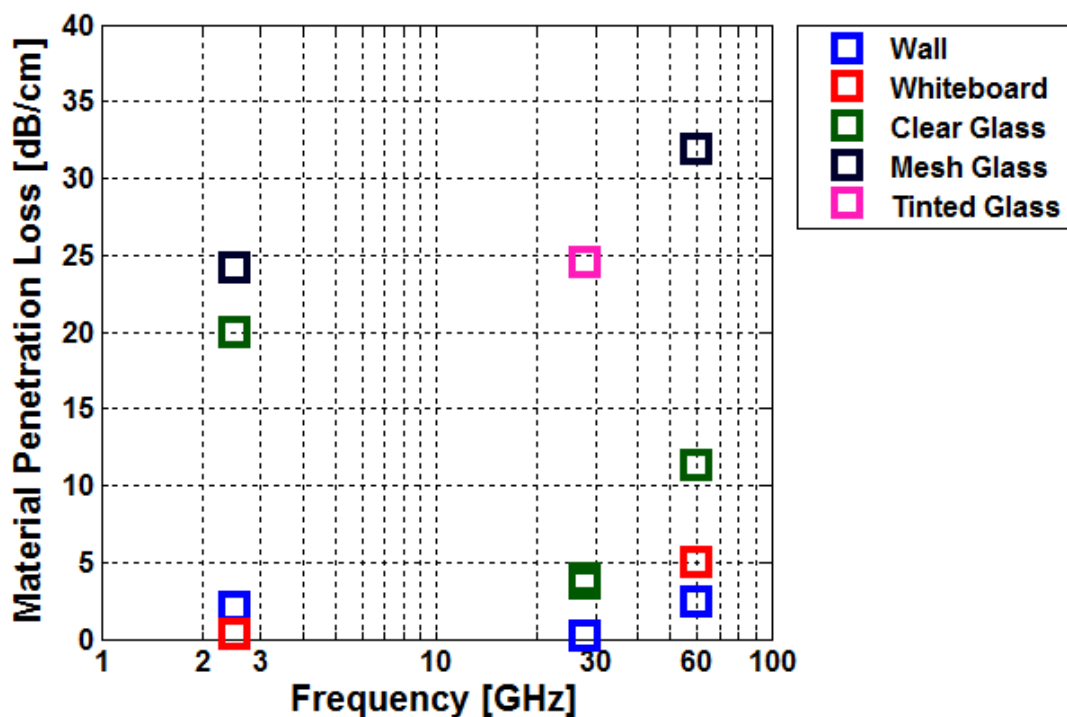


Figure 8. 2.5 GHz, 28 GHz, and 60 GHz normalized material penetration losses from indoor measurements with common types of glass and walls lumped into common datasets [Rappaport 2013] [And2002][Zhao 2013] [Nie 2013].

4.5 Blockage in all Environments

As the radio frequency increases, its propagation behaves more like optical propagation and may become blocked by intervening objects. Typically, two categories of blockage are considered: dynamic blockage and geometry-induced blockage. Dynamic blockage is caused by the moving objects (i.e., cars, people) in the communication environment. The effect is transient additional loss on the paths that intercept the moving object. Figure 9 shows such an example from 28 GHz measurement done by Intel/Fraunhofer HHI in Berlin. In these experiments, time continuous measurements were made with the transmitter and receiver on each side of the road that had on-off traffic controlled by traffic light. Note that the time periods when the traffic light is red is clearly seen in the figure as periods with little variation as the vehicles are static at that time. When the traffic light

is green, the blocking vehicles move through the transmission path at a rapid pace as is seen in the figure. The variations seen when the light is red are explained by vehicles turning the corner to pass between the transmitter and receiver. Figure 10 shows a blockage measurement at 28 GHz due to passing by bus and lorry. The signal attenuation at LOS path is observed to be 8 dB – 30 dB. Signal fluctuation is observed during the period of blockage perhaps due to windows in the bus and lorry. The aggregated omni signal attenuation is observed to be around 10 dB – despite the high attenuation on the LOS path, some of the NLOS paths can still go through. Figure 11 shows a blockage measurement at 15 GHz by garbage truck [Ökvist 2016]. The signal was transmitted from two carriers, each with 100 MHz bandwidth. The signal attenuation is observed to be 8 – 10 dB. A gap between drivers compartment and trash bin can be observed, where temporal recovery of signal strength is observed. Figure 12 shows a blockage measurement at 73.5 GHz by human movement. The measurement setup is shown in Figure 13, where the transmitter and receiver are placed at 5 m apart and 11 blocker bins are measured each separated by 0.5 m. The average LOS blockage shadowing values across the blockage bins range from 22 dB to more than 40 dB. The lowest shadowing value is achieved when the blocker is standing in the middle of the transmitter and receiver. When the blocker moves closer to the transmitter or the receiver, the blockage shadowing increases, This implicates that more NLOS paths are blocked when the blocker is at close distance to the transmitter and receiver. Based on the above measurement results, we can observe that blocking only happens in some directions, multipath from other directions probably not affected. The effect of blockage can be modelled as additional shadow fading on the affected directions.

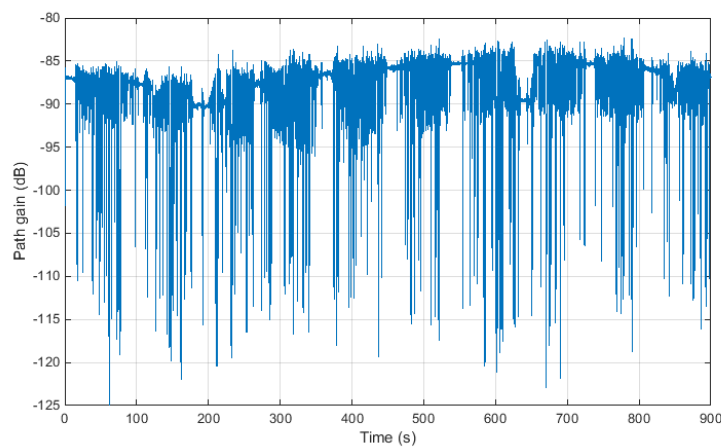


Figure 9 Example of dynamic blockage from a measurement snapshot at 28 GHz by Intel/Fraunhofer HHI

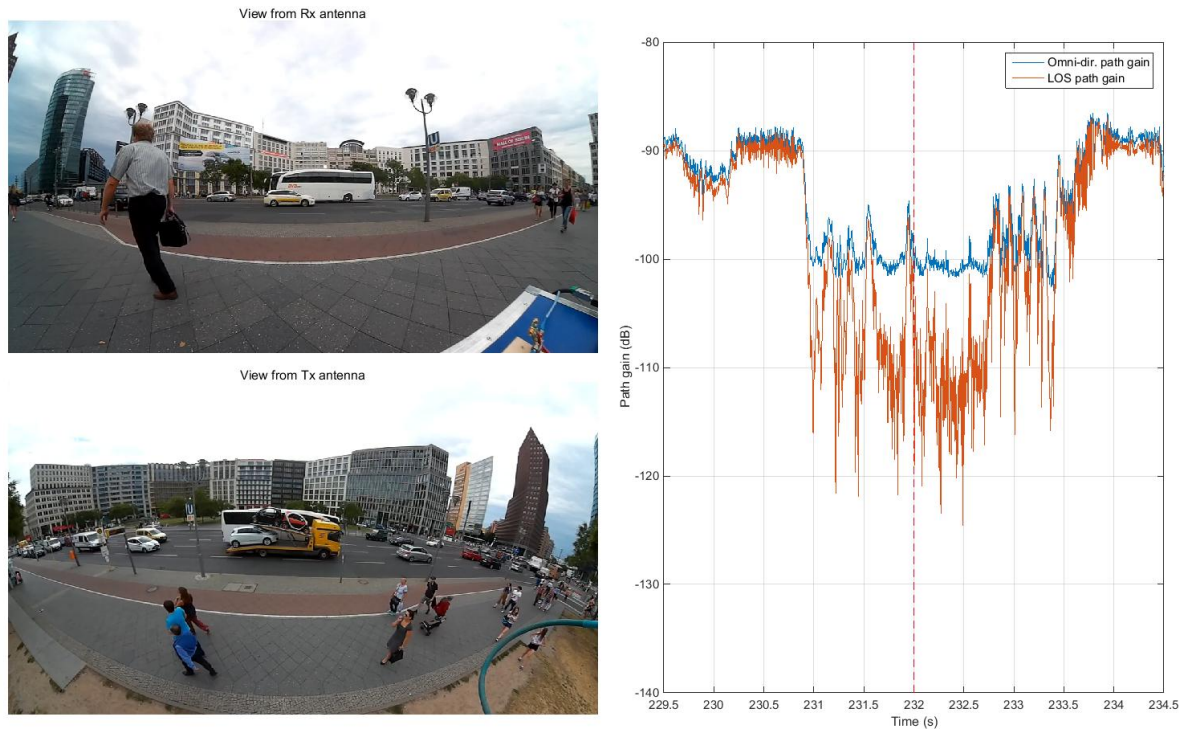


Figure 10 blockage measurement at 28 GHz by distant bus + lorry by Intel/Fraunhofer HHI

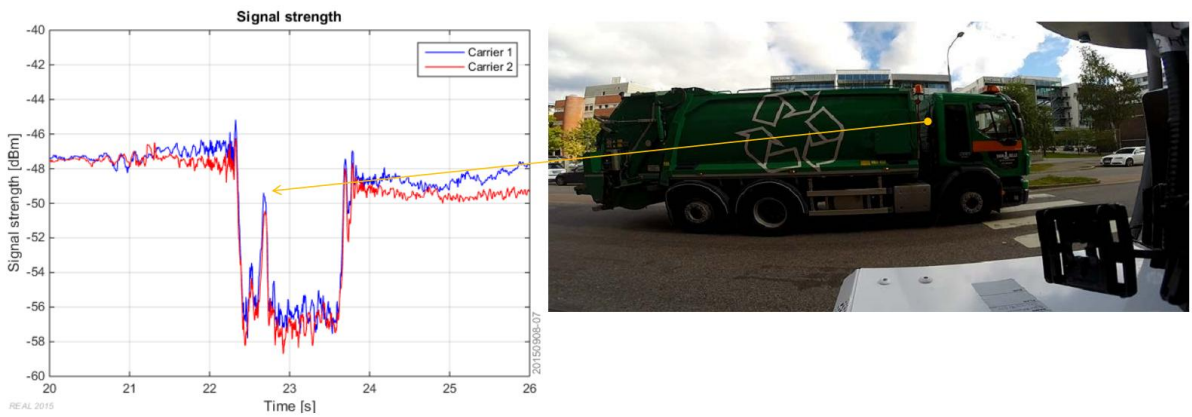


Figure 11 Blockage measurement at 15GHz by garbage truck by Ericsson

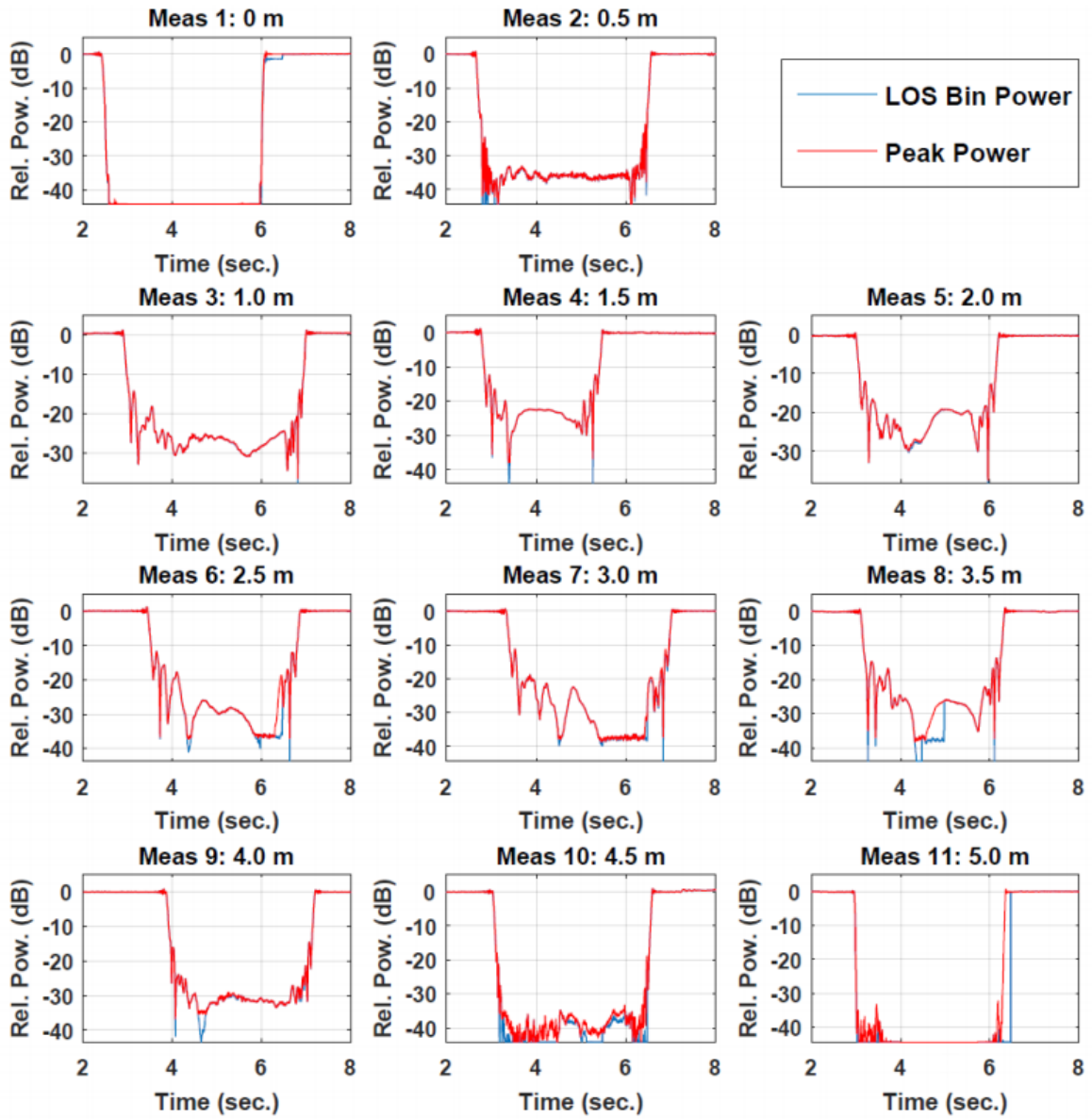


Figure 12 Blockage measurement at 73.5 GHz by human being by NYU

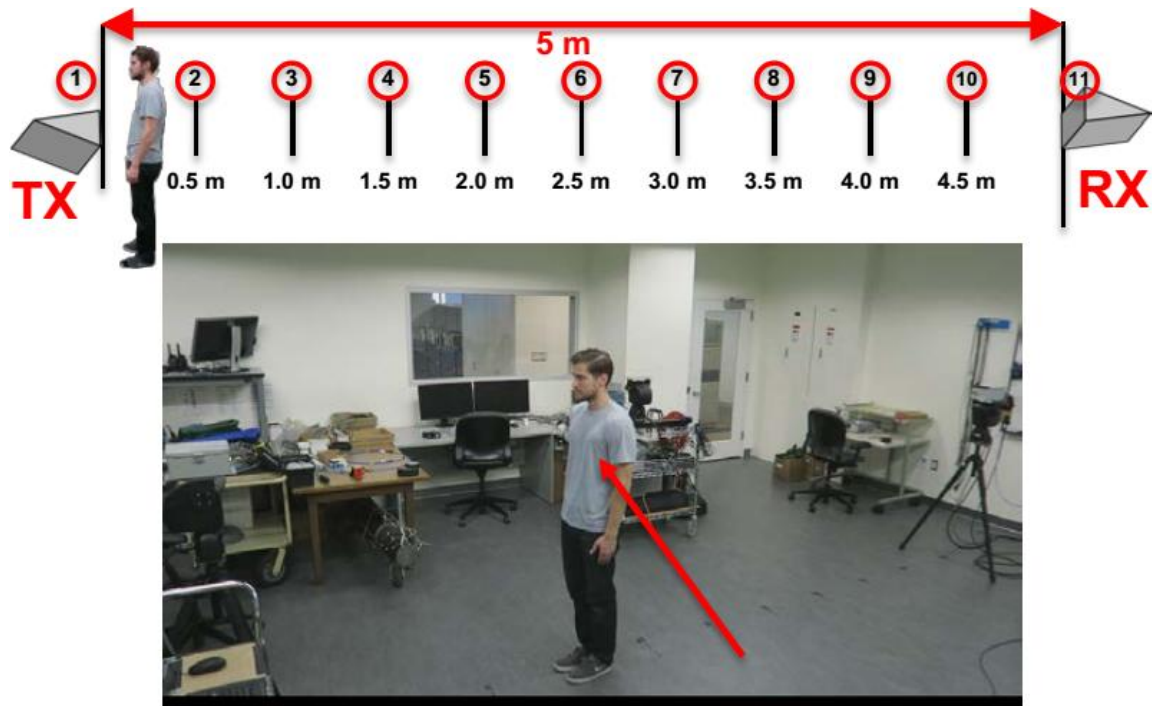


Figure 13 measurement setup of human being blockage measurement in NYU

Geometry-induced blockage, on the other hand, is a static property of the environment. It is caused by objects in the map environment that block the signal paths. The propagation channels in geometry-induced blockage locations are dominated by diffraction and sometimes by diffuse scattering. The effect is an exceptional additional loss beyond the normal path loss and shadow fading. Figure 14 illustrates examples of diffraction-dominated and reflection-dominated regions in an idealized scenario. As compared to shadow fading caused by reflections, diffraction-dominated shadow fading could have different statistics (e.g., different mean, variance and coherence distance).

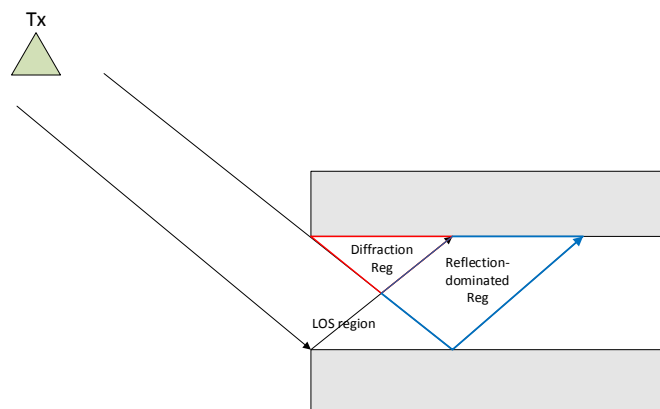


Figure 14 Example of diffraction-dominated and reflection-dominated regions (idealized scenario)

5 Channel Modelling Considerations

Table 1 summarizes a review of the 3GPP 3D channel model [3GPP TR36.873] capabilities. A plus sign “+” means that the current 3GPP 3D channel model supports the requirement, or the necessary

changes are very simple. A minus sign “-” means that the current channel model does not support the requirement. This evaluation is further split into two frequency ranges: below 6 GHz and above 6 GHz. Note that in the table, LSP stands for large-scale parameter.

Table 1. Channel Modelling Considerations

Attribute	Requirement	Below 6 GHz	Above 6 GHz	Improvement addressed in this white paper	Comments
#1 Scenarios	Support of new scenarios such as indoor office, stadium, shopping mall etc.	-	-	✓	Current 3GPP model supports UMi and UMa
#2 Frequency Range	0.5 GHz – 100 GHz supported	+	-	✓	Current 3GPP model 2 – 6 GHz
	Consistency of channel model parameters between different frequency bands	-	-	✓	E.g. shadowing, angle of departure, and in carrier aggregation
#3 Bandwidth	~100 MHz BW for below 6 GHz, 2 GHz BW for above 6 GHz	+	-	✓	
#4 Spatial Consistency	Spatial consistency of LSPs with fixed BS	+	-	✓	LSP map (2D or 3D)
	Spatial consistency of LSPs with arbitrary Tx / Rx locations (D2D / V2V)	-	-	✗	Complexity issue (4D or 6D map)
	Fair comparison of different network topologies	-	-	✗	
	Spatial consistency of SSPs	-	-	✓	Autocorrelation of SSPs
	UDN / MU Consistency	-	-	✓	Sharing of objects / clusters
	Distributed antennas and extremely large	-	-	✓	

	arrays				
	Dynamic channel (smooth evolution of SSPs and LSPs)	-	-	✓	Tx / Rx / scatterer mobility Possible methods for modelling varying DoDs and DoAs are discussed in the Appendix
#5 Large Array Support	Spherical wave	-	-	✗	Also far field spherical
	High angular resolution down to 1 degree	-	-	✗	Realistic PAS?
	Accurate modelling of Laplacian PAS	-	-	✗	20 sinusoids problem
	Very large arrays beyond consistency interval	-	-	✓✗	Via spatial consistency modelling
#6 Dual-mobility support (D2D, V2V)	Dual Doppler	+	-	✗	Not yet done, but should be easy
	Dual angle of arrival (AoA)	+	-	✗	Not yet done, but should be easy
	Dual Antenna Pattern (mobile antenna pattern at both ends of the link)	+	-	✗	Not yet done, but should be easy
	Arbitrary UE height (e.g. different floors)	-	-	✗	
	Spatially consistent multi-dimensional map	-	-	✗	Complexity issue (4D or 6D map)
#7 LOS Probability	Spatially consistent LOS probability / LOS existence	-	-	✓	
#8 Specular Reflection		?	-	✗	Important in mmW

#9 Path Loss	Frequency dependent path loss model	+	-	✓	
	Power scaling (directive antennas vs. omnidirectional)	?	-	✓	
	Multiple NLOS cases	?	-	✓	Important in mmW
#10 Shadowing	Log-normal shadowing	+	-	✓	Shadow fading (SF) parameters needed for high frequency
	Body shadowing	-	-	✓	
#11 Blockage	Blockage modelling	-	-	✓	
#12 Cluster definition	3GPP 3D cluster is defined as fixed delay and Laplacian shape angular spread.	+	-	✓	It is not guaranteed that the Laplacian shape cluster is valid for mmW.
#13 Drop concept (block stationarity)	APs and UEs are dropped in some manner (e.g., hexagonal grid for 3GPP)	+	-	✓	It is not sure if the drop concept works perfectly in mmWave. Also it is not clear how to test beam tracking, for instance.
#14 Accurate LSP Correlation	Consistent correlation of LSPs is needed.	-	-	✗	The current 3GPP model provides different result depending on the order of calculation (autocorrelation, cross-correlation)
#15 Number of Paths	The number of paths needs to be accurate across frequency.	+	-	✗	The current model is based on low frequency measurements.

#16 Moving Environment	Cars, people, vegetation etc.	-	-	✓	
#17 Diffuse Propagation	Specular vs. diffuse power ratio, modelling of diffuse scattering	+	-	✘	Most mmW measurements report specular only despite the fact that diffuse exists

5.1 Support for a large frequency range

One of the outcomes of WRC-15 is that there will be studies of bands in the frequency range between 24.25 and 86 GHz for possible future IMT-2020 designation [ITU 238]. For the 3GPP studies, the broader range of 6 GHz to 100 GHz should be studied for modelling purposes. Furthermore, as mentioned in [3GPP RP-151606], possible implication of the new channel model on the existing 3D channel model for below 6 GHz should also be considered. It is worth noting that the frequency range of 3GPP 3D model is limited to LTE / LTE Advanced bands: “The applicable range of the 3D channel model is at least for 2-3.5 GHz” [3GPP TR36.873]. Therefore a significant improvement is needed in terms of frequency range for modelling tools.

In addition to the frequency range, the channel model should be frequency consistent, i.e. the correlation of LSPs and SSPs between frequency bands should be realistically modelled, and the LOS state and indoor state should not change randomly over frequency.

5.2 Support for high bandwidths

Many scenarios for 5G high frequency services postulate very high data rates up to several gigabits/second for user services. Such high throughput communications will require channels of very wide bandwidth (up to several gigahertz). The bands to be studied under the ITU-R Resolution [ITU 238] cover frequency bands up to 100 GHz (including 66 GHz – 76 GHz). The implication is that one operator may be allocated multiple gigahertz wide channels for operation. Therefore, the channel modelling should include support for scenarios with bandwidths up to several gigahertz. This implies that the delay resolution of the modelled channel needs to be much improved compared to [3GPP TR36.873] to produce realistic frequency domain characteristics over several GHz. This will likely require modifications of the cluster distributions in delay and the sub-path distributions within clusters.

5.3 Modelling of spatial consistency

The requirement of spatial consistency is probably the most challenging to meet with simple extensions to the current “drop-based” models, as there are multiple aspects of the channel conditions, including large-scale parameters and small-scale parameters, that would need to vary in a continuous and realistic manner as a function of position. These conditions will include the LOS/NLOS state, the indoor/outdoor state, and of course the parameters for the associated clusters of multipath components characterized by angles, delays, and powers. Preferably the inclusion of spatial consistency should not come at the cost of a high implementation or simulation complexity, and the channel statistics should be maintained.

Three different approaches for introducing spatial consistency modelling will be outlined here. At this point, no preference is given to any of the methods since they all have different benefits and drawbacks.

5.3.1 Method using Spatially consistent random variables

In this approach, the spatial consistency of channel clusters are modelled in the 3GPP 3D channel model [3GPP TR 36.873] by introducing spatial consistency to the channel cluster specific random variables, LOS/NLOS and indoor/outdoor states.

1) Spatially consistent cluster specific random variables

The channel cluster specific random variables include:

- a) Cluster specific random delay in step 5
- b) Cluster specific shadowing in step 6
- c) Cluster specific offset for AoD/AoA/ZoD/ZoA in step 7
- d) Cluster specific sign for AoD/AoA/ZoD/ZoA in step 7

Among these cluster specific random variables, the first three are continuous random variables and are made spatially consistent using the following method. The fourth variable is discrete and is generated per drop instead of varying spatially to avoid discontinuous sign changes.

The spatially consistent random variables can be generated by interpolating i.i.d. random variables deployed in the simulation area. For example in Figure 15, one spatially consistent uniform distributed random variable can be generated by dropping four complex normal distributed i.i.d. random variables on four vertex of one grid with d_{corr} (e.g. $d_{corr}=50$) de-correlation distance and interpolated using these i.i.d. random variables. The de-correlation distance could be a scenario specific parameter. In order to save simulation complexity, a grid may be generated only if there are actual users dropped within the grid area.

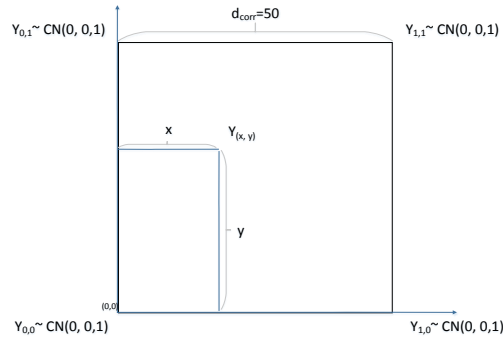


Figure 15 Example of generating one spatially consistent random variable.

Assuming $Y_{0,0}$, $Y_{0,1}$, $Y_{1,0}$, $Y_{1,1}$ are the i.i.d. complex normal random numbers generated on the four vertex of one grid, the complex normal number $Y_{x,y}$ at position (x, y) can be interpolated as equation (x.1):

$$Y_{(x,y)} = \sqrt{1 - y/d_{corr}}(\sqrt{1 - x/d_{corr}}Y_{0,0} + \sqrt{x/d_{corr}}Y_{1,0}) + \sqrt{y/d_{corr}}(\sqrt{1 - x/d_{corr}}Y_{0,1} + \sqrt{x/d_{corr}}Y_{1,1}) \quad (x.1)$$

One uniform random number can be generated using the phase of the interpolated complex normal random number as equation (x.2):

$$X_n = |\text{angle}(Y_{(x,y)})/\pi| \quad (\text{x.2})$$

where $|\cdot|$ operation ensures there is no abrupt change of the interpolated random number X_n between 0 and 1 along a trajectory. This will be desired when the uniform random number is used to generate cluster specific random delay in step 5 because otherwise the delay of one cluster could change between infinity to zero along a trajectory.

The spatially consistent normal distributed random variable can be generated by dropping normal distributed random variables on the vertex of one grid and interpolated among the random variables.

The cluster specific random variables should be applied to one cluster before clusters are sorted based on its random delay.

This method can be extended to additional dimensions, e.g. temporal/frequency, to generate spatial/temporal/frequency consistent random numbers.

2) Spatially consistent LOS/NLOS state

Variation 1: The spatially consistent LOS/NLOS state can be generated by comparing a spatially consistent uniform distributed random number with the LOS probability at a given position. Soft LOS/NLOS state can be generated by filtering the binary LOS/NLOS state over space. Figure 16 gives one example of generating the soft LOS/NLOS state and its effect. The soft LOS/NLOS state at a given position is calculated using the average of nine binary LOS/NLOS states at nine positions on the square centred by the position of interests. The middle plot depicts the spatially consistent binary LOS/NLOS state with 50 meter de-correlation distance. The right plot depicts the spatially consistent soft LOS/NLOS state with 50 meter de-correlation distance and 1 meter transition distance.

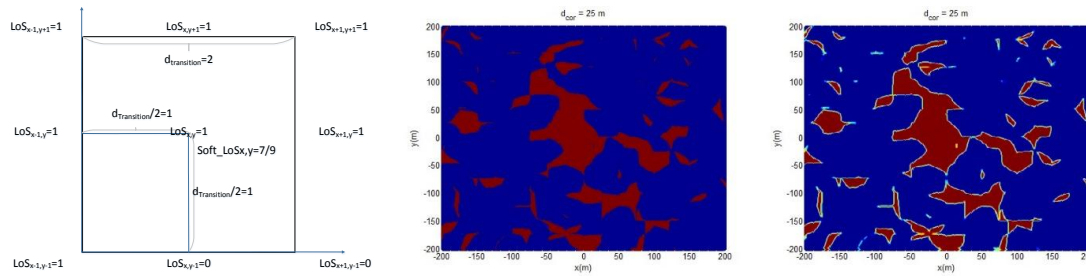


Figure 16 Example of generating one soft LOS/NLOS state.

Variation 2: In this variation, a spatially consistent Gaussian number G with autocorrelation distance d_{LOS} is generated. This is combined with a threshold value F determined via

$$F(d) = \sqrt{2} \text{erf}^{-1}(2P_{LOS}(d) - 1)$$

Here d is the distance and $P_{LOS}(d)$ is the LOS probability function. The soft LOS state is determined by a function approximating knife-edge diffraction:

$$LOS_{soft} = \frac{1}{2} + \frac{1}{\pi} \arctan \left(\sqrt{\frac{d_{LOS}}{\lambda}} (G + F) \right)$$

An examples of the soft LOS/NLOS state using this method is given in Figure 17. Note that the transition becomes more rapid with increasing frequency and that the transition will behave similarly as in some of the reported blocking measurements in the Annex.

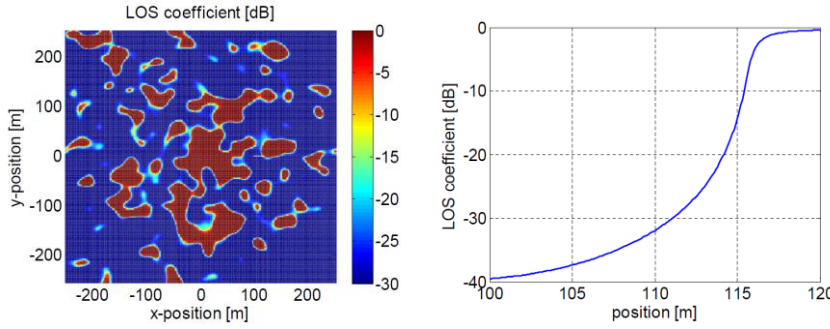


Figure 17 Example of spatially consistent soft LOS state using second variant (left) and a transition from NLOS to LOS (right)

3) Spatially consistent indoor/outdoor state

Spatially consistent indoor/outdoor state can be generated by comparing a spatially consistent uniform distributed random number with the indoor/outdoor probability at a given position. Similarly as soft LOS/NLOS state, soft indoor/outdoor state can be introduced by filtering binary indoor/outdoor state over space. Alternatively, transitions between the outdoor and indoor states can be avoided through modifications of the mobility model if this would be more desirable.

4) Spatially consistent path loss

Based on the soft LOS/NLOS and soft indoor/outdoor states, spatially consistent path loss can be defined using the soft LOS/NLOS and indoor/outdoor states as equation (x.3).

$$PL(LOS_{soft}, INDOOR_{soft}) = PL_{LOS} * LOS_{soft} + PL_{NLOS} * (1 - LOS_{soft}) + INDOOR_{soft} * PenerationLoss \quad (x.3)$$

Since penetration loss is a function of indoor distance, we can make penetration loss to be spatially consistent to have spatially consistent path loss for indoor state.

5) Spatially consistent fast fading channels

Based on the soft LOS/NLOS and indoor/outdoor states, the spatially consistent fast fading channel matrix can be generated using equation (x.4).

$$H(LOS_{soft}, INDOOR_{soft}) = \sqrt{1 - INDOOR_{soft}} (H_{outdoor_LOS} * \sqrt{LOS_{soft}} + H_{outdoor_NLOS} * \sqrt{1 - LOS_{soft}}) + \sqrt{INDOOR_{soft}} * H_{Indoor} \quad (x.4)$$

To summarize, this method can be implemented with a similar complexity as the spatially consistent large-scale parameters which are already a part of most drop-based models such as [3GPP TR36.873]. Smooth variations of angles and delays will be induced, although these will not fully resemble variations seen in measurements. Instead, they will tend to be a bit too smooth and synthetic, and the rate of variations can sometimes be unphysically high, This method will maintain the channel statistics which is a very desirable characteristic.

5.3.2 Geometric Stochastic Approach

Spatial consistency means that channel realizations including large-scale parameters (LSPs) and small-scale parameters (SSPs) would need to vary in a continuous and realistic manner as a function of position in geometry. Two features of spatial consistency are important. Firstly, user equipments (UEs) sharing similar locations should have correlated LSPs, and the LSPs should be crucially dependent on UE's position instead of random allocation in each drop as done in 3GPP SCM. Moreover, the path loss including shadow fading should vary smoothly as UE moves in geometry, even in a drop duration. This is particularly important to the evaluation of multiuser MIMO or multiuser beam-forming techniques. Secondly, SSPs in a drop (e.g. angle, power, and delay) should be dynamically changing with position. More accurately, the new model realizes time-variant angles and cluster death and birth as UE is moving which is important to evaluate mobility and beam tracking for 5G communications.

Geometry stochastic approach for spatial consistency might be the suitable solution to extend 3GPP SCM with small changes in sense of backward compatibility. The modified procedures for the new model based on 3GPP SCM [1] is summarized as follows.

- 3GPP SCM step 1 and 2: Pre-compute the LSPs for each grid, grid shape can be rectangular with side length of spatial consistent distance. See item-C.
- 3GPP SCM step 3 and 4: Every UE takes the LSPs of the grid that the UE locates. See item-C. Calculate the path loss based on UE's position. See item-A and item-B.
- 3GPP SCM step 5: Add the decision of cluster birth and death. If yes, take the procedure of cluster birth and death in item-E.
- 3GPP SCM step 11: Update the angles based on item-D at the beginning of the step.

A. Geometry position

Geometry positions of UE, scatters, and BS are the fundamental information of SCM, and are fixed in a drop. Actually the position of UE is time variant as UE is moving. Suppose the moving speed of UE is v and moving direction is ϕ_v in global coordination system (GCS), the position of UE at time t is given by

$$X_{UE}(t) = \begin{pmatrix} d(t_0) \sin(\theta_{z0D}) \cos(\phi_{AoD}) + v(t-t_0) \cos(\phi_v) \\ d(t_0) \sin(\theta_{z0D}) \sin(\phi_{AoD}) + v(t-t_0) \sin(\phi_v) \\ h_{UE} \end{pmatrix},$$

where $d(t_0)$ is the distance between BS and UE at previous time t_0 . Notice that the time interval $t-t_0$ can be a sub-frame duration as used in 3GPP.

B. Time-variant Path loss

The path loss is crucially depending on the position of UE or distance between BS and UE. Since BS's position is fixed at $X_{BS} = (0, 0, h_{BS})^T$, the distance between BS and UE at time t is

$$d(t) = |X_{BS} - X_{UE}(t)|.$$

With the path loss model for above 6 GHz or 3GPP path model for sub-6GHz, the path loss at time t can be updated accordingly. The correlated shadow fading in different positions are discussed in section 7.2.1 in 3GPP TR 36.873. The correlated shadow fading is given by

$$F(d) = \alpha.F_1 + \sqrt{1-\alpha^2}.F_2,$$

where $\alpha = \exp(-d/d_{cor})$, d_{cor} is the correlation distance of shadow fading, F_1 and F_2 are the shadow fading allocated in two neighboring grids.

C. Position-based Large-scale Parameters (LSPs)

3GPP SCM allocate LSPs randomly for each UE. Two UEs may have much different LSPs although they are close in locations. The fact is the LSPs of the two UEs should be similar which leads to channel impulse response with high correlation. In order to circulate the problem, we divide each cell under a BS's coverage into multiple grids. Each grid is spatial consistent in sense of large-scale fading characteristics. Each grid is configured with a set of LSPs following the given probability density function defined in 3GPP SCM. Grid centre is assumed as the location in calculating LSPs. In the step to generate the LSPs for a UE channel, it firstly checks which grid the UE locates, and then take the LSPs of the corresponding grid to the UE channel. In this way, UE sharing the same grid will have the same LSPs.

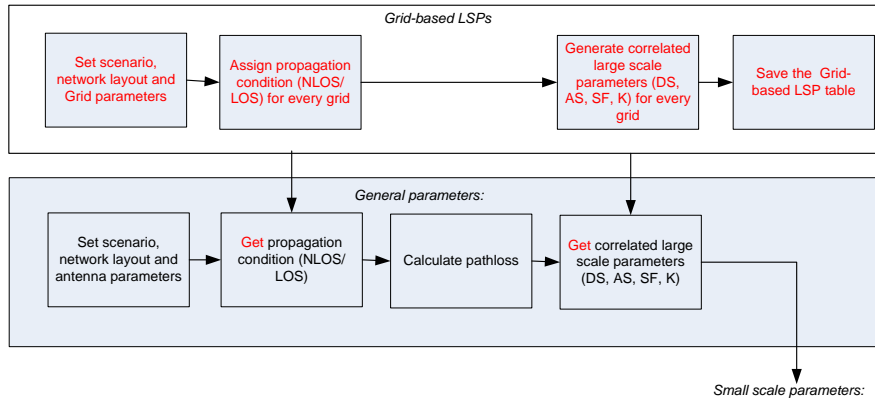


Fig. 1 LSPs generation procedure

Fig. 1 illustrates the procedure to generate LSPs where red texts are the new steps based on 3GPP TR 36.873. Notice that the grid-based LSPs are calculated only once and are saved as a table. Most LSPs of UEs are taken from the table. Thus, the computational complexity of LSPs is lower than 3GPP SCM.

D. Time-variant Angle

Variant angles are introduced for each ray including azimuth angle of departure and arrival (AoD, AoA) and zenith angle of departure and arrival (ZoD, ZoA) in [Wang2015]. Since UE's position at time t is available, the angles can be updated with transmitter and receiver information in the global coordination system (GCS). Linear approximation is an efficient way to reduce complexity with acceptable errors. The linear method for variant angles are generally formulated as [Wang 2015]

$$\theta_{n,m,Angle}(t) = \theta_{n,m,Angle}(t_0) + S_{n,m,Angle}(t - t_0),$$

where the sub-index ‘‘Angle’’ represents AoA, AoD, ZoA, or ZoD in SCM. $S_{n,m,Angle}$ is the slope which describes the changing ratio of time-varying angles. For LOS cluster, the expression of AoD and ZoD slopes are given by [Wang2015]

$$S_{ZOD} = -S_{ZOA} = \frac{v \cos(\phi_v - \phi_{AOD}(t_0))}{(h_{BS} - h_{UE}) / \cos(\theta_{ZOD}(t_0))}, \quad S_{AOD} = S_{AOA} = -\frac{v \sin(\phi_v - \phi_{AOD}(t_0))}{(h_{BS} - h_{UE}) \tan(\theta_{ZOD}(t_0))}.$$

For NLOS cluster with one reflection ray, the model can be simplified by introducing a virtual UE which is the mirror image of UE based on the reflection surface. The simplified slopes in NLOS channel are given by [Wang2015]

$$S_{ZOD} = -S_{ZOA} = -\frac{v \sin(\phi_v + \phi_{AOD}(t_0) - \phi_{RS})}{(h_{BS} - h_{UE}) / \cos(\theta_{ZOD}(t_0))}, \quad S_{AOD} = -S_{AOA} = -\frac{v \cos(\phi_v + \phi_{AOD}(t_0) - \phi_{RS})}{(h_{BS} - h_{UE}) \tan(\theta_{ZOD}(t_0))},$$

where ϕ_{RS} is the angle of the reflection surface and it can be deduced from the initial ϕ_{AOD} and ϕ_{AOA} .

E. Cluster Birth and Death

Cluster birth and death are assumed to happen at the same time in order to keep a fixed number clusters as defined in 3GPP SCM. Scatters are assumed to be independent with each other. In this sense, cluster birth and death can be modeled with Poisson process if looking the rate of cluster birth/death in time. Accurately, the cluster birth/death will happen at time t with the probability

$$\Pr(t) = 1 - \exp(-\lambda_c(t - t_0)),$$

where t_0 is the previous time that cluster birth/death happened. The model has single parameter λ_c which represents the average number of cluster birth/death per second, and hence is very simple in channel simulations. The single parameter λ_c is essentially depending on the number of birth/death in a spatial consistency distance and UE moving speed. For cluster death, the cluster selection can be based on the cluster power from weak to strong since weak cluster is easy to change [WINNER]. For cluster birth, new cluster can copy the cluster (power, delay, and angles) from nearest grid. The priority of cluster selection is based on the cluster power from weak to strong. When UE is moving to the neighboring grid, the clusters will be replaced by the new clusters of neighboring grid gradually and hence keep spatial consistency in sense cluster.

5.3.3 Method using geometric locations of clusters (Grid-based GSCM, GGSCM)

According to the drop concept of the conventional GSCMs (SCM, WINNER, IMT-Advanced, 3GPP 3D, etc.), the receivers (Rx’s) are located randomly and the propagation parameters are randomly

drawn from the pre-defined probability distributions. The channel is assumed to be stationary along a short distance (segment), but this assumption does not hold for longer distances, therefore the parameters need to be re-calculated (new drop/segment). This approach is called as block-stationary modelling in which large scale (LS) and small scale (SS) parameters are fixed during the segment and fully different between the segments. The transition from a segment to another provides a rapid change of channel model parameters thus the channel is discontinuous. To improve the reality and time evolution, it is possible to interpolate between the segments. However, it is difficult to ensure spatial consistency especially between nearby users in multi-user case. Therefore, a new method (partly based on [METIS_D1.2]) is proposed and drafted in the following.

In the method, called Grid-based GSCM (GGSCM), cluster and path angles and delays are translated into geometrical positions (x, y) of the corresponding scatterers, see Figure 18. The benefit is that the cluster and path evolution in delay and angle can be naturally traced and will have very realistic variations.

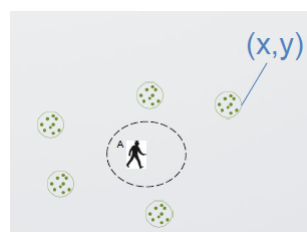


Figure 18 Clusters are translated into geometric positions

This method needs to be complemented with some birth/death process to maintain uniformity of clusters during movement. An example clarifies this discussion. Let us consider a case of three users: A, B, and C (Figure 19). Users A and C are far away from each other. They may assume independent clusters. However, the users A and B are located nearby. The current 3GPP-3D model assumes independent small scale parameters (SSPs), which lead to non-physical situation, and too optimistic MU-MIMO throughput evaluations. Figure 20 illustrates the thinking of spatially consistent case in which all or some of the clusters are shared between nearby users.



Figure 19. The problem of independent clusters of nearby users (current GSCM).

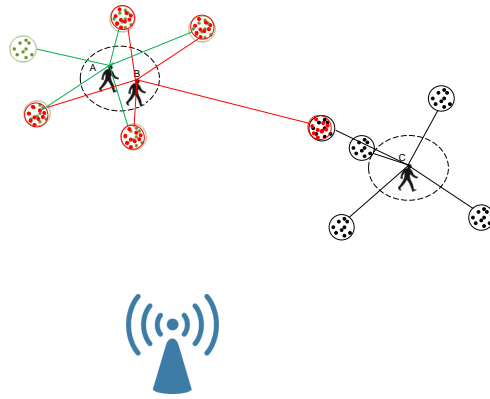


Figure 20. Shared clusters (necessary improvement).

Figure 21 depicts the situation in which a high number of users are “dropped” onto a 2-dimensional map. Each user has a ring around, and the radius of that ring is equal to the correlation distance (or stationarity interval). If another user is located inside that ring, the spatial consistency has to be taken into account. Otherwise, current method of random SSPs is acceptable.

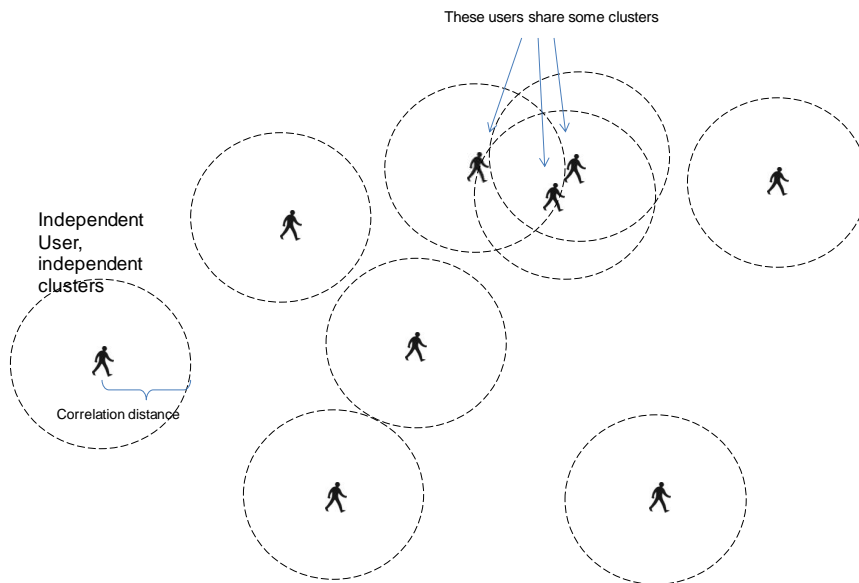


Figure 21. Dropping of users.

In the case of nearby users, the clusters should be interpolated between the users. User B takes the N strongest clusters (N is the number of clusters defined per scenario).



Figure 22. User centric selection of clusters.

The interpolation can be done along a route of based on a pre-defined “grid” (Grid based GSCM, GGSCM). In the GGSCM approach a discrete two-dimensional map of possible Rx locations is defined. Instead of drawing LSPs and SSPs for the actual user locations, the cluster parameters are drawn for every grid point. Then the cluster parameters for the actual Rx locations are interpolated between four nearest grid points. The grid can be intuitively understood as a drop in which the distance between two adjacent users is constant in x and y dimensions. The drops are independent between the GPs, i.e., LSPs and SSPs are randomly drawn from the pre-defined distributions (similar to the legacy GSCM).

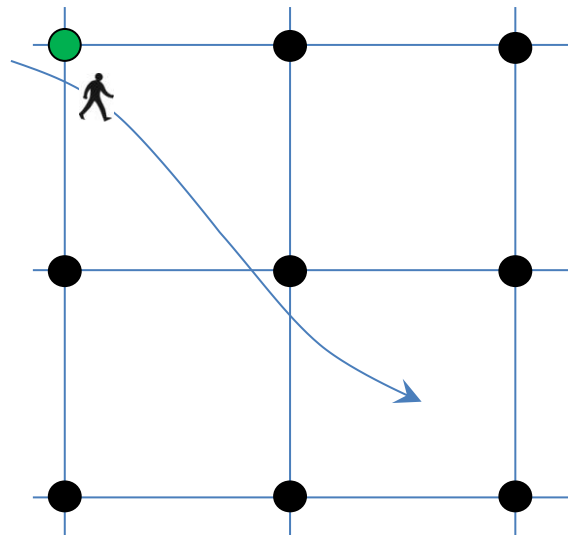


Figure 23. Grid model (GGSCM): Calculate new cluster information at each grid point. Interpolate clusters between the four grid points.

The locations of the clusters have to be defined in (x, y) or (x, y, z) coordinates. The maximum distance between Rx (or Tx) and the cluster location is determined from the geometry of Rx and Tx locations, AoA, AoD, and delay. This geometry is an ellipse with focal points at Rx and Tx locations, and the major axis equals to the delay multiplied by the speed of light. In the case of single bounce,

the cluster is located on the locus of an ellipse defined by AoA, AoD, and delay τ (see Figure 24, SBC, single bounce cluster). In the case of multi-bounce, the same locus defines upper bound of the distance of the cluster, i.e. the cluster can be anywhere in the segment between Tx (or Rx) and the locus (see Figure 24, FBC/LBC, first/last bounce cluster). A distribution for that cluster location could be uniform between the two ends of said segment. Because the AoA, AoD, and delay are randomly drawn in the GSCM, most likely the geometry of these three parameters does not fit to the ellipse. Thus the 50% of the cluster locations may be based on Rx-side cluster parameters and another 50% based on Tx-side cluster parameters.

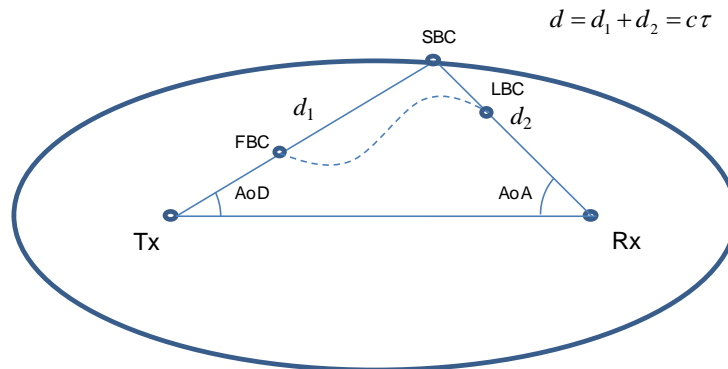


Figure 24. Location of a cluster.

After fixing the physical locations, drifting of LSPs and SSPs are enabled for a short distance movement as illustrated in Figure 25. Implementation of the drifting is straightforward and is fully based on the geometry (for each impulse response, phase, delay, and angle of arrival is recalculated). This supports dynamic channels and simulation of very large arrays.

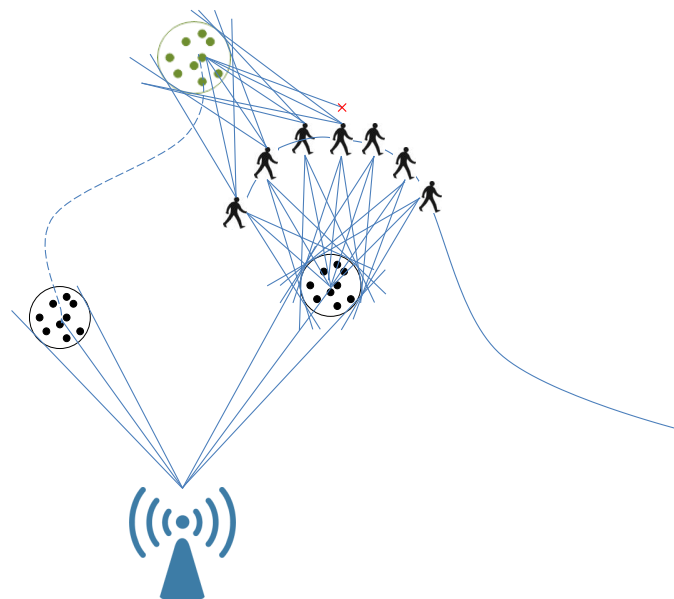


Figure 25. Drifting of angles and delays.

This approach allows also spatially consistent LOS (and specular reflection). Since the Tx, Rx and scatterers have physical coordinates, also a simple map for LOS (and specular reflection) can be created.

The clusters may be calculated only for the grid points and on the need basis to avoid excessive use of memory. A smooth birth-death process of clusters can be realized by weighting the cluster powers in each grid point based on the distance from Rx. All clusters of the four closest grid points are active and the clusters are selected by cutting the weakest clusters away. If the number of a cluster in the scenario of interest is $N = 20$, the total number of clusters in any position between the grid points is $4*N = 80$, but only 20 strongest clusters are selected. The strength of the cluster is scaled by a path loss from the cluster location to the Rx. This approach keeps the number of clusters constant, and allows smooth birth-death process.

5.4 Support for large arrays

Due to the high path loss for the high frequency bands and the stringent 5G performance requirements, many systems will make use of large antenna arrays (beamforming and/or Massive-MIMO) to assure a suitable link budget. Massive MIMO systems will also employ a high number of antenna elements, that will extend over many wavelengths in space. The channel model should support systems using large antenna arrays.

The traditional GSCM model (and also the 3GPP 3D model) assumes the same propagation conditions (plane wave, angle of arrival) for all the individual antenna elements in an array. However this approximation becomes inaccurate when the number of antenna elements is large and may cover an area of many wavelengths.

While the far field criterion is often seen as guaranteeing plane waves, unfortunately this is not always true for large antenna arrays. Spherical waves may need to be taken into account for larger distances and for the short ranges expected for the millimetre wave communications links.

The phase error from the centre of the antenna array to the most distant antenna element can be easily calculated from the geometry. With values $1\lambda < D < 10\lambda$, the error is within $22.0^\circ \dots 22.5^\circ$. For beam forming and interference cancellation, the modelling error should be less than, say $\ll 5^\circ$. Therefore, the plane wave assumption is true only if the distance is larger than $4d$ (to be on the safe side, $8d$ is recommended). The far field distance d for a massive MIMO antenna for the millimetre wave frequencies of interest would normally be between 5 to 10 meters, implying that the minimum antenna to cluster distance to safely utilize planar wavefront modelling would be in the range 40 to 80 meters, which is beyond the deployment scenarios many cases. As a consequence, spherical wave modelling may become important for 5G channel modelling with very large array manifolds.

The 3GPP 3D model assumes a Laplacian power angular spectrum (PAS) may be adequately modelled by 20 equal amplitude sinusoids. This approximation may be sufficient for small arrays. However, large arrays require accurate angular resolution, otherwise they will see each sinusoid as a separate specular wave, which is non-physical. This problem was studied in the contribution [Anite Telecoms 2014] and in the reference [W. Fan 2015].

In the 3GPP 3D channel model, the pairing between azimuth and elevation angles is done randomly, i.e. each azimuth angle is randomly paired with an elevation angle, and the total number of sub-rays is still 20. Different realizations provide different pairing of elevation and azimuth angles. Figure 26

shows an example of random pairing. The projection to azimuth or elevation plane provides the Laplacian shape, but the projections to other planes do not necessarily correspond. This causes a correlation error in the order of 0.11 ... 0.15 (absolute values) [Anite Telecoms 2014].

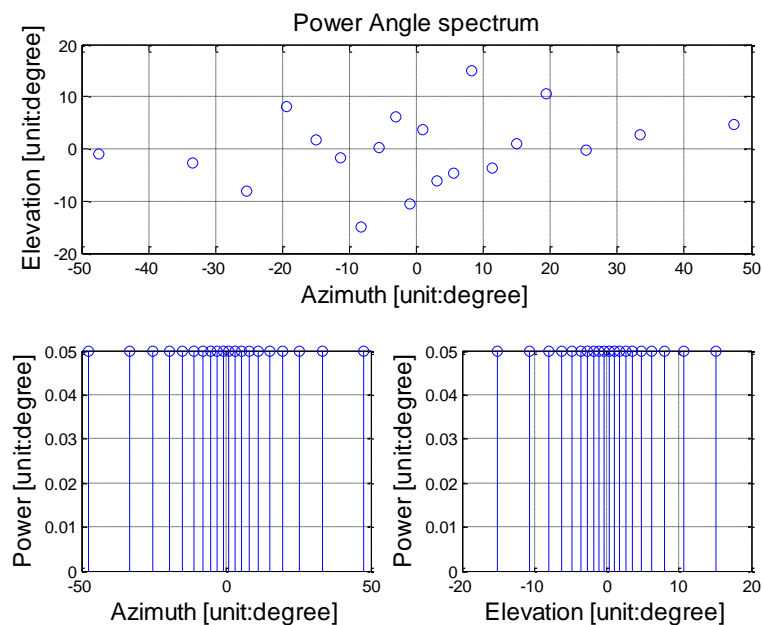


Figure 26 Random pairing of azimuth and elevation angles.

In addition to the spherical wave effect and other alignment problems, very large arrays may see different propagation effects between the different elements of the array. While the minimum size of an extremely large array is not well defined, one may say that an array becomes “large” when it is larger than the consistency interval (or stationarity interval or correlation distance). The correlation distance of large scale parameters varies significantly depending on the details of the environment. For example, in WINNER II it varies from 0.5 to 120 m. Within these distances, all small scale parameters such as angle of arrival, delay, Doppler, polarization, may be different across the array. Also large scale parameters such as shadowing may affect only a sub-set of antenna elements in the array. This is also likely the case with distributed antennas and cooperative networks. The existing 3GPP 3D channel model assumes the same propagation effects across the entire antenna array. This may not be the case for many of the future deployment scenarios.

5.5 Dual mobility support

Dual mobility in the D2D and V2V scenarios causes different Doppler models, different spatial correlation of large-scale and small-scale parameters than in the conventional cellular case. The conventional cellular models presume at least one end of the radio link is fixed (usually the base station). The corresponding Doppler spectrum and characteristic fast fading distribution have not been extensively modelled. To allow modelling for D2D and V2V 5G scenarios, in which both ends of the link may be in motion and experience independent fading, Doppler shift and channel conditions further additions to the channel models are required to accommodate these parameters.

5.6 Dynamic blockage modelling

The dynamic blockage could be modelled as additional shadow fading on certain channel directions. Assuming the distance between the blocker and transmitter is much farther away than the

distance between the blocker and receiver, the blocking effect can be applied to channel receiving directions for simplicity. An example of two blockers is illustrated in Figure 27. Assume the position of receiver is in the origin, we can describe one blocker in Cartesian/polar coordinate system using below parameters:

- 1) Centre of the blocker (φ, θ, r) , where φ, θ, r represent the azimuth angle, zenith angle, and radius of the centre of the blocker
- 2) Azimuth angular span of the blocker (AoA span) $A \approx w/r$, where w is the width of the assumed rectangular blocking surface
- 3) Zenith angular span of the block (ZoA span) $Z \approx h/r$, where h is the height of the assumed rectangular blocking surface

Assume the AoA/ZoA of one channel cluster is (φ_n, θ_n) . The blockage effect for this cluster is modelled if the $|\varphi_n - \varphi| < A$ and $|\theta_n - \theta| < Z$, and the blockage effect of one edge of the blocker is modelled using a knife edge diffraction model for the four edges of the blocker as (1) in Cartesian coordinate system or (2-1) and (2-2) in polar coordinate system:

$$F_{h_1|h_2|w_1|w_2} = \frac{\text{atan}\left(\pm\frac{\pi}{2}\sqrt{\frac{\pi}{\lambda}\left((D_{1h_1|h_2|w_1|w_2}-r_1)+(D_{2h_1|h_2|w_1|w_2}-r_2)\right)}\right)}{\pi} \quad (1)$$

where $D_{1h_1|h_2|w_1|w_2}$ and $D_{2h_1|h_2|w_1|w_2}$ are the distance from transmitter/receiver to the four edges of the blocker, r_1 and r_2 are the perpendicular distance from transmitter/receiver to the blocking surface.

$$F_{h_1|h_2|w_1|w_2} \approx \frac{\text{atan}\left(\pm\frac{\pi}{2}\sqrt{\frac{\pi}{\lambda}r(1-\cos(\varphi_1|\varphi_2|\theta_1|\theta_2))}\right)}{\pi} \quad (2-1)$$

where h_1, h_2, w_1, w_2 represent the four edges of the blocker; the plus sign is used for shadow zone and minus sign is used for LOS zone; and:

$$\begin{cases} \varphi_1 = \frac{A}{2} - (\varphi_n - \varphi) \\ \varphi_2 = \frac{A}{2} + (\varphi_n - \varphi) \\ \theta_1 = \frac{Z}{2} - (\theta_n - \theta) \\ \theta_2 = \frac{Z}{2} + (\theta_n - \theta) \end{cases} \quad (2-2)$$

Be noted that if the distance from the transmitter to the blocker is much larger than the blocker size, (1) will result in similar blockage effect as (2-1) and (2-2).

Finally, the additional shadowing loss of one blocker applied to this cluster is:

$$L_{dB} = -20\log_{10}\left(1 - (F_{h_1} + F_{h_2})(F_{w_1} + F_{w_2})\right) \quad (3)$$

And if one channel cluster is blocked by multiple blockers, the additional shadowing by multiple blockers are summed up. To summarize we have below proposals for blockage model:

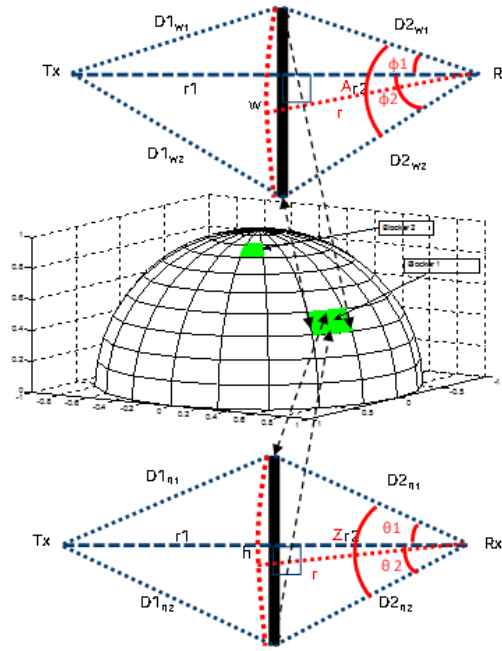


Figure 27, Example of a blocker modelling in the polar coordinated system

For single link simulation, we can define blocker trajectory, size and distance based on experiences either in Cartesian coordinate or polar coordinate systems. And the blocker size/distance is deterministic in the simulations.

For full system level simulation, we can fix the blocker distance and randomly generate the azimuth centre of the blocker using two uniformly distributed random variables $u_1, u_2 \sim U(0,1)$, and the centre of the blocker $(\varphi, \theta, r) = (2\pi u_1, \frac{\pi}{2} - \frac{\pi u_2}{4}, 2)$. The random variables u_1 can be generated with spatial/temporal consistency according to section 5.3.1 with correlation distance d_{corr} and correlation time t_{corr} to model the blocker movement around the receiver in the azimuth dimension. For example, $d_{corr} = 50\text{m}$ and $t_{corr} = \frac{\pi}{2} r/v$. For random variable u_2 , it can be generated per drop with spatial consistency. Thus the blocker does not move in the zenith dimension but two near-by receivers still observe correlated blockage effect. Table 2 gives some configuration examples for the blocker. The moving speed in system level is the mean moving speed of the blocker. The instantaneous moving speed around a particular receiver is statistically distributed.

For multiple blockers, each blocker can be configured with one blocker specific parameter sets.

Table 2 Typical configuration of blocker

	Typical set of screens	Screen dimensions
Indoor;	Human	Cartesian: $w=0.3\text{m}; h=1.7\text{m}; r = 2\text{m}; v=3\text{km/h}$
Outdoor		Polar: $A=0.15\text{rad}; Z = 0.85\text{rad}; r = 2\text{m};$

		$v_p=0.42\text{rad/s}$; $t_{\text{corr}}=3.77\text{s}$; $d_{\text{corr}}=50\text{m}$ (outdoor); $d_{\text{corr}}=5\text{m}$ (indoor)
Outdoor	Vehicle	Cartesian: $w=4.8\text{m}$; $h=1.4\text{m}$; $r = 10\text{m}$; $v = 30\text{km/h}$ Polar: $A=0.48\text{rad}$; $Z = 0.14\text{rad}$; $r = 10\text{m}$; $v_p=0.83\text{rad/s}$; $t_{\text{corr}}=1.88\text{s}$; $d_{\text{corr}}=50\text{m}$

In Figure 28, this model is compared to measurement results for blocking by a passing garbage truck. The truck has been modelled by two rectangular screens with sizes according to the sizes of the drivers compartment and container, and the trajectory to the screens has been matched to the trajectory of the truck. The only fitted model parameters are the speed of the truck (25 km/h) and the K-factor in the channel (9 dB). As can be seen, the model reproduces the measured signal strength drops and transitions exceptionally well.

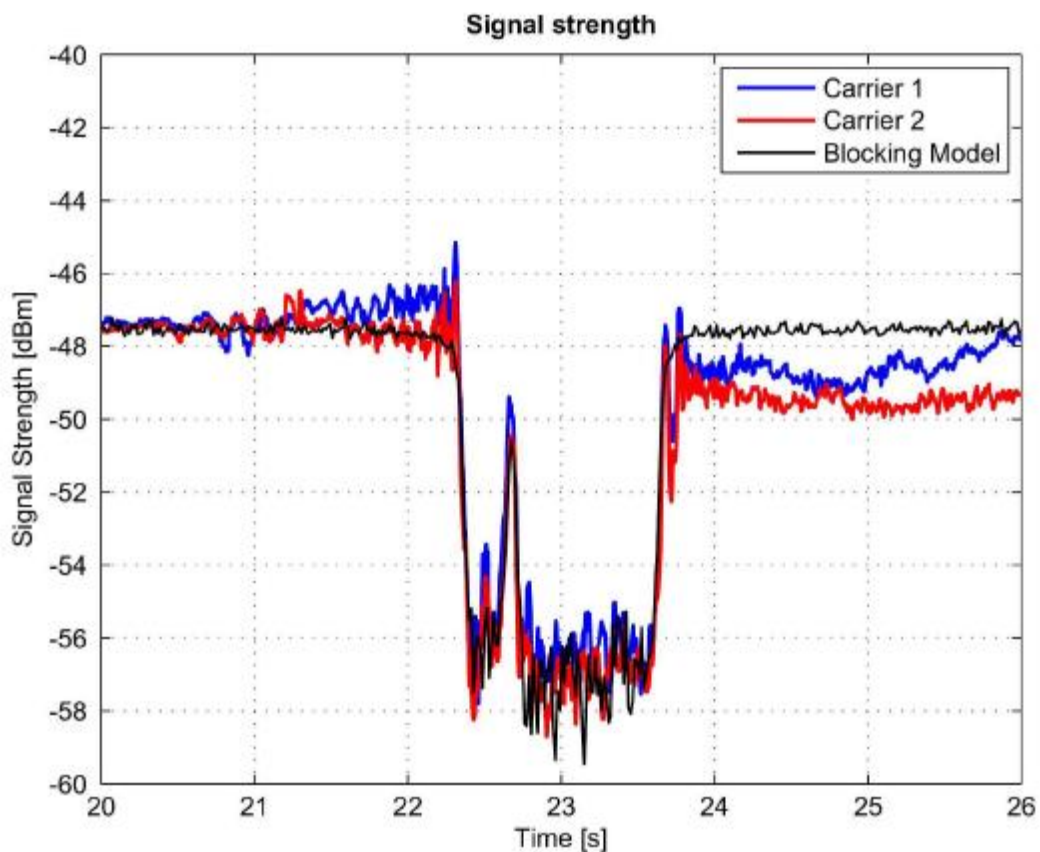


Figure 28 Comparison between the proposed blocking model and measurements [Ökvist 2016]

5.7 Foliage loss

Measurements and modelling of foliage loss at higher frequencies can be found in [Schwering 1988],[Chavero 1999],[Rappaport ICC 2015],[ITU-R P.833]. The loss increases with frequency and

penetration depth through the foliage. Modelling approaches such as [ITU-R P.833] can also account for contributions from diffracted, ground-reflected and scattered waves. It is important not to account for such losses twice in the channel model. In a stochastic path loss model the model is parameterized using measurements in the scenarios of interest. In the UMa and UMi case this will include path loss measurements in urban areas which often include trees and other vegetation. Thus, in a stochastic path loss model the effect of the foliage is already included. It is therefore unnecessary to add an explicit foliage loss model.

5.8 Atmospheric losses

In the UMa and UMi scenarios, the link distances could potentially be up to hundreds of meters and interference may need to be modelled from transmitters that are up to a few kilometres distant. The path loss model as a function of frequency will be a key component of the channel model. It is known that atmospheric losses can become significant at higher frequencies and longer ranges. Figure 29 illustrates the measured atmospheric effects for normal and dry air compiled for the ITU. These are expressed in terms of dB/km of path length. It can be seen that for the mmWave bands below about 100 GHz, the attenuation is dominated by the oxygen absorption peak at about 60 GHz. This peak is about 15 dB/km or about 0.015 dB/metre. For the other frequencies below 100 GHz, the absorption is about ten times less (or 0.001 dB/metre). In dry air the loss is much lower. For distances of tens of meters in the InH and UMi these losses are not significant compared to other effects of the environment (e.g. clutter and buildings). For 100+ metre ranges in the UMa scenario the 1.5 dB loss is of small consequence compared to other effects.

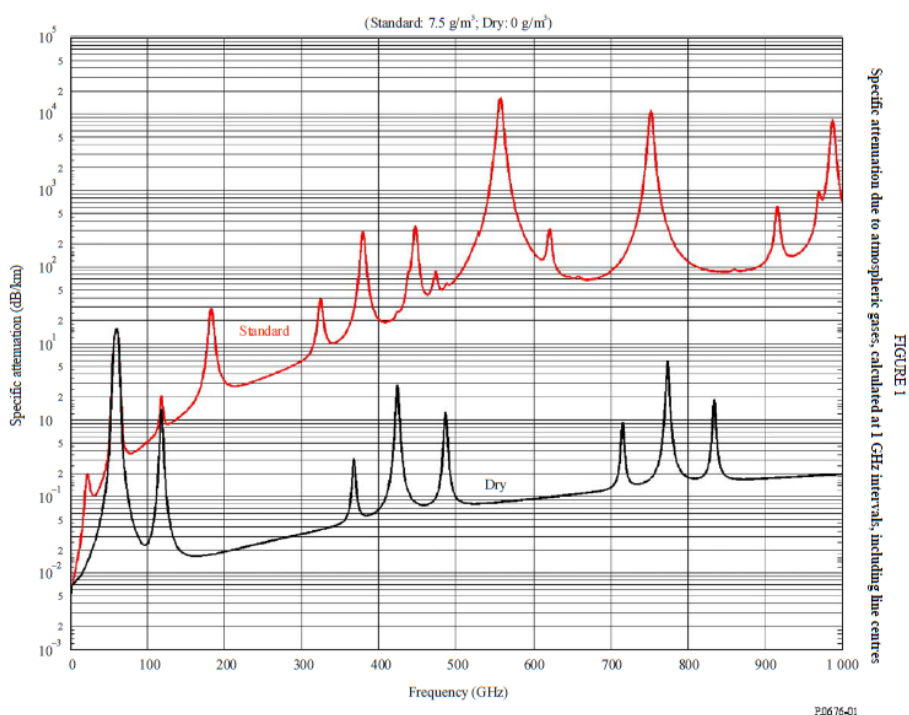


Figure 29 Attenuation by atmospheric gases in the 0-1000 GHz range. Source: Rec ITU-R P.676-9 (02/2012) Attenuation by atmospheric gases

Figure 30 illustrates the measured rain attenuation for various rain-rates compiled for the ITU. These are expressed in terms of dB/km of path length. Rainfall is not a consideration in the InH scenario

(indoors). For the outdoor scenarios, at 100 metre path lengths, the rainfall would cause less than 0.4, 0.8 or 2.0 dB loss for signals close to 100 GHz [Rappaport 2015]. As the average rain-rate is less than the peak, the average loss would be somewhat less and also less for lower frequencies. In periods of heavy rain the path loss may also be accompanied by scattering from the raindrops.

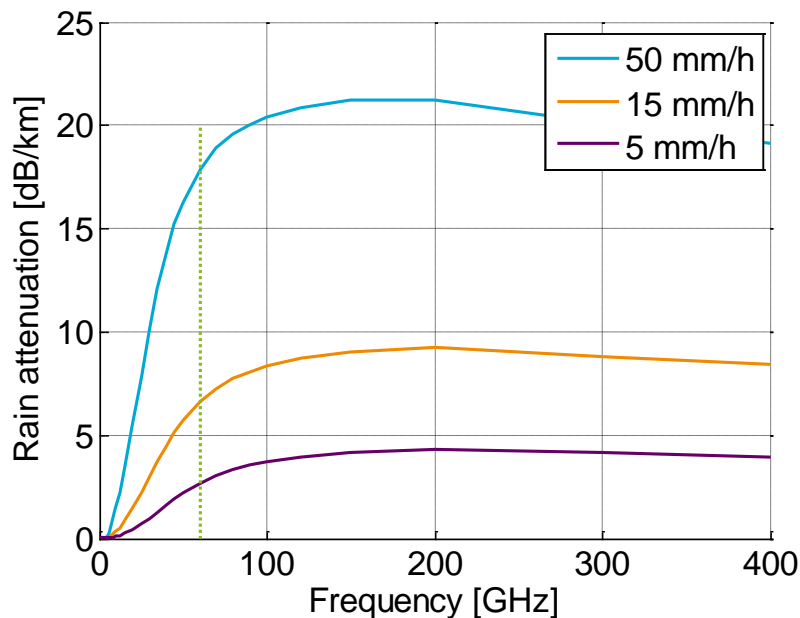


Figure 30 Rain attenuation for different rain intensities. Source: Rec ITU-R P.838-2 Specific attenuation model for rain for use in prediction methods

Overall, in most InH, UMi and UMa scenarios the effects of atmospheric loss and rainfall will be insignificant compared to other factors of the environmental. For scenario deployments in the 100 metre range they may be worthwhile taking into account.

Since the attenuation due to water vapour will be insignificant for the typical link distances in the considered scenarios it doesn't seem necessary to model water vapour attenuation. While rain attenuation could become significant for longer link distances and at higher frequencies, it will be very rare with rain heavy enough to impact the shorter link distances that will be applicable in the agreed scenarios. In typical 3GPP RAN1 simulations the time variability of the link quality is not modelled, unlike the ITU sharing and coexistence studies where worst case interference conditions have a higher importance. Therefore modelling of rain attenuation may be optional and only applied to sharing and coexistence studies.

Oxygen absorption may become significant around the 60 GHz peak as shown in Figure 29. The effect on the path loss can easily be accounted for using known models such as given by Rec ITU-R P.676 [ITU-R P.676]. However, there is a secondary effect that may result in noticeable reductions of delay and angular spread. This reduction is caused by the multipath components having longer path length than the direct path and will suffer a slightly greater oxygen absorption. In order to have a joint model parameterization over the full frequency range at longer ranges, it is proposed that measurements of e.g. channel impulse responses are compensated for the oxygen absorption loss at different delays. An example of the path loss and delay spread results before and after such compensation is shown in [R1-160846]. By this procedure it is possible to characterize the

frequency-dependence of the channel dispersion without the notch-like effect near the oxygen peak disrupting any smoother trends. This process means that the oxygen loss should be applied in a separate modelling step. This can be done by attenuating each cluster (path) in the generated channel impulse response by a loss $\alpha \cdot c \cdot \tau_n$ [dB] where α [dB/m] is the oxygen loss, c [m/s] is the speed of light, and τ_n [s] is the cluster (path) delay.

6 Pathloss, Shadow Fading, LOS and Blockage Modelling

6.1 LOS probability

The definition of LOS used in this white paper is discussed in this sub-section together with other LOS models. The LOS state is here determined by a map-based approach, i.e., by considering the transmitter (AP) and receiver (UE) positions and whether any buildings or walls are blocking the direct path between the AP and the UE. The impact of objects not represented in the map such as trees, cars, furniture, etc. is modelled separately using shadowing/blocking terms. An attractive feature of this LOS definition is that it is frequency independent, as only buildings and walls are considered in the definition.

The first LOS probability model considered, the d_1/d_2 model, is the current 3GPP/ITU model [3GPP TR36.873] [ITU M.2135-1]:

$$p(d) = \min\left(\frac{d_1}{d}, 1\right) \left(1 - e^{-d/d_2}\right) + e^{-d/d_2}, \quad (1)$$

where d is the 2D distance in meters and d_1 and d_2 can both be optimized to fit a set of data (or scenario parameters).

The next LOS probability model considered, the NYU (squared) model, is the one developed by NYU in [Samimi 2015]:

$$p(d) = \left(\min\left(\frac{d_1}{d}, 1\right) \left(1 - e^{-d/d_2}\right) + e^{-d/d_2} \right)^2, \quad (2)$$

where again d_1 and d_2 can be optimized to fit a given set of data (or scenario parameters).

An investigation into the LOS probability for the UMa environment was conducted using all of the UMa measured and ray-tracing data listed in the appendix. In addition to comparing the two models considered above with optimized d_1 and d_2 values, the data was also compared to the current 3GPP UMa LOS probability model (eqn (1)) for a UE height of 1.5 m with $d_1=18$ and $d_2=63$. A summary of the results is given in Table 3 and the three models are compared to the data in Figure 31. In terms of mean squared error (MSE) between the LOS probability from the data and the models, the NYU (squared) model had the lowest MSE, but the difference was small. It is worth noting, however, that the NYU (squared) model is conservative, as it predicts zero likelihood of LOS at closer distances than the other models. Given that the current 3GPP UMa model was a reasonable match to the data and included support for 3D placement of UEs, it is recommended that the current 3GPP LOS probability model for UMa be used for frequencies above 6.0 GHz. The 3GPP UMa model specifically is [3GPP TR36.873]:

$$p(d) = \left(\min\left(\frac{18}{d}, 1\right) \left(1 - e^{-d/63}\right) + e^{-d/63} \right) (1 + C(d, h_{UT})), \quad (3)$$

where h_{UT} is the height of the UE in m and:

$$C(d, h_{UT}) = \begin{cases} 0, & h_{UT} < 13m \\ \left(\frac{h_{UT}-13}{10}\right)^{1.5} g(d), & 13 \leq h_{UT} \leq 23m \end{cases} \quad (4)$$

$$g(d) = \begin{cases} (1.25e^{-6})d^2 \exp(-d/150), & d > 18m, \\ 0, & \text{otherwise} \end{cases} \quad (5)$$

Note that for indoor users d is replaced by the 2D distance to the outer wall.

Table 3. Comparison of the LOS probability models for the UMa environment

	d1	d2	MSE
3GPP UMa	18	63	0.020
d1/d2 model	20	66	0.017
NYU (squared)	20	160	0.015

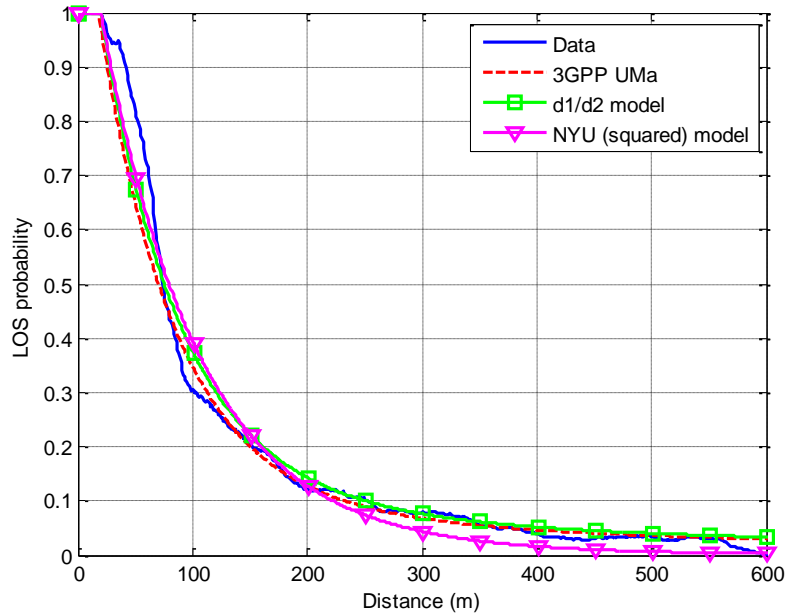


Figure 31. UMa LOS probability for the three models considered.

For the UMi scenario, it was found that the 3GPP LOS probability formula [3GPP TR36.873] is sufficient for frequencies above 6 GHz. The fitted d1/d2 model in (1) provides a better fitted model, however, the errors between the data and the 3GPP LOS probability model over all distances are

small. That formula is the same as (1) with $d_1=18$ m and $d_2=36$ m with d being replaced by the 2D distance to the outer wall for indoor users. Note that the 3GPP UMi LOS probability model is not a function of UE height like the UMa LOS probability model.

Table 4. Comparison of the LOS probability models for the UMi environment

	d1	d2	MSE
3GPP UMi	18	36	0.023
d1/d2 model	20	39	0.001
NYU (squared)	22	100	0.026

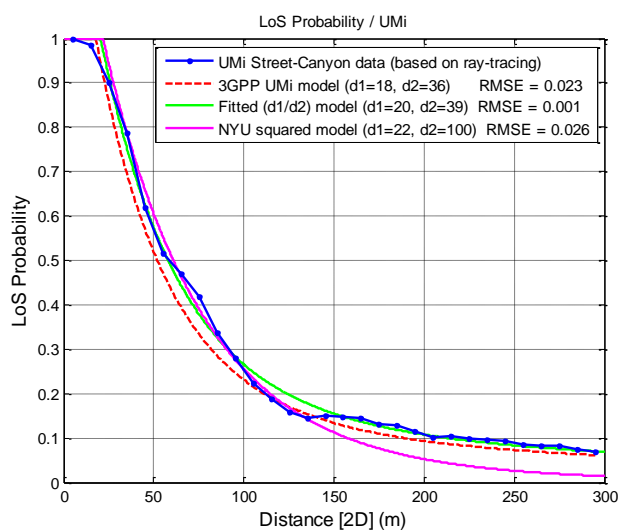


Figure 32. UMi LOS probability for the three models considered.

Since the 3GPP 3D model [3GPP TR36.873] does not include an indoor scenario, and the indoor hotspot scenario in e.g. the IMT advanced model [ITU M.2135-1] differs from the office scenario considered in this white paper, an investigation on the LOS probability for indoor office has been conducted based on ray-tracing simulation, e.g., [Jarvelainen 2016]. Different styles of indoor office environment were investigated, including open-plan office with cubical area, closed-plan office with corridor and meeting room, and also hybrid-plan office with both open and closed areas. It has been verified that the following model fits the propagation in indoor office environment best of the four models evaluated.

$$P_{LoS} = \begin{cases} 1, & d \leq 1.2 \\ \exp(-(d-1.2)/4.7), & 1.2 < d < 6.5 \\ \exp(-(d-6.5)/32.6) \cdot 0.32, & d \geq 6.5 \end{cases} \quad (6)$$

The verification results are shown in Table 5 and Figure 33. The LOS probability model used in ITU IMT-Advanced evaluation [ITU M.2135-1] and WINNER II [WINNER II D1.1.2] are also presented here for comparison. For the ITU and WINNER II model, parameterization results based on new data vary a lot from the original model. The results show that the new model has a good fit to the data in an

average sense and can be used for 5G InH scenarios evaluation. However, note the high variability between different deployments and degrees of openness in the office area.

Table 5. Comparison of the LOS probability models for the InH environment

Models	Original	Updated/New	MSE
ITU model	$P_{LOS} = \begin{cases} 1, & d \leq 18 \\ \exp(-(d-18)/27), & 18 < d < 37 \\ 0.5, & d \geq 37 \end{cases}$	$P_{LOS} = \begin{cases} 1, & d \leq 1.1 \\ \exp(-(d-1)/4.9), & 1.1 < d < 9.8 \\ 0.17, & d \geq 9.8 \end{cases}$	0.0499
WINNER II model (B3)	$P_{LOS} = \begin{cases} 1, & d \leq 10 \\ \exp(-(d-10)/45), & d > 10 \end{cases}$	$P_{LOS} = \begin{cases} 1, & d \leq 1 \\ \exp(-(d-1)/9.4), & d > 1 \end{cases}$	0.0572
WINNER II model (A1)	$P_{LOS} = \begin{cases} 1, & d \leq 2.5 \\ 1 - 0.9(1 - (1.24 - 0.61 \log_{10}(d))^3)^{1/3}, & d > 2.5 \end{cases}$	$P_{LOS} = \begin{cases} 1, & d \leq 2.6 \\ 1 - 0.9(1 - (1.16 - 0.41 \log_{10}(d))^3)^{1/3}, & d > 2.6 \end{cases}$	0.0473
New model	N/A	$P_{LOS} = \begin{cases} 1, & d \leq 1.2 \\ \exp(-(d-1.2)/4.7), & 1.2 < d < 6.5 \\ \exp(-(d-6.5)/32.6) \cdot 0.32, & d \geq 6.5 \end{cases}$	0.0449

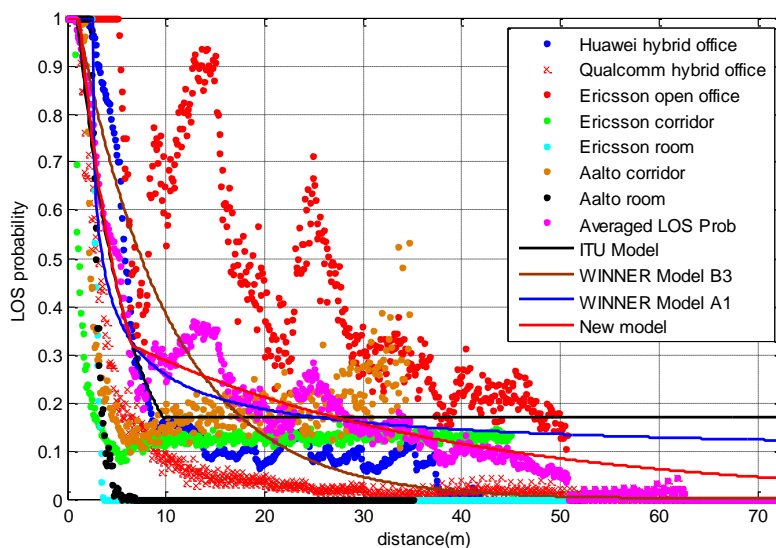


Figure 33. Indoor office LOS probability for three models considered

6.2 Path loss models

To adequately assess the performance of 5G systems, multi-frequency path loss (PL) models, LOS probability, and blockage models will need to be developed across the wide range of frequency bands and for operating scenarios. Three PL models are considered in this white paper; namely the close-in (CI) free space reference distance PL model [Andersen 1995][Rappaport 2015][SunGCW2015], the close-in free space reference distance model with frequency-dependent path loss exponent (CIF) [MacCartney 2015], [Haneda 2016] and the Alpha-Beta-Gamma (ABG) PL model [Hata 1980] [Piersanti ICC2012][[MacCartney GC2013] [MacCartney 2015] [Haneda 2016]. These models are

described in the following text and are then applied to various scenarios. Note that the path loss models currently used in the 3GPP 3D model is of the ABG model form but with additional dependencies on base station or terminal height, and with a LOS breakpoint. It may also be noted that the intention is to have only one path loss model (per scenario and LOS/NLOS) but that the choice is still open for discussion.

Table 6 shows the parameters of the CI, CIF, and ABG path loss models for different environments for omni-directional antennas. It may be noted that the models presented here are multi-frequency models, and the parameters are invariant to carrier frequency and can be applied across the 0.5-100 GHz band.

The CI PL model is given as [Rappaport 2015][MacCartney 2015] [SunGCW2015]

$$PL^{CI}(f, d)[dB] = FSPL(f, 1 m) + 10n \log_{10} \left(\frac{d}{1 m} \right) + X_{\sigma}^{CI}, \quad (7)$$

where f is the frequency in Hz, n is the PLE, d is the distance in meters, X_{σ}^{CI} is the shadow fading (SF) term in dB, and the free space path loss (FSPL) at 1 m, and frequency f is given as:

$$FSPL(f, 1 m) = 20 \log_{10} \left(\frac{4\pi f}{c} \right), \quad (6)$$

where c is the speed of light.

The ABG PL model is given as :

$$PL^{ABG}(f, d)[dB] = 10\alpha \log_{10}(d) + \beta + 10\gamma \log_{10}(f) + X_{\sigma}^{ABG}, \quad (7)$$

where α captures how the PL increase as the transmit-receive in distance (in meters) increases, β is a the floating offset value in dB, γ captures the PL variation over the frequency f in GHz., and X_{σ}^{ABG} is the SF term in dB.

The CIF PL model is an extension of the CI model, and uses a frequency-dependent path loss exponent given by:

$$PL^{CIF}(f, d)[dB] = FSPL(f, 1 m) + 10n \left(1 + b \left(\frac{f - f_0}{f_0} \right) \right) \log_{10} \left(\frac{d}{1 m} \right) + X_{\sigma}^{CIF} \quad (9)$$

where n denotes the path loss exponent (PLE), and b is an optimization parameter that captures the slope, or linear frequency dependency of the path loss exponent that balances at the centroid of the frequencies being modeled (e.g., path loss increases as f increases when b is positive). The term f_0 is a fixed reference frequency, the centroid of all frequencies represented by the path loss model, found as the weighed sum of measurements from different frequencies, using the following equation:

$$f_0 = \frac{\sum_{k=1}^K f_k N_k}{\sum_{k=1}^K N_k} \quad (10)$$

where K is the number of unique frequencies, and N_k is the number of path loss data points corresponding to the k^{th} frequency f_k . The input parameter f_0 represents the weighted frequencies of all measurement (or Ray-tracing) data applied to the model. The CIF model reverts to the CI model when $b = 0$ for multiple frequencies, or when a single frequency $f = f_0$ is modelled. For InH, a dual-slope path loss model might provide a good fit for different distance zones of the propagation environment. Frequency dependency is also observed in some of the indoor measurement campaigns conducted by co-authors. For NLOS, both a dual-slope ABG and dual-slope CIF model can be considered for 5G performance evaluation (they each require 5 modelling parameters to be optimized), and a single-slope CIF model (that uses only 2 optimization parameters) may be considered as a special case for InH-Office [MacCartney 2015]. The dual-slope may be best suited for InH-shopping mall or large indoor distances (greater than 50 m). The dual slope InH large scale path loss models are as follows:

Dual-Slope ABG model :

$$PL_{Dual}^{ABG}(d) = \begin{cases} \alpha_1 * 10 \log_{10}(d) + \beta_1 + \gamma * 10 \log_{10}(f) & 1 < d \leq d_{BP} \\ \alpha_1 * 10 \log_{10}(d_{BP}) + \beta_1 + \gamma * 10 \log_{10}(f) + \alpha_2 * 10 \log_{10}\left(\frac{d}{d_{BP}}\right) & d > d_{BP} \end{cases} \quad (11)$$

Dual-Slope CIF model:

$$PL_{Dual}^{CIF}(d) = \begin{cases} FSPL(f, 1m) + 10n_1 \left(1 + b_1 \left(\frac{f - f_0}{f_0} \right) \right) \log_{10}\left(\frac{d}{1m}\right) & 1 < d \leq d_{BP} \\ FSPL(f, 1m) + 10n_1 \left(1 + b_1 \left(\frac{f - f_0}{f_0} \right) \right) \log_{10}\left(\frac{d_{BP}}{1m}\right) + 10n_2 \left(1 + b_2 \left(\frac{f - f_0}{f_0} \right) \right) \log_{10}\left(\frac{d}{d_{BP}}\right) & d > d_{BP} \end{cases} \quad (12)$$

In the CI PL model, only a single parameter, the path loss exponent (PLE), needs to be determined through optimization to minimize the SF standard deviation over the measured PL data set [SunGCW2015] [Sun VTCS2016] [Rappaport2015]. In the CI PL model there is an anchor point that ties path loss to the FSPL at 1 m, which captures frequency-dependency of the path loss, and establishes a uniform standard to which all measurements and model parameters may be referred. In the CIF model there are 2 optimization parameters (n and b), and since it is an extension of the CI model, it also uses a 1 m free-space close-in reference distance path loss anchor. In the ABG PL model there are three optimization parameters which need to be optimized to minimize the standard deviation (SF) over the data set, just like the CI and CIF PL models [MacCartney2015][Sun VTCS2016]. Closed form expressions for optimization of the model parameters for the CI, CIF, and ABG path loss models are given in [MacCartney 2015], where it was shown that indoor channels experience an increase in the PLE value as the frequency increases, whereas the PLE is not very frequency dependent in outdoor UMa or UMi scenarios [Rappaport 2015],[SunGCW2015],[Thomas VTCS2016],[Sun VTCS2016]. The CI, CIF, and ABG models, as well as cross-polarization forms and closed-form expressions for optimization are given for indoor channels in [MacCartney 2015].

Table 6. CI, CIF and ABG model parameters for different environments

Scenario	CI/CIF Model Parameters	ABG Model Parameters
UMa- LOS	$n=2.0, \sigma_{SF} = 4.1$ dB	NA
UMa- nLOS	$n=3.0, \sigma_{SF} = 6.8$ dB	$\alpha=3.4, \beta=19.2, \gamma=2.3, \sigma_{SF} = 6.5$ dB
UMi-Street Canyon-LOS	$n=2.1, \sigma_{SF} = 3.76$ dB	NA
UMi-Street Canyon-nLOS	$n=3.17, \sigma_{SF} = 8.09$ dB	$\alpha=3.53, \beta=22.4, \gamma=2.13, \sigma_{SF} = 7.82$ dB
UMi-Open Square-LOS	$n=1.85, \sigma_{SF} = 4.2$ dB	NA
UMi-Open Square-nLOS	$n=2.89, \sigma_{SF} = 7.1$ dB	$\alpha=4.14, \beta=3.66, \gamma=2.43, \sigma_{SF} = 7.0$ dB
InH-Indoor Office-LOS	$n=1.73, \sigma_{SF} = 3.02$ dB	NA
InH-Indoor Office-nLOS single slope (FFS)	$n=3.19, b=0.06, f_0= 24.2$ GHz, $\sigma_{SF} = 8.29$ dB	$\alpha=3.83, \beta=17.30, \gamma=2.49, \sigma_{SF} = 8.03$ dB
InH-Indoor-Office nLOS dual slope	$n_1=2.51, b_1=0.12, f_0= 24.1$ GHz, $n_2=4.25, b_2=0.04, d_{BP} = 7.8$ m, $\sigma_{SF}=7.65$ dB	$\alpha_1=1.7, \beta_1=33.0, \gamma=2.49, d_{BP} = 6.90$ m $\alpha_2=4.17, \sigma_{SF} = 7.78$ dB
InH-Shopping Malls-LOS	$n=1.73, \sigma_{SF} = 2.01$ dB	NA
InH-Shopping Malls-nLOS single slope (FFS)	$n=2.59, b=0.01, f_0= 39.5$ GHz, $\sigma_{SF} = 7.40$ dB	$\alpha=3.21, \beta=18.09, \gamma=2.24, \sigma_{SF} = 6.97$ dB
InH-Shopping Malls-nLOS dual slope	$n_1=2.43, b_1=-0.01, f_0= 39.5$ GHz, $n_2=8.36, b_2=0.39, d_{BP} = 110$ m, $\sigma_{SF} = 6.26$ dB	$\alpha_1=2.9, \beta_1=22.17, \gamma=2.24, d_{BP} = 147.0$ m $\alpha_2=11.47, \sigma_{SF} = 6.36$ dB

Note: the parameters of ABG model in the LOS conditions are not mentioned for the UMa and UMi scenarios because the α is almost identical to the PLE of the CI model, and also γ is very close to 2, which indicates free space path loss with frequency, and this is modelled in both the CI and CIF models within the first meter of free space propagation.

Another important issue related to pathloss is shadowing fading. For indoor hotspot, the distance dependency and frequency dependency were investigated for both indoor office and shopping mall. For LOS propagation condition, the frequency and distance dependency is weak. But for NLOS propagation condition, frequency and distance dependency can be observed. The results can be found in Table 7.

Table 7. Distance dependent shadowing for InH

Scenarios	LOS/ NLOS	Models		Value (dB)	Frequency Range	Distance Range
Indoor office	LOS	CI		3	2.44~73GHz	1~73m
	NLOS	Singles lope	ABG	$\min(3.20 \log_{10}(f) + 3.38 \log_{10}(d), 12.5)$		1~86m
			CIF	$\min(2.59 \log_{10}(f) + 4.10 \log_{10}(d), 12.6)$		
		Dual slope	ABG	$\min(2.37 \log_{10}(f) + 3.88 \log_{10}(d), 11.9)$		
			CIF	$\min(2.35 \log_{10}(f) + 3.64 \log_{10}(d), 11.4)$		
Shopping mall	LOS	CI		2	2.9~63GHz	0.5~149m
	NLOS	Singles lope	ABG	$\min(4.62 \log_{10}(d), 10.9)$		2~229m
			CIF	$\min(4.94 \log_{10}(d), 11.7)$		
		Dual slope	ABG	$\min(2.41 + 2.49 \log_{10}(d), 9)$		
			CIF	$\min(2.77 + 2.15 \log_{10}(d), 9)$		

6.3 Building penetration loss modelling

The building penetration loss model according to e.g. [3GPP TR36.873] consists of the following parts:

$$PL = PL_b + PL_{tw} + PL_{in} + N(0, \sigma) \quad (13)$$

where PL_b is the basic outdoor path loss given by the UMa or UMi path loss models, PL_{tw} is the building penetration loss through the external wall, PL_{in} is the inside loss dependent on the depth into the building, and σ is the standard deviation. In the first revision of this white paper and in [Haneda VTC2016] several different frequency-dependent models were proposed. Here the recommended model is described.

The building penetration loss through the external wall is modelled using the composite approach first described in [Semaan Globecom 2014]. In this approach, linear loss as a function of frequency is assumed for any specific material, see Table 8.

Table 8. Material penetration losses

Material	Penetration loss [dB]
Standard multi-pane glass	$L_{glass} = 2 + 0.2 \cdot f$
IRR glass	$L_{IRRglass} = 23 + 0.3 \cdot f$

Concrete	$L_{concrete} = 5 + 4 \cdot f$
----------	--------------------------------

The composite penetration loss is obtained through a weighted average of the transmission through two different materials, where the weight is given by the relative surface area of each material over the façade of the building. Two variants of the model are given, a low loss and a high loss model, see Table 9. An additional loss of 5 dB has been added to the external wall loss to account for non-perpendicular incidence. The indoor loss has been selected at 0.5 dB/m to maintain consistency with [3GPP TR 36.873]. Finally, the standard deviation has been tentatively selected based on the experience from the reported measurements.

Table 9 Recommended building penetration loss model

	Path loss through external wall: PL_{tw} [dB]	Indoor loss: PL_{in} [dB/m]	Standard deviation: σ [dB]
Low loss model	$[5] - 10 \log_{10}(0.3 \cdot 10^{-L_{glass}/10} + 0.7 \cdot 10^{-L_{concrete}/10})$	0.5	[3]
High loss model	$[5] - 10 \log_{10}(0.7 \cdot 10^{-L_{IRRglass}/10} + 0.3 \cdot 10^{-L_{concrete}/10})$	0.5	[5]

A comparison between the model components and aggregate behaviour and the reported measurements can be found in Figure 34. Not included in the figure are additional O2I measurements at 3.5 GHz contributed by CMCC and Bupt for which the total average excess loss (averaged over various incidence angles and for a depth of about 10 m into the building) was 25 and 37 dB for two different buildings. The standard deviation in each building was about 6 dB.

The 12 dB difference between the loss in the two buildings is similar as the difference between the low and high loss models at 3.5 GHz.

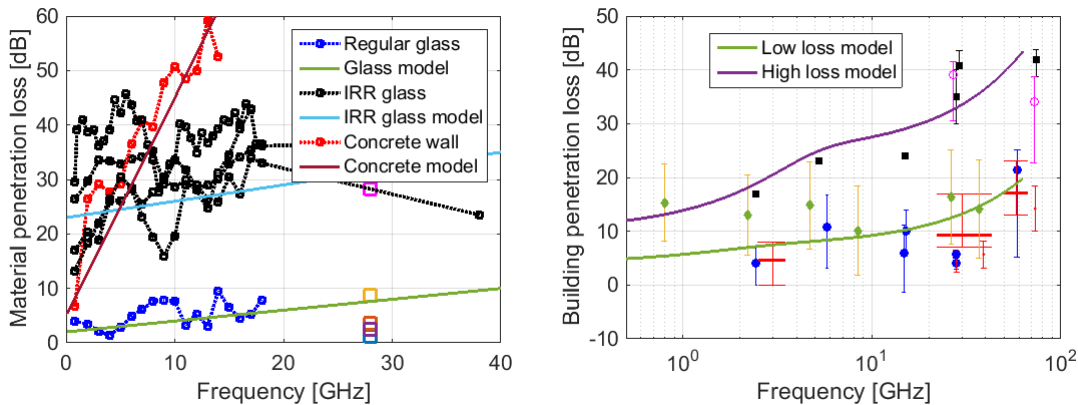


Figure 34 Comparison between the material loss model and measurements (left) and the composite penetration loss model for normal incidence and measurements (right).

6.4 Blockage models

Dynamic blockage and geometry-induced blockage can be modelled by different modelling approaches. The dynamic blockage could be modelled as a component of the small scale fading by including excess shadowing on a number of paths or clusters, as has been proposed in [METIS 2015] or [IEEE 802.11ad]. The geometry-induced blockage could be modelled as a component of the large-scale fading as additional shadow fading with certain occurrence probability.

It is worth noting that the environment also causes transient path gains by, for example, motion of surfaces or objects with strong reflections. The effects of transient path gains cause dynamic shadow fading. Figure 35 illustrates the concept of static shadow fading and dynamic shadow fading. When doing measurements in an uncontrolled environment, the measured instantaneous channel gain most likely includes dynamic shadow fading. By taking the expectation over multiple measurements at each Tx-Rx distance, the dynamic shadow fading can be averaged out. Path loss fitting based on the path gain expectation values gives the static path loss and static shadow fading as described in Section 5.b .

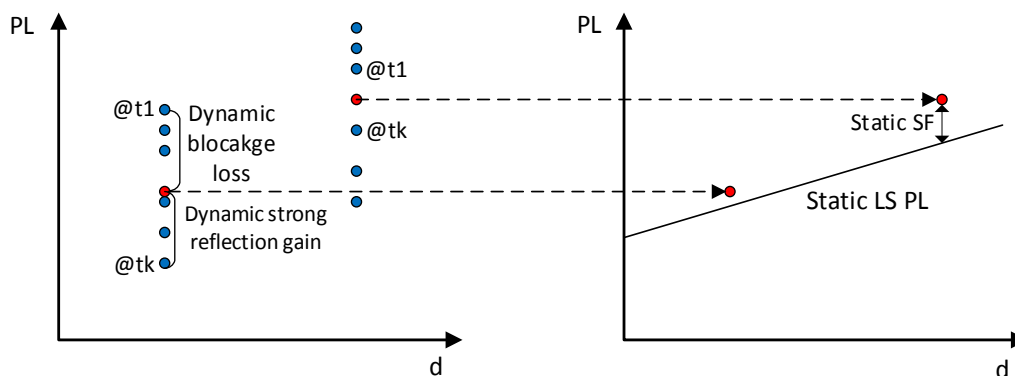


Figure 35 Illustration of static shadow fading and dynamic shadow fading

7 Fast Fading Modelling

7.1 UMi

In the double-directional channel model, the multipath components are described by the delays and the directions of departure and the direction of arrival. Each multipath component is scaled with a complex amplitude gain. Then the double-directional channel impulse response is composed of the sum of the generated double-directional multipath components. The double-directional channel model provides a complete omni-directional statistical spatial channel model (SSCM) for both LOS and NLOS scenarios in UMi environment. These results are analyzed based on the measurement campaign results and mostly the ray-tracing results, which is compared with the measurement campaign done in the same urban area.

For fast-fading modeling, ray-tracing based method is useful to extend the sparse empirical datasets and to analyze the channel characteristics for different frequency ranges with same environments. Ray-tracing results provide full information in spatio-temporal domain, which can be extracted to parameterize the double-directional channel model. The large-scale parameters in SSCM are analyzed from many measurement campaign and ray-tracing simulation, which dataset are summarized in Appendix. As a set of example, large-scale parameters for small-scale fading model in UMi are analyzed using the measurement campaign results and ray-tracing results on UMi street-canyon area in Daejeon, Korea shown in Figure 36, which models the same area conducted the measurement campaign [Hur EuCAP2015]. In the 3D ray-tracing simulation, the TX was placed 16 m above the ground on the sixth-floor height and the RX was placed at 1.5 m above the ground. For the ray tracing simulations, the RX was moved on a 1 m grid in a 200 m x 200 m area. The parameters for ray-tracing simulation and environment description are similarly set to the value used in [Hur JSTSP2016].



Figure 36. Daejeon street canyon environments conducted measurement campaign and used for the ray-tracing study. The BS location is at the sites indicated by the star and the UEs were placed outdoors in the streets canyon areas.

The channel parameters in delay and angular domains are extracted from the detected path information. In the SSCM approach, the channel characteristics are represented by correlated large-scale parameters (LSPs), such as delay spread, angular spread, K-factor and shadow fading factor, which is well described in WINNER-like channel model [WINNER]. All LSPs are modeled by a log-normal distribution with common values of the mean μ and standard variation σ . In [3D-SCM], the LSPs characteristics are described by these common values of log-normal distributions, simply constant model or distance-dependent model. In this work, the new channel model is based on the 3D-SCM approach with same assumptions, and updating the LSP parameter tables by extending frequency up to 100 GHz. Therefore, the frequency dependency of μ and σ is checked if the values can be modeled as a function of frequency or constant over frequency. In delay spread, from the different dataset from measurement and ray-tracing, the linear frequency-dependency over $\log_{10}(f)$ is observed as shown in Figure 37. Furthermore, to avoid infinite DS values with the frequency goes to zero, the linear regression over $\log_{10}(1+f)$ is applied to derive the all LSP characteristics. Also, the DS values in legacy band are close to the current channel model in 3D-SCM parameters, which also shows the similarity of the LSP characteristics. Some parameters with weak frequency-dependency are simply modeled as constant values by averaging the parameters over different dataset. For further modeling purpose, other available channel parameters for extension of

LSP over frequency are described in Appendix, and those derived LPS models are summarized in Table 10 and Table 11.

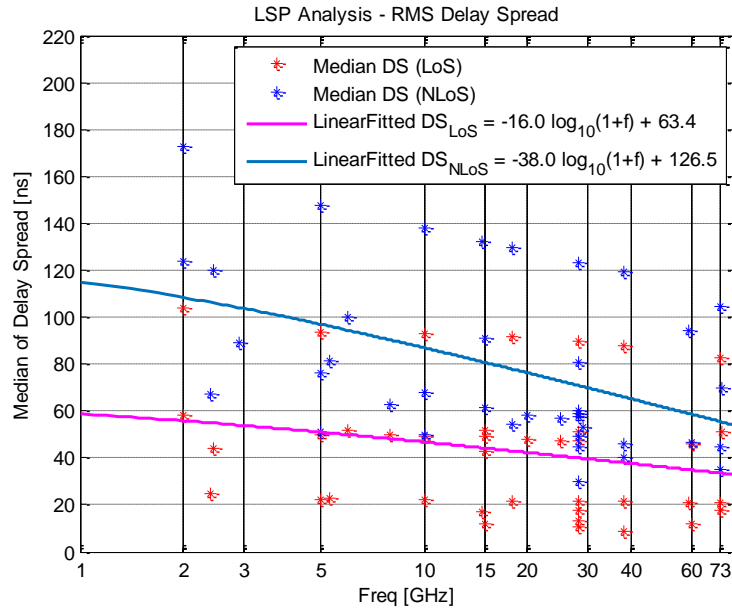


Figure 37. Delay-spread model up to 100 GHz

Table 10. Large-scale parameters for UMi Street-canyon

Scenarios		UMi Street-Canyon	
		LOS	NLOS
Delay spread (DS) $\log_{10}([s])$	μ_{DS}	$-0.2 * \log_{10}(1+f) - 7.20$	$-0.21 * \log_{10}(1+f) - 6.88$
	ε_{DS}	0.39	$0.16 * \log_{10}(1+f) + 0.29$
AoD spread (σ_{ASD}) $\log_{10}([^\circ])$	μ_{ASD}	$-0.05 * \log_{10}(1+f) + 1.21$	$-0.23 * \log_{10}(1+f) + 1.53$
	ε_{ASD}	0.41	$0.11 * \log_{10}(1+f) + 0.33$
AoA spread (σ_{ASA}) $\log_{10}([^\circ])$	μ_{ASA}	$-0.08 * \log_{10}(1+f) + 1.73$	$-0.08 * \log_{10}(1+f) + 1.81$
	ε_{ASA}	$0.014 * \log_{10}(1+f) + 0.28$	$0.05 * \log_{10}(1+f) + 0.3$
ZoA spread (σ_{ZSA}) $\log_{10}([^\circ])$	μ_{ZSA}	$-0.1 * \log_{10}(1+f) + 0.73$	$-0.04 * \log_{10}(1+f) + 0.92$
	ε_{ZSA}	$-0.04 * \log_{10}(1+f) + 0.34$	$-0.07 * \log_{10}(1+f) + 0.41$
Delay scaling parameter r_τ		3	2.1

1. The trend of frequency-dependent on LSP is not observed over all measurement data

Table 11. ZoD model parameters for UMi Street-canyon

Scenarios		UMi Street-Canyon	
		LOS	NLOS
ZoD spread (σ_{ZSD})log ₁₀ ([°])	μ_{ZSD}	$\max[-0.21, -14.8(d_{2D}/1000) + 0.83]$	$\max[-0.5, -3.1(d_{2D}/1000)+0.2]$
	ϵ_{ZSD}	0.35	0.35
ZoD offset	$\mu_{offset,ZOD}$	0	$-10^{\{-1.5\log_{10}(\max(10, d_{2D}))\}+3.3}$

The channel datasets have been analyzed in the spatio-temporal domain applying Agglomerative Algorithm [Walter 2008], for clustering such as delays, angles at the TX and RX side, and the received powers within clusters. Based on the observed clusters in each link, large-scale parameters such as number of clusters and intra-cluster delay spreads and angle spreads are analyzed using the framework in [3D-SCM], and all parameters are extracted by following the methodologies in [WINNER].

The cluster parameters are preliminary derived from some measurement and ray-tracing data, which can be as a preliminary parameters and summarized in Appendix. The ray-tracing data predicts fewer clusters and weak-frequency dependent characteristics. However, the clustering results based on ray-tracing are limited due to some simulation conditions, such as small number of observed path in simulation and the deterministic characteristic of propagation simulation. Further measurement campaigns will be needed to verify these observations. Meanwhile, as a starting point the number of cluster and number of rays in 3D-SCM parameters can be used. Furthermore, in some case it is also required to modify the clustering model to support large BWs and large-sized arrays. It is recommended to further study this through measurements with large bandwidths and/or large antenna arrays.

Table 12. Cluster parameters for UMi Street-canyon

Scenarios		3D-UMi	
		LOS	NLOS
Number of cluster ¹⁾	N	12	19
Number of rays per cluster	M	20	20
Cluster DS	$\mu_{ClusterDS}$	$-12.0*\log_{10}(1+f) + 36.6$	11

Cluster ASD	$\mu_{ClusterASD}$	3	10
Cluster ASA	$\mu_{ClusterASA}$	17	22
Cluster ZSA	$\mu_{ClusterZSA}$	7	7
Cluster SF	$\sigma_{ClusterSF}$	5	$3.09 * \log_{10}(1+f) + 5.72$

1. Ray-tracing results show smaller number of clusters, and recommend to study the effect of large BW and arrays. Currently, it is suggested to use the 3GPP 3D number of clusters as a starting point.

7.2 UMa

UMa large-scale fading parameters were determined using measurements at 28 GHz in Lindholmen and Molndal Sweden, 6 GHz data taken on the BUPT campus, and a ray-tracing study performed in Aalborg, Denmark as shown in Figure 38. This ray tracing environment was chosen as there were real-world measurements also made in the same area [Nguyen16]. Specifically there were two APs used in the study which both have a height of 25 m. The UE height was 1.5 m and isotropic antennas were employed at both the AP and UE. Note that no other objects, such as vehicles, trees, light poles, and signs, were included in this ray-tracing study but they were present when measurements were taken. The maximum number of rays in the simulation was 20, no transmissions through buildings were allowed, the maximum number of reflections was four, the maximum number of diffractions was one for frequencies above 10 GHz and was two for frequencies of 10 GHz and below. Six frequencies were considered in this study which were 5.6, 10, 18, 28, 39.3, and 73.5 GHz.

Two philosophies were used in determining the final set of UMa parameters since there was a very limited set of data available. The first was to make the model consistent with the 3GPP model below 6 GHz and second was to use ray tracing mostly to determine trends (e.g., how delay spread changes with frequency) instead of absolute values of the LSPs. The large-scale parameters found for the NLOS and LOS UMa environment are given in the Appendix (Table 23 through Table 36). The delay and azimuth angle spreads were found to decrease in frequency and are modelled as a linear decrease with the log of frequency. No clear frequency trend was found for the correlation of the LSPs so it was determined to reuse the ones from the 3GPP 3D channel model. Also there was no clear evidence to change the correlation distances of the LSPs, so again the values from the 3GPP 3D channel model were retained.

Finally, an investigation into the clustering of the rays in this ray-tracing study was performed. To determine clusters, the agglomerative algorithm was employed. The results showed that the average number of clusters and the average number of rays per cluster were both fairly consistent across the different carrier frequencies. However, the cluster delay spreads tended to decrease with increasing frequency in both LOS and NLOS and hence it was determined to model that frequency dependency. In interpreting these results, especially the average number of rays per cluster, it should be noted that the number of modelled rays was limited to 20 in the simulations, Hence it was decided to still retain

the 3GPP modelling of the number of clusters and the number of rays per cluster until more study with addition measurements or more detailed ray tracing is available.

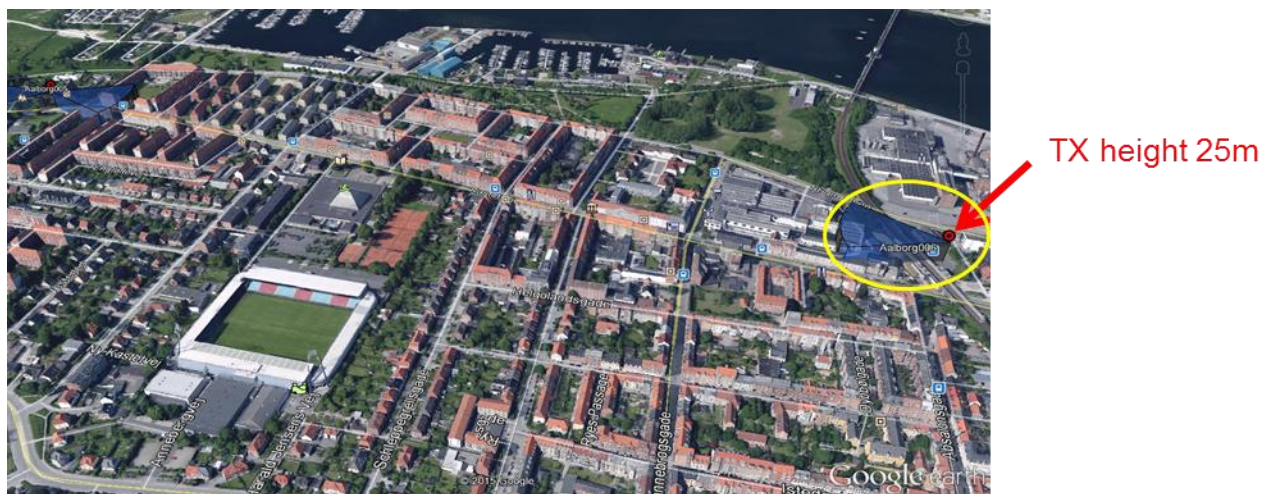


Figure 38. Aalborg, Denmark environment used for ray-tracing study. The AP (Tx) location was at the site indicated and UEs were placed outdoors in the streets and open areas.

7.3 InH

For InH scenarios, an investigation of fast fading modelling has been conducted based on both measurement and ray-tracing. Both indoor office and shopping mall environments have been investigated at frequencies including 2.9GHz, 3.5GHz, 6GHz, 14GHz, 15GHz, 20 GHz, 28 GHz, 29GHz, 60GHz, and 73 GHz. Some preliminary analysis on large-scale channel characteristics have been summarized from Table 37 to Table 41. Some small-scale channel characteristics have been summarized in Table 42 and Table 43. Although it is still too early to apply these results to the full frequency range up to 100 GHz, these preliminary investigations have provided insight into the differences across the extended frequency range.

The preliminary analysis results shown in Table 13 and Table 14 illustrate the frequency dependency of large-scale channel characteristics across the measured frequency range. For some LSPs, frequency dependency can be observed, but for some other LSPs, the frequency dependency observed is not strong. Since for some cases, the number of data samples for frequencies available for analysis is limited, it is not easy to come to conclusion yet. And also for certain measurement, frequency dependency is not observed. These observations indicate that, for some of the LSPs, frequency dependency could be considered for channel modelling for the frequency range up to 100 GHz.

Table 13. Analysis on frequency dependency on LSP for indoor office

Model		LOS			NLOS		
		fitting	Avg.	IMT-A ¹	fitting	Avg.	IMT-A ¹
DS	Median [ns]	$-0.77 \cdot \log_{10}(1+f) + 30.61$	28.22	N/A	$-11.64 \cdot \log_{10}(1+f) + 54.53$	38.94	N/A

	μ_{DS}	$-0.28*\log_{10}(1+f)-7.31$	-7.71	-7.70	$-0.35*\log_{10}(1+f)-7.06$	-7.55	-7.41
	σ_{DS}	$0.04*\log_{10}(1+f)+0.18$	0.24	0.18	$0.10*\log_{10}(1+f)+0.04$	0.19	0.14
ASA	Median [°]	$11.47*\log_{10}(1+f)+9.23$	26.77	N/A	$-17.89*\log_{10}(1+f)+71.83$	44.48	N/A
	μ_{ASA}	$0.07*\log_{10}(1+f)+1.39$	1.51	1.62	$-0.22*\log_{10}(1+f)+1.98$	1.6	1.77
	σ_{ASA}	$1.78*\log_{10}(1+f)-2.46$	0.60	0.22	$1.90*\log_{10}(1+f)-2.66$	0.6	0.16
ZSA	Median [°]	$-5.90*\log_{10}(1+f)+29.77$	7.13	N/A	$-0.56*\log_{10}(1+f)+8.14$	5.97	N/A
	μ_{ZSA}	$-0.52*\log_{10}(1+f)+1.60$	0.76	N/A	$-0.03*\log_{10}(1+f)+0.89$	0.77	N/A
	σ_{ZSA}	$0.07*\log_{10}(1+f)+0.005$	0.12	N/A	0.08	0.08	N/A
K	μ_K	$0.84*\log_{10}(1+f)+2.12$	3.38	7	N/A	N/A	N/A
	σ_K	$-0.58*\log_{10}(1+f)+6.19$	4.16	4	N/A	N/A	N/A
ASD	μ_{ZSD}	N/A	1.08	1.60	N/A	N/A	1.62
	σ_{ZSD}	N/A	0.23	0.18	N/A	N/A	0.25
ZSD	μ_{ZSD}	N/A	0.40	N/A	N/A	N/A	N/A
	σ_{ZSD}	N/A	0.23	N/A	N/A	N/A	N/A

1.The IMT-A results for InH are based on 2D channel model

Table 14. Analysis on frequency dependency on LSP for shopping mall

Model		LOS			NLOS		
		fitting	Avg.	IMT-A ¹	fitting	Avg.	IMT-A ¹
DS	Median [ns]	$-13.31*\log_{10}(1+f)+60.24$	41.75	N/A	$-23.90*\log_{10}(1+f)+89.31$	56.12	N/A
	μ_{DS}	$-0.13*\log_{10}(1+f)-7.27$	-7.47	-7.70	$-0.13*\log_{10}(1+f)-7.01$	-7.21	-7.41
	σ_{DS}	$0.007*\log_{10}(1+f)+0.30$	0.31	0.18	$0.007*\log_{10}(1+f)+0.19$	0.21	0.14
ASA	Median [°]	$-19.01*\log_{10}(1+f)+67.41$	39.06	N/A	$5.43*\log_{10}(1+f)+29.02$	37.13	N/A

	μ_{ASA}	$-0.21 \cdot \log_{10}(1+f) + 1.83$	1.51	1.62	$0.10 \cdot \log_{10}(1+f) + 1.54$	1.7	1.77
	σ_{ASA}	$-0.08 \cdot \log_{10}(1+f) + 0.38$	0.25	0.22	$-0.13 \cdot \log_{10}(1+f) + 0.35$	0.15	0.16
ZSA	Median [η]	$9.64 \cdot \log_{10}(1+f) - 8.56$	5.82	N/A	$0.46 \cdot \log_{10}(1+f) + 3.35$	4.05	N/A
	μ_{ZSA}	$0.38 \cdot \log_{10}(1+f) + 0.16$	0.75	N/A	$0.15 \cdot \log_{10}(1+f) + 0.54$	0.77	N/A
	σ_{ZSA}	$-0.33 \cdot \log_{10}(1+f) + 0.73$	0.23	N/A	$-0.08 \cdot \log_{10}(1+f) + 0.26$	0.13	N/A
K	μ_K	$-2.53 \cdot \log_{10}(1+f) + 4.34$	0.57	7	N/A	N/A	N/A
	σ_K	$-0.44 \cdot \log_{10}(1+f) + 3.85$	3.19	4	N/A	N/A	N/A
ASD	Median [η]	$1.03 \cdot \log_{10}(1+f) + 19.96$	23.5	N/A	$-19.33 \cdot \log_{10}(1+f) + 86.74$	57.91	N/A
	μ_{ZSD}	$0.18 \cdot \log_{10}(1+f) + 1.09$	1.36	1.60	$-0.14 \cdot \log_{10}(1+f) + 1.93$	1.72	1.62
	σ_{ZSD}	$-0.11 \cdot \log_{10}(1+f) + 0.55$	0.17	0.18	$0.04 \cdot \log_{10}(1+f) + 0.06$	0.14	0.25
ZSD	Median [η]	$1.97 \cdot \log_{10}(1+f) + 1.04$	3.98	N/A	$-5.95 \cdot \log_{10}(1+f) + 16.96$	8.09	N/A
	μ_{ZSD}	$0.18 \cdot \log_{10}(1+f) + 0.38$	0.67	N/A	$-0.25 \cdot \log_{10}(1+f) + 1.27$	0.89	N/A
	σ_{ZSD}	$-0.25 \cdot \log_{10}(1+f) + 0.75$	0.37	N/A	$0.01 \cdot \log_{10}(1+f) + 0.17$	0.19	N/A

1. The IMT-A results for InH are based on 2D channel model

For small-scale fading, according to the Table 42 and Table 43, so far the results only collected for limited number of frequencies. They can be used as start point for further investigation on related topics.

7.4 O2I channel modelling

The measurements of O2I channel characteristics in terms of large-scale and small-scale parameters are summarized in Table 44. For comparison, the O2I model parameters of the 3D channel model [3GPP TR 36.873] are given in the leftmost column. No obvious frequency-dependence of these parameters can be spotted. Furthermore, the values seem to be mostly in line with the O2I scenario in the 3D channel model except for the delay spread which is lower. However, one should note that the measurements are exclusively in LOS to the building with fairly short distances while the O2I scenario should capture both LOS and NLOS conditions. As some of the measurements suggest that the delay spread is mainly dependent on the outdoor part of the propagation path it seems reasonable that in NLOS there would be larger delay spreads than what has been measured.

Based on the currently available data three different approaches can be considered:

1. The existing 3D O2I LSP and SSP parameter values from [3GPP TR 36.873] could be applied also for the frequency range up to 100 GHz. Note that the building penetration loss model is frequency-dependent as already described.
2. The existing 3D O2I LSP and SSP parameter values from [3GPP TR 36.873] could be modified to reflect the new measurements. All parameters are modelled as frequency-independent except the building penetration loss.
3. Split the O2I scenario into a LOS variant parameterized using the new measurements in Table 44, and a NLOS variant parameterized using possible future NLOS O2I measurements.

8 Step-by-step procedure for generating channels

The 12-step procedure described in 36.873 should serve as a good starting point for modelling of channels up to 100 GHz. Some modifications of existing steps or additions of new steps may be required to comply with the modelling proposals presented in this white paper.

9 List of contributors

This paper reflects the outcome from an ad-hoc industry working group that included the following participants.

<i>Company</i>	<i>Contact name</i>	<i>Email Address</i>
Aalto University	Katsuyuki Haneda Sinh Le Hong Nguyen Jan Jarvelainen Afroza Khatun,	Katsuyuki.haneda@aalto.fi sinh.nguyen@aalto . jan.jarvelaine@aalto.fi afroza.khatun@aalto.fi
BUPT	Jianhua Zhang Lei Tian	jhzhang@bupt.edu.cn tianlbupt@bupt.edu.cn
CMCC	Guangyi Liu Hui Tong Yi Zheng	liuguangyi@chinamobile.com tonghui@chinamobile.com zhengyi@chinamobile.com ,
Ericsson	Henrik Asplund	henrik.aspland@ericsson.com
Huawei	Wen Tong, Jian Li, Yi Wang, David Steer, Tommi Jamsa, Jia He	tongwen@huawei.com Calvin.li@huawei.com , yi.wang@huawei.com , david.steer@huawei.com tommi.jamsa@huawei.com hejia83@huawei.com
INTEL	Clara Li, Tommaso Balercia, Yuan Zhu, Wenting Chang	Clara.q.li@intel.com, tommaso.balercia@intel.com yuan.y.zhu@intel.com wenting.chang@intel.com
KT Corporation	Sunguk Lee, YoungSuk Kim	Sunguk.lee@kt.com , youngsuk.kim@kt.com

Nokia	Amitava Ghosh, Tim Thomas	amitava.ghosh@nokia.com , timothy.thomas@nokia.com
NTT DOCOMO	Takehiro Nakamura, Yuichi Kakishima, Tetsuro Imai, Haralabos Papadopoulos	nakamura@nttdocomo.com kakishima@docomoinnovations.com imaite@nttdocomo.com hpapadopoulos@ docomoinnovations.com
NYU	Theodore (Ted) S. Rappaport, George R. MacCartney, Mathew K. Samimi, Shu Sun	tsr@nyu.edu gmac@nyu.edu mks@nyu.edu ss7152@nyu.edu
Qualcomm	Ozge Koymen	okoymen@qti.qualcomm.com
Samsung	Sooyoung Hur, Jeongho Park, Charlie Zhang	sooyoung.hur@samsung.com , jeongho.jh.park@samsung.com , jianzhong.z@samsung.com
University of Bristol	Evangelos Mellios	Evangelos.mellios@bristol.ac.uk
University of Southern California	Andreas F.Molisch	molisch@usc.edu

10 Acknowledgements

ETRI has contributed with measurement results that have been included in the analysis and processing performed by the contributors.

<i>Company</i>	<i>Contact name</i>	<i>Email Address</i>
ETRI	Myung-Don Kim Jae-Joon Park	mdkim@etri.re.kr jjpark@etri.re.kr

11 Appendix

11.1 Overview of measurement campaigns

The basis for this white paper is the open literature in combination with recent and ongoing propagation channel measurements performed by the cosignatories of this white paper, some of which are as yet unpublished. These measurements along with the main observations and conclusions are described in the accompanying Annex. The following tables give an overview of these recent measurement activities in different frequency bands and scenarios.

11.1.1 UMi street canyon O2O

Band	Party	GHz	Pathloss & Shadowing	Large Scale Parameters	Small Scale Parameters

< 30 GHz	NYU	1.8	•	•	•
	CMCC	6	●	●	Aug.
	DCM	8	●		
	CMCC	10	TBD	TBD	
	Intel	10	July.	Sep.	Sep.
	Nokia/Aalborg	2, 10, 18	●		
	CMCC	14	Sep.	Sep.	
	Aalto	15	Sep.	Sep.	Sep.
	Huawei	15			
	Ericsson	15	●	●	●
	DCM	20, 26	●	Sep. (20)	Sep. (20)
	Huawei	28	●	Nov.	Nov.
	Intel	28	Sep.	Nov.	Nov.
	NYU	28	● [Summer 2012]	● [Summer 2012]	● [Summer 2012]
	NYU	28	Sep.	Sep.	Sep.
	Samsung	28	●	●	●
	Ericsson	28			
	Nokia/Aalborg	28	●	●	
	CMCC	28	Sep.	Sep.	
	Aalto	28	●	●	●
Qualcomm	29	Oct.	TBD	TBD	

Band	Party	GHz	Pathloss & Shadowing	Large Scale Parameters	Small Scale Parameters
30 - 60 GHz	Huawei	30-40			
	DCM	37	●		
	NYU	38			
	Intel	40, 60	July (60) Sep. (40)	Sep (60) Nov. (40)	Sep. (60) Nov. (40)

	Ericsson	60			
	Huawei	60	Nov.	Nov.	Nov.
	Qualcomm	60	Oct.	TBD	TBD
> 60 GHz	Aalto	63	Sep.	Sep.	Sep.
	Huawei	73	●	Nov.	Nov.
	NYU	73	● [Summer 2013]	● [Summer 2013]	● [Summer 2013]
	Intel	75, 82	Sep.	Nov.	Nov.

11.1.2 UMi open square O2O

Band	Party	GHz	Pathloss & Shadowing	Large Scale Parameters	Small Scale Parameters
< 30 GHz	Nokia / AAU	10	•		Madrid-grid
	CMCC	14	Sep.	Sep.	
	Nokia / AAU	2, 10,18	●		
	Nokia/AAU	28	●		
	Samsung	28	TBD (July or Sep)	TBD (Sep)	TBD (Sep)
	Qualcomm	29	●	TBD	TBD
30 - 60 GHz	Qualcomm	60	Sept	TBD	TBD
	Univ. of Bristol	60	TBD (Spring 2016)	TBD (Spring 2016)	TBD (Spring 2016)
60 GHz	Aalto	63	•	•	•

	NYU	73	● [Spring 2014]	● [Spring 2014]	

11.1.3 UMi O2I

Band	Party	GHz	Pathloss & Shadowing	Large Scale Parameters	Small Scale Parameters
< 30 GHz	NYU	1.9, 5.85	•		
	DCM	8, 26	July		
	Nokia/Aalborg	10	●		
	Ericsson	6, 15, 28	●	●	●
	Nokia/Aalborg	20	●		
	Nokia/Aalborg	28	Sep.		
	Samsung	28	TBD (July)		
	NYU	28	● [Summer 2012]	● [Summer 2012]	
	Ericsson	28			
30 - 60 GHz	DCM	37	July		
	Ericsson	60	●	●	●
> 60 GHz					

11.1.4 UMa O2O

Band	Party	GHz	Pathloss & Shadowing	Large Scale Parameters	Small Scale Parameters
< 30 GHz	CMCC	6	Sep.	Sep.	
	Nokia/Aalborg	2, 10, 18, 28	●		
	CMCC	14	TBD	TBD	
30 - 60 GHz	NYU	38	• [Summer 1998 & Summer 2011]	• [Summer 1998 & Summer 2011]	
> 60 GHz					

11.1.5 InH open-plan office

Band	Party	GHz	Pathloss & Shadowing	Large Scale Parameters	Small Scale Parameters
< 30 GHz	NYU	1.3, 1.9, 2.5, 4.0, 5.85	•	•	
	CMCC	6	Sep.	Sep.	
	CMCC	14	●	●	

	Ericsson	15			
	Huawei	15	Sept.	Nov.	Nov.
	DCM	8, 20, 26	●	Sep (20)	Sep (20)
	Huawei	28	●	Sept.	Nov.
	NYU	28	● [Summer 2012 & Summer 2014]	● [Summer 2012 & Summer 2014]	
	Samsung	28	TBD	TBD	TBD
	Ericsson	28	TBD		
	CMCC	28	Sep.	Sep.	
30 - 60 GHz	Huawei	30-40			
	DCM	37	July		
	Ericsson	60			
	NYU	60	● [2000]	● [2000]	
	Univ. of Bristol	60	TBD (Spring 2016)	TBD (Spring 2016)	TBD (Spring 2016)
	Huawei	60	Sept.	Nov.	Nov.
> 60 GHz	Aalto	63, 70	•	•	•
	Huawei	72	●	Sept.	Nov.
	NYU	73	● [Spring & Summer 2014]	● [Spring & Summer 2014]	

11.1.6 InH closed-plan office

Band	Party	GHz	Pathloss & Shadowing	Large Scale Parameters	Small Scale Parameters
< 30 GHz	NYU	1.3, 1.9, 2.5, 4.0, 5.85	•	•	

	Intel	10, 28	Sep	Nov	Nov
	Ericsson	2, 4, 6, 15	●	●	●
	NYU	28	● [Summer 2012 & Summer 2014]	● [Summer 2012 & Summer 2014]	
	Samsung	28	TBD	TBD	TBD
	Ericsson	28	TBD		
	Qualcomm	29	●	TBD	TBD
30 - 60 GHz					
	Intel	40	Sep	Nov	Nov
	Ericsson	60	●	●	●
	NYU	60	● [2000]	● [2000]	
Qualcomm	60	July	TBD	TBD	
> 60 GHz	Aalto	63, 70	•	•	•
	NYU	73	● [Spring & Summer 2014]	● [Spring & Summer 2014]	
Intel	75, 82	Sep.	Nov	Nov	

11.1.7 InH shopping mall

Band	Party	GHz	Pathloss & Shadowing	Large Scale Parameters	Small Scale Parameters
< 30 GHz	CMCC	6	TBD	TBD	
	Nokia/Aalborg	2, 10, 18	●		

	Intel	10, 28	Sep.	Nov	Nov
	CMCC	14	Jul.	Jul.	
	Aalto	15	●	●	●
	Aalto	28	●	●	●
	Samsung	28	●	●	●
	Nokia/Aalborg	28	Sep.		
	Qualcomm	29	June	TBD	
30 - 60 GHz	Intel	40	Sep.	Nov	Nov
	Qualcomm	60	June	TBD	
	Univ. of Bristol	60	TBD (Spring 2016)	TBD (Spring 2016)	TBD (Spring 2016)
> 60 GHz	Aalto	63, 70	•	•	•
	Intel	75, 82	Sep.	Nov	Nov

11.2 Overview of ray-tracing campaigns

11.2.1 UMi street canyon O2O

Band	Party	GHz	Pathloss & Shadowing	Large Scale Parameters	Small Scale Parameters	Location Details
< 30 GHz	Aalto	15	Nov.	Nov.	Nov.	Greater Helsinki area
	Aalto	28	Nov.	Nov.	Nov.	Greater Helsinki area
	Samsung	28	●	●	●	Daejeon, Korea / Same location for measurement campaign
	Samsung	28	●	●	●	Ottawa
	Samsung	28	●	●	●	NYU Campus / Same location for NYU measurement

						campaign
	USC	28	●	●	●	
	Nokia	5.6,10.25, 28.5	●	●	●	Madrid-grid
30 - 60 GHz	Nokia	39.3	•	•	•	Madrid-grid
> 60 GHz	Aalto	63	Nov.	Nov.	Nov.	Greater Helsinki area
	Nokia	73	●	●	●	NYU Campus plus Madrid-grid

11.2.2 UMi open square O2O

Band	Party	GHz	Pathloss & Shadowing	Large Scale Parameters	Small Scale Parameters	Location Details
< 30 GHz	Nokia	5.6,10.25, 28.5	•	•	•	Madrid-grid
	Univ. of Bristol	28	TBD (Spring 2016)	TBD (Spring 2016)	TBD (Spring 2016)	Bristol / London
30 - 60 GHz	Nokia	39.3	•	•	•	Madrid-grid
	Univ. of Bristol	40 / 60	TBD (Spring 2016)	TBD (Spring 2016)	TBD (Spring 2016)	Bristol / London

> 60 GHz	Aalto	63	•	•	•	Helsinki city center
	Nokia	73.5	●	●	●	Madrid-grid

11.2.3 UMa O2O

Band	Party	GHz	Pathloss & Shadowing	Large Scale Parameters	Small Scale Parameters	Location Details
< 30 GHz	Nokia	5.6,10.25, 28.5	•	•	•	Madrid-grid
	Nokia/Aalborg	10, 18, 28	Sep.	Sep.	Oct.	Aalborg (same location as measurement campaigns)
	Samsung	28	●	●	●	Ottawa
	Samsung	28	●	●	●	NYU Campus
	Univ. of Bristol	28	TBD (Spring 2016)	TBD (Spring 2016)	TBD (Spring 2016)	Bristol / London
30 - 60 GHz	Univ. of Bristol	40 / 60	TBD (Spring 2016)	TBD (Spring 2016)	TBD (Spring 2016)	Bristol / London
	Nokia/Aalborg	39.3	Sep.	Sep.	Oct.	Aalborg (same location as measurement campaigns)
	Nokia	39.3	●	●	●	Madrid-grid
> 60 GHz	Nokia/Aalborg	73.5	Sep.	Sep.	Oct.	Aalborg (same location as measurement campaigns)
	Nokia	73.5	●	●	●	Madrid-grid

11.2.4 InH open-plan office

Band	Party	GHz	Pathloss & Shadowing	Large Scale Parameters	Small Scale Parameters	Location Details
< 30 GHz	Samsung	28	TBD	TBD	TBD (Sep)	Open-Office
30 - 60 GHz						
> 60 GHz	Nokia	73	•	•	•	Open-office at NYU campus

11.2.5 InH closed-plan office

Band	Party	GHz	Pathloss & Shadowing	Large Scale Parameters	Small Scale Parameters	Location Details
< 30 GHz						

30 - 60 GHz						
> 60 GHz	Aalto	63, 70	•	•	•	Large office, meeting room, cafeteria

11.2.6 InH shopping mall

Band	Party	GHz	Pathloss & Shadowing	Large Scale Parameters	Small Scale Parameters	Location Details
< 30 GHz	Samsung	28	TBD	TBD	TBD (Sep)	Shopping-mall like environment / Same location for measurement campaign
30 - 60 GHz						
60 GHz	Aalto	63, 70	•	•	•	A shopping mall in

Table 17. Angle spread ASA datasets of UMi street-canyon

UMi Street-Canyon		Ray-tracing Samsung - Ottawa										Ray-tracing Samsung - Daejeon								Ray-tracing Samsung - NYU Campus								
Frequency [GHz]		2	5	8	10	15	20	25	28	60	2.4	5	10	18	28	38	73	2	5	10	18	28	38	73				
ASA	LoS	Distribution	Log-Normal										Log-Normal								Log-normal							
		Med [deg]	44.23	43.25	42.99	42.87	43.05	43.25	43.15	43.37	42.91	43.27	41.80	41.54	41.33	41.21	41.22	40.82	84.04	79.68	79.32	78.56	77.45	76.87	72.91			
		mu [log10(deg)]	1.65	1.64	1.63	1.63	1.63	1.64	1.63	1.64	1.63	1.64	1.62	1.62	1.62	1.61	1.62	1.61	1.92	1.90	1.90	1.90	1.89	1.89	1.86			
		sigma [log10(deg)]	0.30	0.31	0.32	0.32	0.32	0.33	0.33	0.33	0.34	0.28	0.31	0.32	0.33	0.34	0.34	0.35	0.26	0.26	0.26	0.27	0.27	0.28	0.29			
	NLoS	Distribution	TBD										TBD								TBD							
		Med [deg]	82.52	53.78	53.70	57.72	59.86	61.51	64.20	65.88	74.18	54.68	46.94	40.31	45.03	44.41	45.50	51.26	71.30	55.85	52.30	55.97	59.86	59.59	59.40			
		mu [log10(deg)]	1.92	1.73	1.73	1.76	1.78	1.79	1.81	1.82	1.87	1.74	1.67	1.61	1.65	1.65	1.66	1.71	1.85	1.75	1.72	1.75	1.78	1.78	1.77			
		sigma [log10(deg)]	0.29	0.40	0.41	0.40	0.39	0.40	0.39	0.40	0.41	0.28	0.36	0.46	0.39	0.42	0.44	0.37	0.38	0.43	0.45	0.45	0.43	0.44	0.45			
	PDP-cutoff Value [dB]		No cutoff										No cutoff								No cutoff							
	PathPower-cutoff Value [dB]		-170										-170								-170							

UMi Street-Canyon		Ray-tracing Intel				Measurement Samsung - DJ	Measurement Samsung/KT -PyCh	Measurement NYU WIRELESS-NYC	Measurement ETRI - Daejeon	Measurement Aalto Univ.				Measurement CMCC				
Frequency [GHz]		6	15	28	73.5	28	28	28	73	28	38	5.3	15	28	60	3.5	6	
ASA	LoS	Distribution																
		Med [ns]	51.00	51.00	51.00	51.00			50.90	50.90	16.8	18.2	17.38	10.5	19.8	14.5	56	51.29
		mu [log10(deg)]	1.71	1.71	1.71	1.71			1.69	1.69	1.23	1.26	1.24	1.02	1.30	1.16	1.75	1.71
		sigma [log10(deg)]							0.27	0.27	0.25	0.22	0.53				0.19	0.12
	NLoS	Distribution																
		Med [ns]	61.60	52.80	50.60	39.60	33.48	43.11	25.20	37.00	42.2	38.7	27.54				69	60.26
		mu [log10(deg)]	1.79	1.72	1.70	1.60	1.52	1.63	1.40	1.57	1.63	1.59	1.4				1.84	1.78
		sigma [log10(deg)]					0.21		0.34	0.32	0.21	0.16	0.34				0.15	0.15
	PDP-cutoff Value [dB]		Unknown				Unknown	Unknown	Unknown	25	Unknown				Unknown			
	PathPower-cutoff Value [dB]		Unknown				Unknown	Unknown	Unknown	Unknown	Unknown				Unknown			

Table 18. Angle spread ZSA datasets of UMi street-canyon.

UMi Street-Canyon		Ray-tracing Samsung - Ottawa										Ray-tracing Samsung - Daejeon								Ray-tracing Samsung - NYU Campus								
Frequency [GHz]		2	5	8	10	15	20	25	28	60	2.4	5	10	18	28	38	73	2	5	10	18	28	38	73				
ZSA	LoS	Distribution	TBD										TBD								TBD							
		Med [deg]	2.67	2.89	2.90	2.91	2.92	3.18	3.19	3.19	3.52	7.02	5.60	5.00	4.65	4.07	4.11	3.76	3.72	3.72	3.84	3.87	3.88	3.91	3.94			
		mu [log10(deg)]	0.43	0.46	0.46	0.46	0.46	0.50	0.50	0.50	0.55	0.85	0.75	0.70	0.67	0.61	0.61	0.57	0.57	0.57	0.58	0.59	0.59	0.59	0.60			
		(optional mu model)	Distance-dependent model $\mu = \max(a \cdot d_{2D}/1000 + b, c)$										Distance-dependent model $\mu = \max(a \cdot d_{2D}/1000 + b, c)$								Distance-dependent model $\mu = \max(a \cdot d_{2D}/1000 + b, c)$							
		a Avg. -33	-32.40	-36.29	-36.39	-36.43	-36.44	-42.52	-42.57	-42.58	-49.83	-26.58	-29.87	-30.92	-31.55	-32.10	-32.11	-34.66	-29.75	-31.98	-33.23	-33.73	-36.38	-12.55	-8.00			
		b Avg. 1.9	1.86	1.89	1.89	1.89	1.89	1.95	1.95	1.95	1.97	2.05	2.11	2.12	2.12	2.11	2.08	2.05	1.83	1.86	1.86	1.86	1.89	1.27	1.25			
	c Avg. 0.37	0.34	0.37	0.37	0.37	0.40	0.40	0.40	0.40	0.43	0.19	0.25	0.28	0.31	0.35	0.40	0.50	0.41	0.41	0.42	0.42	0.42	0.41	0.37				
	sigma [log10(deg)]	0.43	0.46	0.46	0.46	0.46	0.50	0.50	0.50	0.55	0.85	0.75	0.70	0.67	0.61	0.61	0.57	0.57	0.57	0.58	0.59	0.59	0.59	0.60				
	NLoS	Distribution	TBD										TBD								TBD							
		Med [deg]	7.23	7.55	7.44	7.58	7.50	7.52	7.50	7.50	7.62	8.31	8.46	8.76	9.38	9.98	10.59	12.44	7.27	6.31	5.90	5.85	5.86	5.83	5.81			
mu [log10(deg)]		0.86	0.88	0.87	0.88	0.87	0.88	0.87	0.88	0.88	0.92	0.93	0.94	0.97	1.00	1.02	1.09	0.86	0.80	0.77	0.77	0.77	0.77	0.76				
sigma [log10(deg)]		0.25	0.42	0.41	0.34	0.29	0.27	0.23	0.23	0.20	0.30	0.35	0.47	0.44	0.40	0.34	0.23	0.36	0.40	0.40	0.36	0.35	0.35	0.34				
PDP-cutoff Value [dB]		No cutoff										No cutoff								No cutoff								
PathPower-cutoff Value [dB]		-170										-170								-170								

UMi Street-Canyon		Measurement NYU WIRELESS-NYC		Measurement CMCC		Measurement Aalto Univ.		
Frequency [GHz]		28	73	3.5	6	5.3		
ZSA	LoS	Distribution						
		Med [ns]	4	4	7.24	24	4.17	
		mu [log10(deg)]	0.6	0.6	0.86	1.38	0.62	
		sigma [log10(deg)]	0.09	0.09	0.02	0.13		
	NLoS	Distribution						
		Med [ns]	6.1	3.5	7.76	22.9	3.74	
		mu [log10(deg)]	0.79	0.54	0.89	1.36	0.57	
		sigma [log10(deg)]	0.3	0.15	0.42	0.21		
	PDP-cutoff Value [dB]		Unknown		Unknown		Unknown	
	PathPower-cutoff Value [dB]		Unknown		Unknown		Unknown	

Table 19. Angle spread ZSD datasets of UMi street-canyon.

UMi Street-Canyon			Ray-tracing										Ray-tracing										Ray-tracing									
			Samsung - Ottawa										Samsung - Daejeon										Samsung - NVU Campus									
Frequency [GHz]			2	5	8	10	15	20	25	28	60	2.4	5	10	18	28	38	73	2	5	10	18	28	38	73							
ZSD	LoS	Distribution	TBD										TBD										TBD									
		Med [deg]	0.53	0.54	0.54	0.54	0.55	0.59	0.59	0.59	0.63	3.14	1.53	1.50	2.32	2.02	1.81	1.44	0.73	0.68	0.69	0.70	0.71	0.71	0.72							
		mu [log10(deg)]	-0.28	-0.27	-0.27	-0.27	-0.26	-0.23	-0.23	-0.23	-0.20	0.50	0.19	0.18	0.37	0.31	0.26	0.16	-0.14	-0.17	-0.16	-0.16	-0.15	-0.15	-0.14							
		3D-SCM mu model	Distance-dependent model $\mu = \max(a \cdot d_{2D}/1000 + b, c)$										Distance-dependent model $\mu = \max(a \cdot d_{2D}/1000 + b, c)$										Distance-dependent model $\mu = \max(a \cdot d_{2D}/1000 + b, c)$									
		a Avg. -14.8	-17.64	-19.64	-19.70	-20.99	-21.05	-20.57	-20.67	-20.60	-11.65	-11.29	-15.95	-16.10	-12.05	-12.16	-12.22	-12.00	-11.64	-11.63	-12.04	-11.83	-11.55	-10.39	-8.00							
	b Avg. 0.83	0.85	0.86	0.86	0.89	0.88	0.84	0.85	0.84	0.58	0.93	0.96	0.96	0.86	0.84	0.83	0.78	0.82	0.79	0.80	0.79	0.78	0.74	0.67								
	c Avg. -0.21	-0.27	-0.25	-0.25	-0.25	-0.24	-0.22	-0.21	-0.21	-0.20	-0.23	-0.30	-0.30	-0.29	-0.29	-0.28	-0.27	-0.12	-0.14	-0.12	-0.11	-0.10	-0.10	-0.11								
	sigma [log10(deg)]	0.34	0.36	0.36	0.36	0.37	0.36	0.36	0.36	0.37	0.39	0.42	0.42	0.40	0.39	0.39	0.37	0.30	0.30	0.30	0.31	0.31	0.31	0.31								
	NLoS	Distribution	TBD										TBD										TBD									
		Med [deg]	0.50	0.49	0.48	0.48	0.48	0.48	0.49	0.48	0.49	0.70	0.64	0.62	0.61	0.62	0.65	0.64	0.69	0.56	0.51	0.49	0.48	0.47	0.46							
mu [log10(deg)]		-0.30	-0.31	-0.32	-0.32	-0.32	-0.32	-0.31	-0.31	-0.31	-0.16	-0.20	-0.20	-0.22	-0.20	-0.18	-0.19	-0.16	-0.25	-0.30	-0.31	-0.32	-0.33	-0.33								
3D-SCM mu model		Distance-dependent model $\mu = \max(a \cdot d_{2D}/1000 + b, c)$										Distance-dependent model $\mu = \max(a \cdot d_{2D}/1000 + b, c)$										Distance-dependent model $\mu = \max(a \cdot d_{2D}/1000 + b, c)$										
a Avg. -3.06		-2.35	-2.27	-2.12	-1.92	-2.42	-2.61	-2.51	-2.65	-2.30	-5.50	-4.63	-5.56	-4.74	-5.20	-5.00	-4.76	-0.61	-0.74	-1.27	-2.28	-2.74	-3.01	-3.20								
b Avg. 0.18	0.12	0.05	0.01	-0.04	0.03	0.06	0.03	0.06	0.04	0.53	0.41	0.43	0.36	0.38	0.36	0.33	0.08	0.01	0.05	0.16	0.20	0.22	0.24									
c Avg. 0.5	-0.27	-0.49	-0.63	-0.64	-0.71	-0.74	-0.75	-0.77	-0.63	-0.33	-0.53	-0.36	-0.38	-0.32	-0.29	-0.29	-0.21	-0.40	-0.42	-0.50	-0.51	-0.51	-0.54									
sigma [log10(deg)]	0.30	0.42	0.43	0.41	0.40	0.39	0.38	0.37	0.28	0.28	0.35	0.28	0.30	0.26	0.24	0.23	0.42	0.42	0.38	0.35	0.33	0.33	0.33									
PDP-cutoff Value [dB]			No cutoff										No cutoff										No cutoff									
PathPower-cutoff Value [dB]			-170										-170										-170									

UMi Street-Canyon			Measurement		Measurement		Measurement		
			NYU WIRELESS-NYC		CMCC		Aalto Univ		
Frequency [GHz]			28	73	3.5	6	5.3		
ZSD	LoS	Distribution							
		Med [ns]			7.41	19.05	9.01		
		mu [log10(deg)]			0.87	1.28	0.95		
		sigma [log10(deg)]			0.39	0.29			
		3D-SCM mu model							
	NLoS	Distribution							
		Med [ns]			2.88	10.96	16.98	3.69	
		mu [log10(deg)]			0.46	1.04	1.23	0.57	
		sigma [log10(deg)]			0.18	0.65	0.44		
		3D-SCM mu model							
PDP-cutoff Value [dB]			Unknown		Unknown		Unknown		
PathPower-cutoff Value [dB]			Unknown		Unknown		Unknown		

Table 20. Cluster Parameters of UMi street-canyon.

UMi Street-Canyon			Ray-tracing										3GPP 3D-SCM UMi
			Samsung - Ottawa										
Frequency [GHz]			2.0	5.0	8.0	10.0	15.0	20.0	25.0	28.0	60.0		
Number of Cluster, N	LoS	median	6	6	6	6	6	6	5	5	5	12	
	NLoS	median	5	6	6	5	5	5	5	5	5		19
Number of rays per cluster, M	LoS	median	4	4	4	4	4	4	4	4	4	20	
		Mean	4.22	3.90	4.03	4.13	4.22	4.16	4.32	4.40	4.33		
	NLoS	Median	2	2	2	2	3	3	3	3	3	20	
		Mean	4.48	4.53	4.48	4.59	4.62	4.64	4.72	4.71	4.82		
Cluster DS	LoS	median	31.17	25.43	24.96	24.59	23.29	21.44	21.59	17.83	13.87		
	NLoS	median	10	13.58	13.76	13.93	11.48	10.56	10.64	11	8.04		
Cluster ASD	LoS	median	3.70	3.88	3.28	3.34	3.50	3.01	2.92	2.89	2.70	3	
	NLoS	median	1.87	2.13	1.58	1.79	1.62	1.54	1.76	1.54	1.87		10
Cluster ZSA	LoS	median	2.64	2.58	2.47	2.47	2.62	2.59	2.51	2.51	2.89	7	
	NLoS	median	1.55	1.54	1.46	1.54	1.52	1.53	1.48	1.54	1.54		7
Cluster SF	LoS	std	5.25	5.74	6.03	6.30	6.58	5.66	3.96	5.69	3.76	3	
	NLoS	std	6.72	8.36	8.53	8.83	10.03	9.97	10.30	10.47	10.52		3

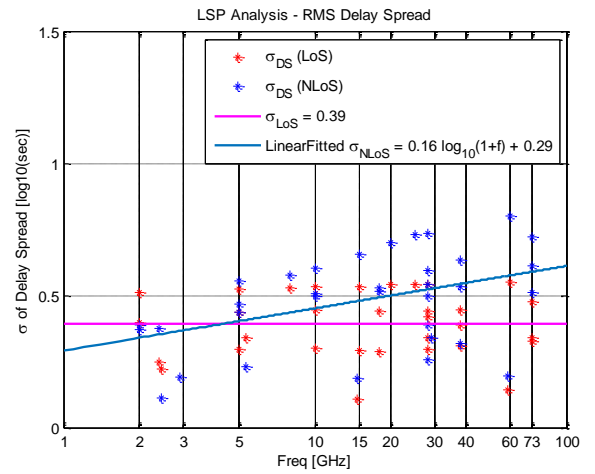
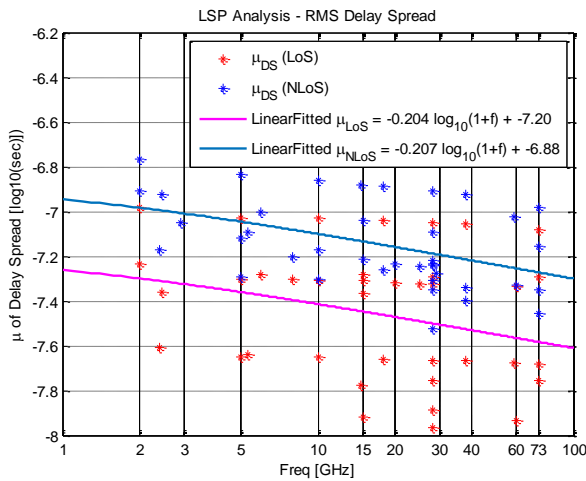


Figure 39. Delay Spread modeling for parameters of log-normal distributions over frequency

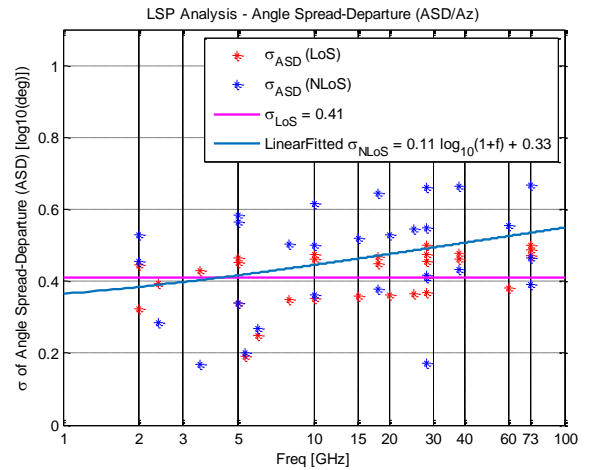
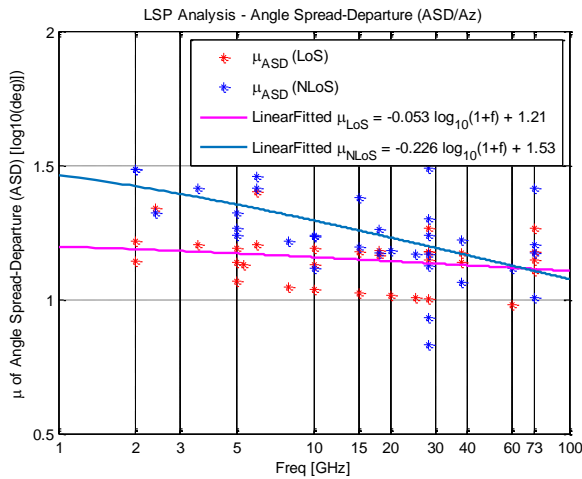


Figure 40. Angle Spread/ASD modeling for parameters of log-normal distributions over frequency

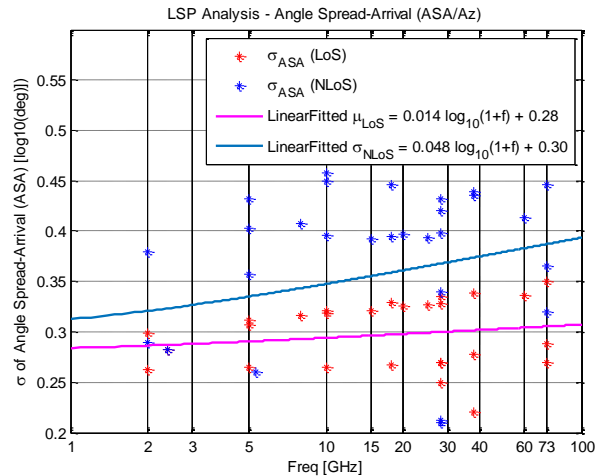
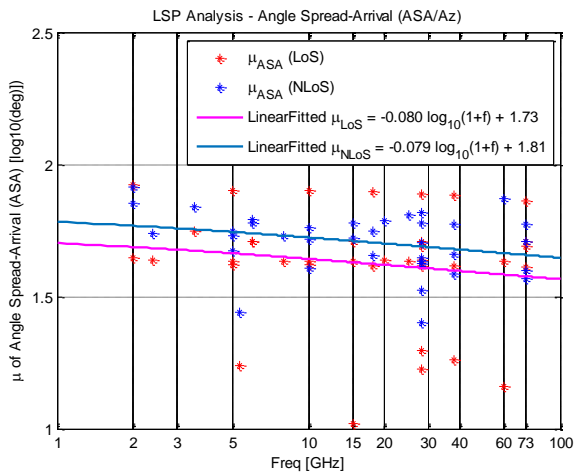


Figure 41. Angle Spread/ASA modeling for parameters of log-normal distributions over frequency

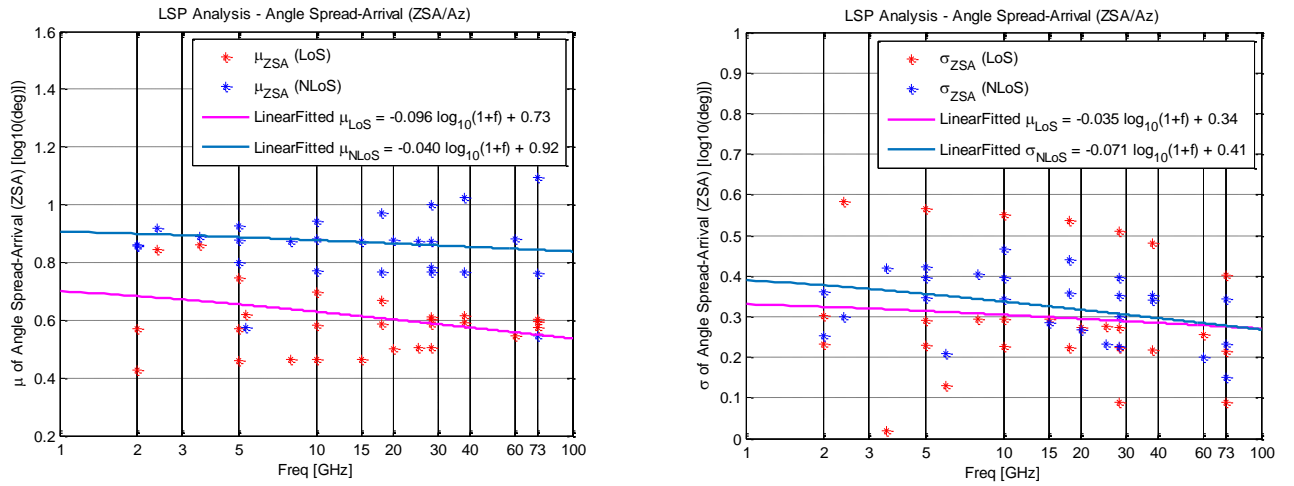


Figure 42. Angle Spread/ZSA modeling for parameters of log-normal distributions over frequency

Table 21. Preliminary UMi cluster parameters

	28 GHz ¹		73 GHz ²	
	LoS	NLoS	LoS (28-73 Combined)	NLoS
Clustering Algorithm	K-Means algorithm		K-Means algorithm	
Ave. number of clusters	6	6	5.0	4.6
Ave. number of rays per cluster	10	10	12.4	13.2
Cluster DS (nsec)	TBD	TBD	TBD	TBD
Cluster ASA (degrees)	3.3	6.7	6.7	5.2
Cluster ASD (degrees)	2.7	5.7	1.5	2.1
Cluster ZSA (degrees)	3.9	4.9	1.8	1.5
Cluster ZSD (degrees)	1.2	1.6	N/A	0.8
Per-cluster shadow fading (dB)	5	5	13.6	17.4

Table 22. Preliminary UMi correlations for large-scale parameters

	28 GHz ¹		73 GHz ²	
	LoS	NLoS	LoS(28-73 Combined)	NLoS
ASD vs. DS	-0.25	0.37	0.32	0.054
ASA vs. DS	0.35	0.43	0.49	0.282
ASA vs. SF	-0.01	0.03	0.54	0.042
ASD vs. SF	-0.24	0.16	-0.04	0.009
DS vs. SF	0.22	0.30	0.35	-0.177
ASD vs. ASA	-0.67	0.09	0.72	-0.256
ZSD vs. SF	0.23	0.13	N/A	-0.430

ZSA vs. SF	0.16	0.10	0.16	-0.389
ZSD vs. DS	0.27	0.50	N/A	0.950
ZSA vs. DS	0.14	0.19	0.44	0.108
ZSD vs. ASD	-0.32	0.36	N/A	0.49
ZSA vs. ASD	-0.39	0.10	0.95	-0.263
ZSD vs. ASA	0.33	0.20	N/A	0.950
ZSA vs. ASA	0.37	0.02	0.72	0.232
ZSD vs. ZSA	0.92	0.52	N/A	-0.960

1. From Samsung based on ray-tracing
2. From NYU based on measurement [Samimi EUCAP2016]

11.3.2 UMa

Table 23. UMa NLOS channel model parameters (part 1)

Parameters		Symbol	NLOS UMa	
			3GPP ≤6 GHz	>6 GHz
Delay Spread	DS median [ns] (linear scale)	median	360.67	-
	logDS = log10(DS / 1ns)	μ	2.56	2.72-0.204log10(f/1 GHz)
		σ	0.39	0.39
Azimuth / Departure Angle Spread	ASD median [deg](linear scale)	median	25.78	-
	logASD = log10(ASD / 1deg)	μ	1.41	1.5-0.1144log10(f/1 GHz)
		σ	0.28	0.28
Azimuth / Arrival Angle Spread	ASA median [deg](linear scale)	median	74.2	-
	logASA = log10(ASA / 1deg)	μ	1.87	2.08-0.27*log10(f/1 GHz)
		σ	0.11	0.11

Table 24. UMa NLOS channel model parameters (part 2)

Parameters		Symbol	NLOS UMa	
			3GPP	>6 GHz
Zenith / Departure Angle Spread	[based on 3D-SCM] Mean of lgZSD $\mu = \max(ad + b, c)$ ($d = 2D$ -distance in m)	a	-0.0021	-0.0021
		b	0.75	0.75
		c	-0.5	-0.5
ZoD offsets	ZoD_Offset = $e^{-10^{(a \log_{10}(\max(b, d) + c))}}$ [deg] ($d = 2D$ -distance in m)	a	-0.62	$0.208 \log_{10}(f/1 \text{ GHz}) - 0.782$
		b	10	25
		c	1.93	$-0.13 \log_{10}(f/1 \text{ GHz}) + 2.03$
		e	0	$7.66 \log_{10}(f/1 \text{ GHz}) - 5.96$
	Std. dev. of $\log_{10}(\text{ZoD_Offset})$	σ	-	0.19

Table 25. UMa NLOS channel model parameters (part 3)

Parameters		Symbol	NLOS UMa	
			3GPP	>6 GHz
Zenith / Arrival Angle Spread	ZSA median [deg] (linear scale)	median	18.2	-
	$\lg\text{ZSA} = \log_{10}(\text{ZSA} / 1\text{deg})$	μ	1.26	$-0.3236 \log_{10}(f/1 \text{ GHz}) + 1.512$
		σ	0.16	0.16
ZoA offsets		-	0	0

Table 26. UMa NLOS channel model parameters (part 4)

Parameters	Symbol	NLOS UMa	
		3GPP	>6 GHz
Shadow fading [dB]	SF	6	6.8
XPR [dB]	μ	7	7
	σ	3	3
Delay distribution		Exponential	
AoD and AoA distribution		Wrapped Gaussian	
ZoD and ZoA distribution		Laplacian	
Delay scaling parameter		2.3	2.3

Table 27. UMa NLOS channel model parameters (part 5)

Parameters	Sym bol	NLOS UMa		
		3GPP	>6 GHz	
Clustering	Number of Cluster	N	20	20
	Number of subpath	M	20	20
	Cluster DS [ns]		-	$-53\log_{10}(f/1 \text{ GHz})+151.4$
	Cluster ASD [deg]		2	2
	Cluster ASA [deg]		15	15
	Cluster ZSD [deg]		$(3/8)10^{(u_ZSD)}$	$(3/8)10^{(u_ZSD)}$
	Std. dev. of log10(clust ZSD)		-	0.75
	Cluster ZSA [deg]		7	7
	Std. dev. of log10(clust ZSA)		-	0.69
	Per-cluster shadowing std [dB]		3	3

Table 28. UMa NLOS channel model parameters (part 6)

		Symbol	NLOS UMa
			3GPP and >6 GHz
Correlation distance [m]	DS [s]		40
	ASD [deg]		50
	ASA [deg]		50
	ZSD [deg]		50
	ZSA [deg]		50
	SF [dB]		50
	K [dB]		-

Table 29. UMa NLOS channel model parameters (part 7)

Parameters		Symbol	3GPP and >6 GHz
Cross – correlations	ASD [deg] vs DS [s]		0.4
	ASA [deg] vs DS [s]		0.6
	ASA [deg] vs SF [dB]		0
	ASD [deg] vs SF [dB]		-0.6
	DS[s] vs SF[dB]		-0.4
	ASD [deg] vs ASA [deg]		0.4
	ASD [deg] vs K [dB]		-
	ASA [deg] vs K [dB]		-
	DS [s] vs K [dB]		-
	SF [dB] vs K [dB]		-
	ZSD [deg] vs SF [dB]		0
	ZSA [deg] vs SF [dB]		-0.4
	ZSD [deg] vs K [dB]		-
	ZSA [deg] vs K [dB]		-
	ZSD [deg] vs DS [s]		-0.5
	ZSA [deg] vs DS [s]		0
	ZSD [deg] vs ASD [deg]		0.5
	ZSA [deg] vs ASD [deg]		-0.1
	ZSD [deg] vs ASA [deg]		0
	ZSA [deg] vs ASA [deg]		0
ZSD [deg] vs ZSA [deg]		0	

Table 30. UMa LOS channel model parameters (part 1)

Parameters		Symbol	LOS UMa	
			3GPP ≤6 GHz	>6 GHz
Delay Spread	DS median [ns] (linear scale)	median	93.79	-
	logDS = log ₁₀ (DS / 1ns)	μ	1.97	2.045-0.0963log ₁₀ (f/1 GHz)
		σ	0.66	0.66
Azimuth / Departure Angle Spread	ASD median [deg](linear scale)	median	14.17	-
	logASD = log ₁₀ (ASD / 1deg)	μ	1.15	1.06+0.1114log ₁₀ (f/1GHz)
		σ	0.28	0.28
Azimuth / Arrival Angle Spread	ASA median [deg](linear scale)	median	64.51	64.51
	logASA = log ₁₀ (ASA / 1deg)	μ	1.81	1.81
		σ	0.20	0.20

Table 31. UMa LOS channel model parameters (part 2)

Parameters		Symbol	LOS UMa	
			3GPP	>6 GHz
Zenith / Departure Angle Spread	[based on 3D-SCM] Mean of lgZSD μ = max(ad + b, c) (d = 2D-distance in m)	a	-0.0021	-0.0021
		b	0.75	0.75
		c	-0.5	-0.5
ZoD offsets	ZoD_Offset (degrees)		0	0

Table 32. UMa LOS channel model parameters (part 3)

Parameters		Symbol	LOS UMa	
			3GPP	>6 GHz
Zenith / Arrival Angle Spread	ZSA median [deg] (linear scale)	median	8.92	8.92
	lgZSA = log ₁₀ (ZSA / 1deg)	μ	0.95	0.95
		σ	0.16	0.16
ZoA offsets	ZoA_Offset (degrees)		0	0

Table 33. UMa LOS channel model parameters (part 4)

Parameters		Symbol	LOS UMa	
			3GPP	>6 GHz
Shadow fading [dB]		SF	4.0	4.1
K-factor [dB]		μ	9	9
		σ	3.5	3.5
XPR [dB]		μ	8	8
		σ	4	4
Delay distribution			Exponential	
AoD and AoA distribution			Wrapped Gaussian	
ZoD and ZoA distribution			Laplacian in 3GPP	
Delay scaling parameter			2.5	2.5

Table 34. UMa LOS channel model parameters (part 5)

Parameters		Symbol	LOS UMa	
			3GPP	>6 GHz
Clustering	Number of Cluster	N	12	12
	Number of subpath	M	20	20
	Cluster DS [ns]		-	$-70\log_{10}(f/1\text{ GHz})+164.5$
	Cluster ASD [deg]		5	5
	Cluster ASA [deg]		11	11
	Cluster ZSD [deg]		$(3/8)10^{(u_{ZSD})}$	$(3/8)10^{(u_{ZSD})}$
	Std. dev. of log10(clust ZSD)		-	0.64
	Log10 Cluster ZSA		7	7
	Std. dev. of log10(clust ZSA)		-	0.70
	Per-cluster shadowing std [dB]		3	3

Table 35. UMa LOS channel model parameters (part 6)

		Symbol	LOS UMa
			3GPP and >6 GHz
Correlation distance [m]	DS [s]		30
	ASD [deg]		18
	ASA [deg]		15
	ZSD [deg]		15
	ZSA [deg]		15
	SF [dB]		37
	K [dB]		12

Table 36. UMa LOS channel model parameters (part 7)

Parameters		Symbol	LOS UMa
			3GPP and >6 GHz
Cross – correlations	ASD [deg] vs DS [s]		0.4
	ASA [deg] vs DS [s]		0.8
	ASA [deg] vs SF [dB]		-0.5
	ASD [deg] vs SF [dB]		-0.5
	DS[s] vs SF[dB]		-0.4
	ASD [deg] vs ASA [deg]		0
	ASD [deg] vs K [dB]		0
	ASA [deg] vs K [dB]		-0.2
	DS [s] vs K [dB]		-0.4
	SF [dB] vs K [dB]		0
	ZSD [deg] vs SF [dB]		0
	ZSA [deg] vs SF [dB]		-0.8
	ZSD [deg] vs K [dB]		0
	ZSA [deg] vs K [dB]		0
	ZSD [deg] vs DS [s]		-0.2
	ZSA [deg] vs DS [s]		0
	ZSD [deg] vs ASD [deg]		0.5
	ZSA [deg] vs ASD [deg]		0
	ZSD [deg] vs ASA [deg]		-0.3
	ZSA [deg] vs ASA [deg]		0.4
ZSD [deg] vs ZSA [deg]		0	

11.3.3 InH

Table 37. Preliminary Indoor office large-scale channel characteristics (part 1)

		3.5GHz ¹		6GHz ¹		20 GHz ²	28GHz ³	73GHz ⁴	73GHz ⁵		28GHz ⁵	
Scenarios		LOS	NLOS	LOS	NLOS	LOS	LOS	Hybrid	LOS	NLOS	LOS	NLOS
Delay spread (σ_τ) \log_{10} (seconds)	Median(ns)	TBD	TBD	TBD	TBD	TBD	TBD	TBD	14.53	23.06	10.58	23.28
	μ_{DS}	TBD	TBD	TBD	TBD	-7.33	-7.75	-8.1	-7.85	-7.67	-7.97	-7.7
	ϵ_{DS}	TBD	TBD	TBD	TBD	0.1	0.13	0.4	0.18	0.2	0.25	0.2
Delay distribution		TBD	TBD	TBD	TBD	TBD	Exponential	Exponential	Exponential			
AoA spread (σ_{ASA}) \log_{10} (degrees)	Median(deg)	TBD	TBD	TBD	TBD	TBD	TBD	TBD	30.48	37.46	28.24	47.51
	μ_{ASA}	3GPP	3GPP	1.72	1.49	TBD	1.57	1.6	1.46	1.54	1.43	1.66
	ϵ_{ASA}	3GPP	3GPP	0.14	0.23	TBD	0.22	0.37	0.13	0.19	0.14	0.12
AoD spread (σ_{ASD}) \log_{10} (degrees)	Median(deg)	TBD	TBD	TBD	TBD	TBD	TBD	TBD	TBD	TBD	TBD	TBD
	μ_{ASD}	3GPP	3GPP	1.34	1.49	1.8	1.08	1.5	TBD	TBD	TBD	TBD
	ϵ_{ASD}	3GPP	3GPP	0.15	0.08	0.09	0.23	0.26	TBD	TBD	TBD	TBD
ZoA spread (σ_{ZSA}) \log_{10} (degrees)	Median(deg)	TBD	TBD	TBD	TBD	TBD	TBD	TBD	4.37	5.71	9.9	6.24
	μ_{ZSA}	1.02	1.08	1.33	0.95	TBD	0.67	-0.025d+1.18	0.62	0.76	1	0.79
	ϵ_{ZSA}	0.41	0.36	0.07	0.28	TBD	0.17	0.30	0.14	0.08	0.05	0.08
ZoD spread (σ_{ZSD}) \log_{10} (degrees)	Median(deg)	TBD	TBD	TBD	TBD	TBD	TBD	TBD	TBD	TBD	TBD	TBD
	μ_{ZSD}	1.22	1.26	1.25	1.48	0	0.40	-0.040d+1.45	TBD	TBD	TBD	TBD
	ϵ_{ZSD}	0.23	0.67	0.25	0.09	0.48	0.23	0.33	TBD	TBD	TBD	TBD
AoD and AoA distribution		TBD	TBD	TBD	TBD	TBD	Laplacian	Uniform	Wrapped Gaussian			
ZoD and ZoA distribution		Gaussian		TBD	TBD	TBD	Laplacian	Laplacian	Laplacian			
Delay scaling parameter r_τ		TBD	TBD	TBD	TBD	TBD	1.95	2.4	2.03	1.35	2.23	1.78
XPR (dB)	μ_{XPR}	TBD	TBD	TBD	TBD	TBD	TBD	15	10	6	TBD	TBD
	σ_{XPR}	TBD	TBD	TBD	TBD	TBD	TBD	2	7.5	10	TBD	TBD

LOS Ricean K factor (dB) *	μ_k	TBD	8	TBD	N/A	TBD	N/A						
	ϵ_k	TBD	3	TBD	N/A	TBD	N/A						

1. From BUPT based on measurement
2. From DOCOMO based on measurement
3. From KT based on measurement
4. From Nokia/NYU based on ray-tracing
5. From Huawei based on measurement

Table 38. Preliminary Indoor office large-scale channel characteristics (part 2)

		14GHz ¹		28GHz ¹		15GHz ²		2.9GHz ³		29GHz ³		28GHz ⁴		73GHz ⁴	
Scenarios		LOS	NLOS	LOS	NLOS	LOS	NLOS	LOS	NLOS	LOS	NLOS	LOS	NLOS	LOS	NLOS
Delay spread (σ_r) \log_{10} (seconds)	Median(ns)	27.78	36.92	29.35	43.16	22.9	42.4	24	45	25	36	TBD	TBD	TBD	TBD
	μ_{DS}	-7.60	-7.47	-7.55	-7.41	-7.65	-7.43	-7.7	-7.4	-7.6	-7.5	TBD	TBD	TBD	TBD
	ϵ_{DS}	0.27	0.22	0.15	0.17	0.2	0.17	0.29	0.14	0.37	0.18	TBD	TBD	TBD	TBD
Delay distribution		TBD	TBD	TBD	TBD	TBD	TBD	Exponential				TBD	TBD	TBD	TBD
XPR (dB)	μ_{XPR}	TBD	TBD	TBD	TBD	TBD	TBD	TBD	TBD	TBD	TBD	14	10.4	22.8	15.4
	σ_{XPR}	TBD	TBD	TBD	TBD	TBD	TBD	TBD	TBD	TBD	TBD	1.5	9.7	2.4	8

1. From CMCC&BUPT based on measurement
2. From Ericsson based on measurement
3. From Qualcomm based on measurement
4. From NYU based on measurement

Table 39. Preliminary Indoor office large-scale channel characteristics (part 3)

Parameters		3.5GHz ¹		20GHz ²	28GHz ³	73GHz ⁴	28GHz ⁵		73GHz ⁵	
		LOS	NLOS	LOS	LOS	Hybrid	LOS	NLOS	LOS	NLOS
Correlation distance (m)	DS [ns]	TBD	TBD	TBD		TBD	2.26	2.47	1.85	1.69
	ASD [deg]	TBD	TBD	TBD		TBD	2.01	1.83	1.96	0.67

	ASA [deg]	TBD	TBD	TBD		TBD	2.07	2.61	2.06	1.62
	ZSD [deg]	4	4	TBD		TBD	3.01	2/23	3.03	2.02
	ZSA [deg]	4	4	TBD		TBD	2.65	2.54	2.09	0.83
	SF [dB]	TBD	TBD	TBD		TBD	1.64	1.14	0.28	2.45
	K [dB]	TBD	TBD	TBD		TBD	1.62	1.13	0.28	2.41
Cross Correlation	ASD [deg] vs DS [s]	3GPP	3GPP	0.26	0.481	0.47	TBD	TBD	TBD	TBD
	ASA [deg] vs DS [s]	3GPP	3GPP	TBD	0.5433	0.28	0.83	-0.03	0.69	-0.1
	ASA [deg] vs SF [dB]	TBD	TBD	TBD	0.0454	TBD	0.07	-0.55	-0.41	-0.13
	ASD [deg] vs SF [dB]	TBD	TBD	-0.68	0.3111	TBD	TBD	TBD	TBD	TBD
	DS[s] vs SF[dB]	TBD	TBD	-0.33	0.3318	TBD	0.44	0.35	-0.24	0.6
	ASD [deg] vs ASA [deg]	3GPP	3GPP	TBD	0.6236	0.15	TBD	TBD	TBD	TBD
	ASD [deg] vs K [dB]	TBD	TBD	TBD		TBD	TBD	TBD	TBD	TBD
	ASA [deg] vs K [dB]	TBD	TBD	TBD		TBD	TBD	TBD	TBD	TBD
	DS [s] vs K [dB]	TBD	TBD	TBD		TBD	TBD	TBD	TBD	TBD
	SF [dB] vs K [dB]	TBD	TBD	TBD		TBD	TBD	TBD	TBD	TBD
	ZSD [deg] vs SF [dB]	0.18	0	0.02	0.3749	TBD	TBD	TBD	TBD	TBD
	ZSA [deg] vs SF [dB]	0.34	0	TBD	0.3313	TBD	-0.52	-0.01	-0.68	-0.27
	ZSD [deg] vs K [dB]	0	N/A	TBD		TBD	TBD	TBD	TBD	TBD
	ZSA [deg] vs K [dB]	0.1	N/A	TBD		TBD	TBD	TBD	TBD	TBD
	ZSD [deg] vs DS [s]	0	-0.27	0.24	0.1752	0.07	TBD	TBD	TBD	TBD
	ZSA [deg] vs DS [s]	0	-0.06	TBD	0.4963	-0.01	-0.2	-0.12	0.41	-0.24
	ZSD [deg] vs ASD [deg]	0.65	0.35	0.1	-0.3449	0.21	TBD	TBD	TBD	TBD
	ZSA [deg] vs ASD [deg]	0	0.23	TBD	0.5116	0.1	TBD	TBD	TBD	TBD
	ZSD [deg] vs ASA [deg]	0	-0.08	TBD	-0.0418	0.22	TBD	TBD	TBD	TBD
	ZSA [deg] vs ASA [deg]	0.62	0.43	TBD	0.6429	0.06	-0.03	-0.28	0.61	-0.37
ZSD [deg] vs ZSA [deg]	0.05	0.42	TBD	0.0975	0.44	TBD	TBD	TBD	TBD	

1. From BUPT based on measurement
2. From DOCOMO based on measurement
3. From KT based on measurement
4. From Nokia/NYU based on ray-tracing
5. From Huawei based on measurement
- 6.

Table 40. Preliminary Indoor shopping mall large-scale channel characteristics (part 1)

		15GHz ¹		28GHz ¹		63 GHz ¹		2.9GHz ²		29GHz ²		61GHz ²		28GHz ³		38GHz ³		28GHz ⁴		38GHz ⁴	
Scenario		LOS	NLOS	LOS	NLOS	LOS	NLOS	LOS	NLOS	LOS	NLOS	LOS	NLOS	LOS	NLOS	LOS	NLOS	LOS	NLOS	LOS	NLOS
Delay spread (σ_τ)	Median(ns)	45.88	49.69	33.91	39.65	25.68	38.4	49	80	57	71	39	58	TBD	TBD	TBD	TBD	TBD	TBD	TBD	TBD
	$\log_{10}(\text{seconds})$																				
	μ_{DS}	-7.45	-7.31	-7.49	-7.45	-7.62	-7.46	-7.4	-7.1	-7.3	-7.2	-7.5	-7.3	-7.48	-7.28	-7.53	-7.24	-7.38	-6.88	-7.59	-6.9
	ϵ_{DS}	0.31	0.24	0.16	0.25	0.2	0.22	0.3	0.2	0.3	0.23	0.34	0.26	0.37	0.18	0.34	0.13	0.3	0.2	0.49	0.19
Delay distribution		Exponential						Exponential						TBD	TBD	TBD	TBD	TBD	TBD	TBD	TBD
AoA spread (σ_{ASA})	Median(deg)	47.42	34.94	34.52	38.08	35.25	38.37	TBD	TBD	TBD	TBD	TBD	TBD	TBD	TBD	TBD	TBD	TBD	TBD	TBD	TBD
	$\log_{10}(\text{degrees})$																				
	μ_{ASA}	1.62	1.54	1.52	1.56	1.5	1.56	TBD	TBD	TBD	TBD	TBD	TBD	TBD	1.59	1.79	1.53	1.78	1.42	1.84	1.46
	ϵ_{ASA}	0.26	0.23	0.15	0.2	0.16	0.17	TBD	TBD	TBD	TBD	TBD	TBD	0.31	0.08	0.27	0.11	0.26	0.18	0.37	0.09
AoD spread (σ_{ASD})	Median(deg)	24.06	65.3	21.31	55.24	25.19	53.2	TBD	TBD	TBD	TBD	TBD	TBD	TBD	TBD	TBD	TBD	TBD	TBD	TBD	TBD
	$\log_{10}(\text{degrees})$																				
	μ_{ASD}	1.32	1.77	1.35	1.71	1.43	1.68	TBD	TBD	TBD	TBD	TBD	TBD	TBD	TBD	TBD	TBD	TBD	TBD	TBD	TBD
	ϵ_{ASD}	0.26	0.12	0.15	0.15	0.1	0.15	TBD	TBD	TBD	TBD	TBD	TBD	TBD	TBD	TBD	TBD	TBD	TBD	TBD	TBD
ZoA spread (σ_{ZSA})	Median(deg)	3.69	3.92	4.43	4.04	9.34	4.2	TBD	TBD	TBD	TBD	TBD	TBD	TBD	TBD	TBD	TBD	TBD	TBD	TBD	TBD
	μ_{ZSA}	0.63	0.62	0.64	0.62	0.86	0.63	TBD	TBD	TBD	TBD	TBD	TBD	0.77	0.85	0.80	0.91	0.8	0.82	0.79	0.94

$\log_{10}(\text{degrees})$	ϵ_{ZSA}	0.52	0.25	0.44	0.29	0.4	0.24	TBD	TBD	TBD	TBD	TBD	TBD	0.09	0.05	0.03	0.05	0.09	0.02	0.03	0.03	
ZoD spread (σ_{ZSD}) $\log_{10}(\text{degrees})$	Median(deg)	3.36	10.26	4.02	7.45	4.56	6.56	TBD	TBD	TBD	TBD	TBD	TBD	TBD	TBD	TBD						
	μ_{ZSD}	0.63	0.98	0.64	0.87	0.74	0.82	TBD	TBD	TBD	TBD	TBD	TBD	TBD	TBD	TBD						
	ϵ_{ZSD}	0.46	0.19	0.35	0.2	0.3	0.2	TBD	TBD	TBD	TBD	TBD	TBD	TBD	TBD	TBD						
AoD and AoA distribution		Wrapped Gaussian						TBD	TBD	TBD	TBD	TBD	TBD	TBD	TBD	TBD						
ZoD and ZoA distribution		Laplacian						TBD	TBD	TBD	TBD	TBD	TBD	TBD	TBD	TBD						
Delay scaling parameter r_τ		6.79	7.17	10.23	8.62	8.7	8.31	TBD	TBD	TBD	TBD	TBD	TBD	TBD	TBD	TBD						
XPR (dB)	μ_{XPR}	17.12	17.71	16.12	14.48	16.85	16.06	TBD	TBD	TBD	TBD	TBD	TBD	TBD	TBD	TBD						
	σ_{XPR}	5.85	6.74	6.22	6.25	6.62	5.34	TBD	TBD	TBD	TBD	TBD	TBD	TBD	TBD	TBD						
LOS Ricean K factor (dB) *	μ_K	1.36	N/A	0.54	N/A	-0.18	N/A	TBD	N/A	TBD	N/A	TBD	N/A	TBD	N/A	TBD	N/A	TBD	N/A	TBD	N/A	N/A
	ϵ_K	3.49	N/A	2.91	N/A	3.18	N/A	TBD	N/A	TBD	N/A	TBD	N/A	TBD	N/A	TBD	N/A	TBD	N/A	TBD	N/A	N/A

1. From Aalto University based on measurement
2. From Qualcomm based on measurement
3. From ETRI based on measurement in Railway station
4. From ETRI based on measurement in Airport

Table 41. Preliminary Indoor shopping mall large-scale channel characteristics (part 2)

Parameters		15GHz ¹		28GHz ¹		63GHz ¹	
		LOS	NLOS	LOS	NLOS	LOS	NLOS
Correlation distance (m)	DS [ns]	8	2.5	8.5	2	8	0.5
	ASD [deg]	7	6.5	5.5	1	2	1
	ASA [deg]	17.5	7.5	6.5	6	8.5	4.5
	ZSD [deg]	8.5	4.5	7.5	1.5	7.5	0.5
	ZSA [deg]	12.5	3	10	1.5	14.5	2
	SF [dB]	3	7.5	6.5	7.5	15	2
	K [dB]	2	N/A	12.5	N/A	16	N/A

Cross Correlation	ASD [deg] vs DS [s]	0.44	0.16	-0.16	0.32	-0.1	0.54
	ASA [deg] vs DS [s]	0.31	0.51	0.46	0.36	0.62	0.21
	ASA [deg] vs SF [dB]	-0.09	0.08	0.13	0.44	0.31	0.27
	ASD [deg] vs SF [dB]	0.29	0.16	0.38	0.33	0.3	0.33
	DS[s] vs SF[dB]	0.13	0.11	-0.03	0.42	0.21	0.48
	ASD [deg] vs ASA [deg]	-0.37	0.46	-0.3	0.35	-0.07	0.24
	ASD [deg] vs K [dB]	-0.18	N/A	0.34	N/A	0.41	N/A
	ASA [deg] vs K [dB]	-0.13	N/A	-0.28	N/A	-0.07	N/A
	DS [s] vs K [dB]	-0.49	N/A	-0.46	N/A	-0.38	N/A
	SF [dB] vs K [dB]	0.4	N/A	0.49	N/A	0.49	N/A
	ZSD [deg] vs SF [dB]	-0.08	0.01	-0.14	0.29	-0.17	0.45
	ZSA [deg] vs SF [dB]	-0.15	0.09	-0.17	0.29	-0.19	0.23
	ZSD [deg] vs K [dB]	0.01	N/A	0.37	N/A	0.56	N/A
	ZSA [deg] vs K [dB]	-0.07	N/A	0.38	N/A	0.45	N/A
	ZSD [deg] vs DS [s]	-0.43	-0.22	-0.6	0.04	-0.58	0.37
	ZSA [deg] vs DS [s]	-0.35	0.3	-0.5	0.36	-0.16	0.2
	ZSD [deg] vs ASD [deg]	0.28	-0.08	0.21	0.4	0.46	0.33
	ZSA [deg] vs ASD [deg]	0.3	-0.2	0.27	0.03	0.34	-0.1
	ZSD [deg] vs ASA [deg]	-0.54	-0.5	-0.45	-0.01	-0.26	-0.2
	ZSA [deg] vs ASA [deg]	-0.58	0.19	-0.42	0.47	0.08	0.26
ZSD [deg] vs ZSA [deg]	0.92	0.09	0.9	0.22	0.77	0.29	

1. From Aalto University based on measurement

Table 42. Preliminary Indoor office small-scale channel characteristics

Parameters	73GHz ¹	28GHz ²	28GHz ³		73GHz ³	
	Hybrid	LOS	LOS	NLOS	LOS	NLOS
Number of clusters	6	7	3.271	3.5	3.9	4.3

Number of rays per cluster	10	4	52.9	41.82	38.47	35.75
Cluster ASD [deg]	3.2	9.75	TBD	TBD	TBD	TBD
Cluster ASA[deg]	3.7	13.22	15.27	15.35	14.05	10.44
Cluster ZSD[deg]	$10^{(-0.043d+0.09)}$	3.61	TBD	TBD	TBD	TBD
Cluster ZSA[deg]	$10^{(-0.036d-0.18)}$	5.16	8.06	5.42	3.95	4.51
Per cluster shadowing std [dB]	12	TBD	TBD	TBD	TBD	TBD

1. From Nokia/NYU based on ray-tracing
2. From KT based on measurement
3. From Huawei based on measurement

Table 43. Preliminary Indoor shopping mall small-scale channel characteristics

Parameters	15GHz ¹		28GHz ¹		63GHz ¹	
	LOS	NLOS	LOS	NLOS	LOS	NLOS
Number of clusters	6.33	6.98	6.18	6.21	6.23	5.68
Number of rays per cluster	2.7	7.9	3.67	10	7.8	14
Cluster ASD [deg]	5.2	9.87	6.59	11.12	9.98	12.82
Cluster ASA[deg]	5.22	9.34	6.73	10.05	12.27	11.4
Cluster ZSD[deg]	2.52	4.35	2.96	4.75	5.06	4.7
Cluster ZSA[deg]	2.43	2.3	3.17	2.44	6.08	3.03
Per cluster shadowing std [dB]	14	10	16	11	11	11

1. From Aalto based on measurement

11.3.4 O2I

Table 44 Summary of measured small scale channel parameters for the O2I scenario

		36.873	DOCOMO	Ericsson				KT	CMCC/BUPT
Frequency [GHz]			20	2.44	5.8	14.8	58.68	28	3.5
Delay spread (DS) $\log_{10}(\text{[s]})$	m_{DS}	-6.62	-7.29	-7.42	-7.36	-7.24	-7.09	-8.07	
	ϵ_{DS}	0.32	0.34	0.49	0.46	0.53	0.45	0.54	
AoD spread (σ_{ASD}) $\log_{10}(\text{[}^\circ\text{]})$	m_{ASD}	1.25							
	ϵ_{ASD}	0.42							
AoA spread (σ_{ASA}) $\log_{10}(\text{[}^\circ\text{]})$	m_{ASA}	1.76	1.62					1.51	
	ϵ_{ASA}	0.16	0.24					0.30	
ZoA spread (σ_{ZSA}) $\log_{10}(\text{[}^\circ\text{]}^2)$	m_{ZSA}	1.01	0.5					0.43	0.86
	ϵ_{ZSA}	0.43	0.46					0.25	0.26
Shadow fading (SF) [dB]	s_{SF}	7						5.59	

		36.873	DOCOMO	Ericsson				KT	CMCC/BUPT
Frequency [GHz]			20	2.44	5.8	14.8	58.68	28	3.5
Cross-Correlations	ASD vs DS	0.4							
	ASA vs DS	0.4	0.25						
	ASA vs SF	0						0.53	
	ASD vs SF	0.2							
	DS vs SF	-0.5						0.7	
	ASD vs ASA	0							
	ASD vs K	N/A							
	ASA vs K	N/A							
	DS vs K	N/A							
	SF vs K	N/A							
Cross-Correlations ¹⁾	ZSD vs SF	0							-0.15
	ZSA vs SF	0						0.68	0.13
	ZSD vs K	N/A							
	ZSA vs K	N/A							
	ZSD vs DS	-0.6	0.12					0.64	-0.73
	ZSA vs DS	-0.2							-0.53
	ZSD vs ASD	-0.2							-0.21
	ZSA vs ASD	0							0.42
	ZSD vs ASA	0							-0.21
	ZSA vs ASA	0.5	0.15					0.41	0.13
	ZSD vs ZSA	0.5							0.38

		36.873	DOCOMO	Ericsson				KT	CMCC/BUPT
Frequency [GHz]			20	2.44	5.8	14.8	58.68	28	3.5
Cross-Correlations	ASD vs DS	0.4							
Delay distribution		Exp						Exp	
AoD and AoA distribution		Wr G						Lapl	
ZoD and ZoA distribution		Lapl						Lapl	Lapl
Delay scaling parameter r_τ		2.2						2.96	
XPR [dB] ⁶⁾	m	9							
	s	5							
Number of clusters		12	6					2	
Number of rays per cluster		20	50					15	
Cluster ASD		5							
Cluster ASA		8	36					25	
Cluser ZSA ²⁾		3	5					3.7	7
Per cluster shadowing std z [dB]		4							
Correlation distance in the horizontal plane [m] ³⁾	DS	10							
	ASD	11							
	ASA	17							
	SF	7							
	K	N/A							
	ZSA	25							25
	ZSD	25							25

11.4 Processing Methodologies

11.4.1 Physical effects on propagation

As a consequence of shorter wavelengths as the carrier frequency increases, the radio propagation must be modelled with an understanding and consideration of a number of physical effects that occur in the real environment. A deployment scenario, perhaps involving up to a hundred meters of propagation transmission distance with short wavelengths, will encounter multiple different physical transmission effects. It is helpful if these physical effects are included in the overall transmission model to accurately reflect the behavior of the radio propagation environmental conditions.

An illustration of some of the physical effects of propagation is shown in Figure 43. This illustration may be helpful in understanding the multiple regions of physical processes that may be in the environment and affect the radio propagation.

- Zone 1 (close range free space)
Propagation is dominated by the direct path with few reflections.
- Zone 2 (LOS/scattered/waveguide)
Propagation is dominated by the direct path and significant close reflections.
- Zone 3 (NLOS occultation scattered)
Propagation is mainly by the reflections with some direct path energy but these are attenuated by distance.
- Zone 4 (distant NLOS)
Propagation is dominated by a small number of paths that are either not occulted or are a result of a good reflection.
- Zone 5 (too distant)
The illustration also shows a fifth zone in which the signals have become too weak to be useful either through numerous multiple reflections, distance, corners or occultation. In this zone communications is generally impractical.

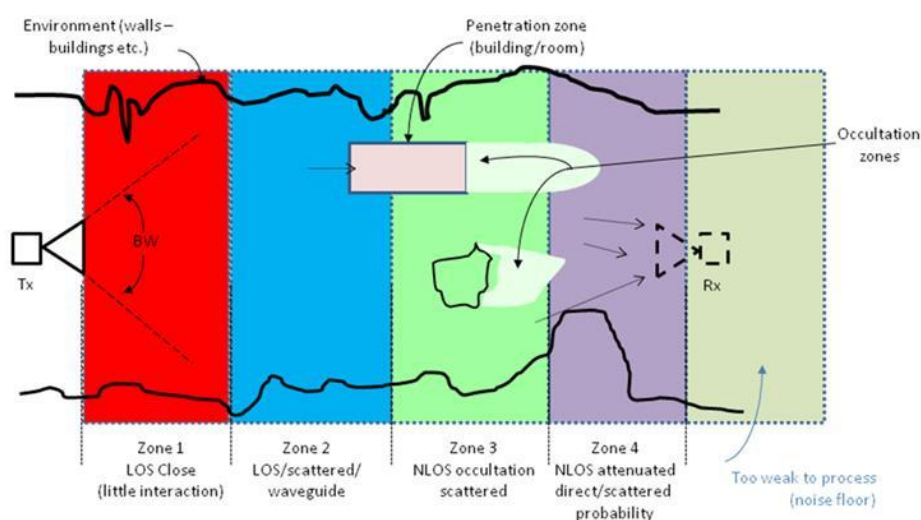


Figure 43. Illustration of multiple physical transmission effects

In each region there is always the possibility of physical blockage or occultation. Because of the small wavelengths, many typical objects in the environment (e.g. people, furniture, machinery, office equipment, etc.) are of a size that they completely block the direct signal, leaving the receiver with little except whatever reflections that may be available. This is shown in the illustration as typically in Zone 3 or 4 but it may occur anywhere. Also in some instances, there may be penetration loss for signals into interior rooms or through walls. The zone size depends on the wavelength, the dimensions and details of the environment, and the antenna beam widths. Not all zones may exist in every deployment environment or signal path. Typically, the signal propagation may experience multiple physical effects on its journey and so the “zones” may overlap in space.

11.4.2 The effects of the antenna pattern

In understanding the measurements of the new 5G channels and the associated channel model parameters, it is helpful to know the characteristics of the antennas used to make the measurements. Some measurement antennas are directive (e.g. horn or array antennas) and consequently may not illuminate reflecting surfaces of the environment during measurements and thus may appear to simplify the environment when compared with measurements made with other non-directional antennas (e.g. omni-directional antennas). In some cases, the test antennas may have significant sidelobes in their radiation pattern and these may make the environment seem more reflective than is physically the case.

Traditionally, measurements in the frequency bands below 6 GHz have used omni-directional antennas. In these bands the transmit antenna “floods” the environment with power in all directions (i.e. sector coverage) and the receive antenna accepts power from all directions at its location. In environments in which there are many reflections the apparent “path loss” may be reduced due to the additional power received from the many reflections. Typically in low frequency bands, the same antenna format (i.e. sector at base station and omni-directional at user equipment) is also used for the operational equipment and so the total-power/omni-directional path loss measurement is appropriate for the operating environment. Propagation studies and operation for these bands has thus been successful because the measurements, modelling and operation are all based on similar antenna characteristics.

In the bands above 6 GHz however, directional antennas (e.g. “horns”) are often used for measurements to help improve the range of the measurements. Directional antenna configurations are also expected to be used for operational equipment including mobile devices and access points as the antenna “gain” they provide may be necessary in the operational system to achieve the needed link budget. However, if the antenna configuration used for the path loss measurements is not the same as used for the operating equipment, then the associated model may not be accurate for modelling link budgets for equipment having different antenna configurations. Equipment with a narrow beam antenna will typically see less received power than would be expected based on a path loss model derived from measurements using omni-directional antennas.

a. Decoupling the antenna pattern

Many of the future systems will be operated using highly directional antennas for at least a portion of their usage. To accurately model these conditions it is necessary to decouple the channel model from the measurement antenna patterns. This is often referred to as “antenna decoupling”. The measurements are in reality the convolution of the measurement antenna patterns and the channel

environment and recovering the channel environment from the measurements involves a “deconvolution” of the measuring antenna patterns from the measurements. The general process for decoupling of the antenna pattern to reconstruct the true signal angular distribution can be summarized in the following steps.

1. Estimate the path of propagation (angular domain/delay domain/both).
2. Remove the antenna pattern (different algorithms).
3. Reconstruct the estimated measured data with antenna pattern.
4. Evaluate the effect of reconstruction and antenna decoupling.

For a typical measurement antenna with a main beam and small side-lobes, the measured angular spectrum will appear as the actual channel “blurred” by the measurement antenna sampling pattern. To recover the true angular distribution of the actual channel it is necessary to undo the convolution between the measuring antenna and the channel. This is not an easy to do as practical signals and beam patterns include zeros or low amplitude regions that may prevent a simple analytical inversion from recovering the real channel. However, with sufficiently well behaved signals (i.e. with well-defined angular clusters and a good ratio between beam strength and its side-lobes) often a good approximations can be made.

Similar measurement decoupling problems are experienced in a number of other sciences and there are several algorithms for deriving the hypothetical true angular distribution from the data. Some of these processes are iterative, in which an initial estimate is gradually corrected based on its comparison to the measured data. A popular practical technique in the RADAR community is the “MUSIC” algorithm [Schmidt] while the Synthetic Aperture Imaging and radio astronomy communities use the “CLEAN” algorithm [Clarke]. The SAGE algorithm has also been applied in this context [Fessler].

11.4.3 Clustering

Different clustering algorithms were considered in support of the channel modelling activities herein described. These algorithms include the Agglomerative algorithm, the k-means algorithm and the time cluster and spatial lobe clustering algorithm.

The agglomerative algorithm is a bottom-up hierarchical clustering algorithm where multipath components (MPCs) are iteratively merged together. It starts with each MPC belonging to a different cluster and, at each step, the most similar clusters are combined. The process repeats until either a stop criterion is met or only one single cluster remains.

The K-means algorithm [Czink VTCF06] groups the multipath components (MPCs) into clusters such that the MPCs within each cluster have similar delay, elevation and azimuth angles. The algorithm identifies each cluster by its centroid position in the parameter space. Each MPC is assigned to the cluster centroid with smallest distance. The algorithm iteratively optimizes the positions of the centroids in order to minimize the total distance from each MPC to its centroid.

In the time cluster and spatial lobe clustering algorithm approach [Samimi GCW2015][Samimi ICC2015] [Samimi EUCAP2016], the time and space dimensions are considered independently, by separately performing data clustering in the temporal and spatial domains, yielding statistics for time clusters and spatial lobes in omnidirectional millimeter wave channels. Time clusters are composed of multipath components traveling close in time delay, and that arrive from potentially different angular

directions in a short propagation time window as seen from field measurements. Spatial lobes represent main directions of arrival (or departure) where energy arrives over the entire time span of the multipath time delay profile. In this modelling framework, a channel impulse response “initial condition” for a particular location or point is generated by separately generating time cluster parameters and spatial lobe parameters independently, and then randomly assigning the different multipath components to different spatial lobes as has been found to occur in millimeter wave channels.

References

- [3GPP TR25.996] 3GPP TR 25.996 (V.12.0.0), "Spatial channel model for Multiple Input Multiple Output (MIMO) simulations," Sep. 2014.
- [3GPP TR36.814] 3GPP TR 36.814 (V9.0.0), "Further advancements for E-UTRA physical layer aspects," Mar. 2010.
- [3GPP TR36.873] 3GPP, TR 36.873 (V12.2.0), "Study on 3D channel model for LTE," July 2015
- [Andersen 1995] J. Andersen, T. Rappaport, and S. Yoshida, "Propagation measurements and models for wireless communications channels," *IEEE Communications Magazine*, vol. 33, no. 1, pp. 42–49, Jan 1995.
- [And2002] C. Anderson, et. al., "In-Building Wideband Multipath Characteristics at 2.5 & 60 GHz," 2002 IEEE Vehicular Technology Conference, Fall 2002.
- [Anite Telecoms 2014] Anite Telecoms, "Some investigations on angular sampling method for 3D spatial cluster", 3GPP R1-140805, Prague, Czech Republic, 10 – 14 February 2014.
- [Baum2015] D. S. Baum, J. Hansen, and J. Salo, "An interim channel model for beyond-3G systems: extending the 3GPP spatial channel model (SCM)," in Proc. IEEE VTC-spring, vol. 5, 2005, pp.3132-3136.
- [Chavero 1999] M. Chavero, et. al., "Impact of Vegetation on the performance of 28 GHz LMDS Transmission," *IEEE MTT-S*, Vol. 3, June 1999, p. 1063-1066.
- [Clark Sept. 1980] An efficient implementation of the algorithm 'CLEAN'; Clark, B. G.; *Astronomy and Astrophysics*, vol. 89, no. 3, pp377-378; Sept 1980.[COST] <http://www.cost2100.org/>
- [Czink VTCF06] N. Czink, et al., "A framework for automatic clustering of parametric MIMO channel data including path powers," in *IEEE VTC-Fall 2006*, September 2006.
- [ETSI 2015] ETSI, "New ETSI Group on Millimetre Wave Transmission starts work," <http://www.etsi.org/news-events/news/866-2015-01-press-new-etsi-group-on-millimetre-wave-transmission-starts-work>
- [Fessler VTC Fall 2014] Space-Alternating Generalized Expectation-Maximization Algorithm; Fessler, J.A.; *IEEE Transactions on Signal Processing*, vol. 42, no. 10, pp2664-2677; Oct 1994.
- [Gustafson 2014] C. Gustafson, et. al. , "On mm-Wave Multipath Clustering and Channel Modeling," *IEEE Transactions on Antennas and Propagation*, vol. 62, no. 3, pp. 1445-1455, March 2014.
- [Haneda 2016] K. Haneda, N. Omaki, T. Imai, L. Raschkowski, M. Peter and A. Roivainen, "Frequency-agile pathloss models for urban street canyons," *IEEE Trans. Ant. Prop.*, 2016.
- [Haneda ICC2016] K. Haneda et al., "Indoor 5G 3GPP-like Channel Models for Office and Shopping Mall Environments," in 2016 IEEE International Conference on Communications Workshops (ICCW), May 2016.

[Haneda VTC2016] K. Haneda et al., "5G 3gpp-like channel models for outdoor urban microcellular and macrocellular environments," in 2016 IEEE VTC 2016- Spring, May 2016. [Online]. Available: <http://arxiv.org/abs/1602.07533>

[Hata 1980] M. Hata, "Empirical formulas for propagation loss in land mobile radio service," IEEE Trans. Veh. Technol., vol. 29, no. 3, pp. 317–325, Aug.1980

[Hur EuCAP2015] S. Hur, et. al., "Wideband Spatial Channel Model in an Urban Cellular Environments At 28 GHz," in Proc. EuCAP2015, April 2015.

[Hur JSTSP2016] S. Hur, et. Al., "Proposal on Millimeter-Wave Channel Modeling for 5G Cellular System", IEEE Journal of Selected Topics in Signal Processing, April 2016.

[ITU M.2135-1] ITU-R Rep M.2135-1, "Guidelines for evaluation of radio interface technologies for IMT-Advanced."

[ITU-R P.676] Recommendation ITU-R P.676-10 "Attenuation by atmospheric gases"

[ITU-R P.833] Recommendation ITU-R P.833-8 "Attenuation in vegetation"

[ITU-R P.838] Recommendation ITU-R P.838-3 "Specific attenuation model for rain for use in prediction methods"

[Jarvelainen 2016] J. Jarvelainen, S. Nguyen, K. Haneda, R. Naderpour and U. T. Virk, "Evaluation of millimeter-wave line-of-sight probability With point cloud data," IEEE Wireless Communications Letters, 2016.

[Karttunen EuCAP2015] A. Karttunen, K. Haneda, J. Jarvelainen and J. Putkonen, "Polarisation Characteristics of Propagation Paths in Indoor 70 GHz Channels," in Proc. 9th European Conf. Ant. Prop. (EuCAP 2015), Lisbon, Portugal, Apr. 2015.

[Larsson EuCAP 2014] C. Larsson, F. Harrysson, B-E. Olsson and J-E. Berg, "An outdoor-to-indoor propagation scenario at 28 GHz", in Proc. of European Conference on Antennas and Propagation (EuCAP) 2014, pp. 3301-3304.

[Liu2012] L. Liu, C. Oestges, J. Poutanen, K. Haneda, P. Vainikainen, F. Quitin, F. Tufvesson, P. D. Doncker, "The COST 2100 MIMO channel model," IEEE Wireless Communications Magazine, Dec., 2012, pp. 92-99.

[MacCartney GC2013] G. MacCartney, J. Zhang, S. Nie, and T. Rappaport, "Path loss models for 5g millimeter wave propagation channels in urban microcells," in 2013 IEEE Global Communications Conference (GLOBECOM), Dec. 2013, pp. 3948–3953.

[MacCartney 2015], G. MacCartney, et. al, "Indoor Office Wideband Millimeter-Wave Propagation Measurements and Channel Models at 28 GHz and 73 GHz for Ultra-Dense 5G Wireless Networks," IEEE Access, October 2015.

[METIS 2013] "Simulation Guidelines," Deliverable D6.1, METIS document number ICT-317669-METIS/D6.1, October 31, 2013.

[METIS 2015] METIS2020, Deliverable D1.4 v3, "METIS Channel Model," July 2015. https://www.metis2020.com/wp-content/uploads/METIS_D1.4_v3.pdf

[MiWEBA 2014] MiWEBA, Deliverable D5.1 “Channel modeling and characterization,” June, 2014, http://www.miweba.eu/wp-content/uploads/2014/07/MiWEBA_D5.1_v1.011.pdf.

[mmMagic] <https://5g-ppp.eu/mmmagic/>

[Nie13] S. Nie, G. R. MacCartney, Jr., S. Sun, T. S. Rappaport, “72 GHz Millimeter Wave Indoor Measurements for Wireless and Backhaul Communications,” in *2013 IEEE 24th Annual International Symposium on Personal, Indoor and Mobile Radio Communications, (PIMRC)*, Sept. 2013, pp. 2429.

[NIST] <http://www.nist.gov/ct/wireless-networks/5gmillimeterwavechannelmodel.cfm>

[Nguyen16] H. C. Nguyen, et al., “An Empirical Study of Urban Macro Propagation at 10, 18, and 28 GHz,” *submitted to VTC-2016/Spring*.

[Ökvist 2016] P. Ökvist, N. Seifi, B. Halvarsson, A. Simonsson, M. Thurfjell, H. Asplund and J. Medbo, “15 GHz Street-level Blocking Characteristics Assessed with 5G Radio Access Prototype” in *2016 IEEE VTC 2016- Spring*, May 2016.

[Piersanti ICC2012] S. Piersanti, L. Annoni, and D. Cassioli, “Millimeter waves channel measurements and path loss models,” in *2012 IEEE International Conference on Communications (ICC)*, June 2012, pp. 4552–4556.

[R1-160846] 3GPP R1-160846, Ericsson, “Street Microcell Channel Measurements at 2.44, 14.8 & 58.68 GHz”, Feb. 2016. Online:

ftp://ftp.3gpp.org/TSG_RAN/WG1_RL1/TSGR1_84/Docs/R1-160846.zip

[Rappaport 2013] T. S. Rappaport et al., “Millimeter Wave Mobile Communications for 5G Cellular: It Will Work!,” in *IEEE Access*, vol.1, pp. 335-349, 2013.

[Rappaport 2015], T. S. Rappaport, et. al.,” Wideband Millimeter-Wave Propagation Measurements and Channel Models for Future Wireless Communication System Design,” *IEEE Trans. Communications*,” Vol. 63, No. 9, , pp. 3029-3056, Sept. 2015.

[Rappaport Book2015] T. S. Rappaport, R. W. Heath, Jr., R. C. Daniels, and J. N. Murdock, *Millimeter Wave Wireless Communications*. Pearson/Prentice Hall 2015.

[Rappaport ICC 2015] T. S. Rappaport and S. Deng, “73 GHz Wideband Millimeter-Wave Foliage and Ground Reflection Measurements and Models,” *2015 IEEE ICC*, June 2015.

[Rodriguez VTC Fall 2014] I. Rodriguez, H. C. Nguyen, N. T. K. Jorgensen, T. B. Sorensen and P. Mogensen, “Radio Propagation into Modern Buildings: Attenuation Measurements in the Range from 800 MHz to 18 GHz”, in *Proc. of IEEE Vehicular Technology Conference (VTC fall)*, 2014, pp. 1-5.

[Samimi 2015] M. K. Samimi, T. S. Rappaport, and G. R. MacCartney, Jr., “Probabilistic omnidirectional path loss models for millimeter-wave outdoor communications,” in *IEEE Wireless Communications Letters*, vol. 4, no. 4, pp. 357-360, Aug. 2015.

[Samimi GCW2015] M. K. Samimi, T. S. Rappaport, “3-D Statistical Channel Model for Millimeter-Wave Outdoor Communications,” in *2015 IEEE Global Communications Conference, Exhibition & Industry Forum (GLOBECOM) Workshop*, Dec. 6-10, 2015.

[Samimi EUCAP2016] M. K. Samimi, T. S. Rappaport, “Local Multipath Model Parameters for Generating 5G Millimeter-Wave 3GPP-like Channel Impulse Response,” accepted for publication in

- the 10th European Conference on Antennas and Propagation (EuCAP'2016), April 2016.[Schwering 1988] F. Schwering, et. al., "Millimeter-Wave Propagation in Vegetation: Experiments and Theory," *IEEE Trans. Geoscience and Remote Sensing*, vol. 23, no. 6, p.355-367, May 1988.
- [Schmidt Mar 1986] Multiple emitter location and signal parameter estimation; Schmidt, R.O. ; *IEEE Transactions on Antennas and Propagation*, vol. 34, Issue: 3; pp276-280; Mar1986.
- [Semaan Globecom 2014] E. Semaan, F. Harrysson, A. Furuskär and H. Asplund, "Outdoor-to-indoor coverage in high frequency bands", *Globecom Workshops 2014*, pp. 393-398.
- [Sun GCW2015], S. Sun, et. al., "Path Loss, Shadow Fading, and Line-Of-Sight Probability Models for 5G Urban Macro-Cellular Scenarios," 2015 IEEE Globecom Workshop, San Diego, Dec. 2015.
- [Sun VTCS2016] S. Sun, et al., "Path Loss Models for 5G Urban Micro- and Macro-Cellular Scenarios," accepted for publication in *IEEE VTC-Spring 2016*, May 2016.
- [Tenerelli1998] P. A. Tenerelli and C. W. Bostian, "Measurement of 28 GHz diffraction loss by building corners", in *Proc. IEEE PIMRC 1998*, vol. 3, pp. 1166-1169, Sep. 1998.
- [Thomas VTCS2016] T. Thomas, et. al., "A Prediction Study of Path Loss Models from 2-73.5 GHz in an Urban-Macro Environment," accepted for publication in *IEEE VTC-Spring 2016*, May 2016.
- [W. Fan 2015] W. Fan, T. Jämsä, J. Ø. Nielsen, G. F. Pedersen, "On Angular Sampling Methods for 3-D Spatial Channel Models", *IEEE Antennas and Wireless Propagation Letters*, Vol. 14, 2015.
- [Walter 2008] Walter, B.; Bala, K.; Kulkarni, M.; Pingali, K., "Fast agglomerative clustering for rendering," in *Interactive Ray Tracing, 2008. RT 2008. IEEE Symposium on*, vol., no., pp.81-86, 9-10 Aug. 2008.
- [Wang 2015] Y. Wang, L. Huang, Z. Shi, K. Liu, and X. Zou, "A millimeter wave channel model with variant angles under 3GPP SCM framework," in *Proc. IEEE PIMRC 2015 Workshop*, Hong Kong, China, Aug. 2015.]
- [Wang 2016] Y. Wang, Z. Shi, L. Huang, Z. Yu, and C. Cao, "An Extension of Spatial Channel Model with Spatial Consistency", in *Proc. IEEE VTC-fall 2016*, Montreal, Sept. 2016.
- [WINNER] WINNER II Channel Models, D1.1.2 V1.2, IST-4-027756 WINNER II Deliverable, 4 February 2008.
- [Zhao 2013] H. Zhao et al., "28 GHz millimeter wave cellular communication measurements for reflection and penetration loss in and around buildings in New York city," in *2013 IEEE International Conference on Communications (ICC)*, pp. 5163-5167, 9-13 June 2013.

List of Acronyms

ABG.....	alpha beta gamma (path loss model)
ASA.....	angle spread of arrival in azimuth (at the UE)
ASD.....	angle spread of departure in azimuth (from the AP)
AP.....	access point
BW.....	bandwidth
CI.....	close in (reference-distance path loss model)
CIF.....	CI model with frequency-dependent path loss exponent
D2D.....	device to device
DS.....	delay spread
ESA.....	elevation angle spread of arrival (at the UE)
ESD.....	elevation angle spread of departure (from the AP)
GHz.....	Giga (billion) Hertz
InH.....	indoor hotspot
LOS.....	line of sight
LSP.....	large scale parameter
MIMO.....	multiple input/multiple output
MSE.....	mean squared error
NLOS.....	non line of sight
O2I.....	outdoor to indoor
O2O.....	outdoor to outdoor
PL.....	path loss
PLE.....	path loss exponent
Rx.....	receiver
SCM.....	spatial channel model
SF.....	shadow fading
SSCM.....	statistical spatial channel model
Tx.....	transmitter
UE.....	user equipment
UMa.....	urban macro
UMi.....	urban micro
V2V.....	vehicle to vehicle
ZBA.....	zenith (elevation) bias angle of arrival (at the UE)
ZBD.....	zenith (elevation) bias angle of departure (from the AP)